Quality Assurance and Control Methods for Serial Production of Superconducting RF Cavities Assembled in Cryomodules

Karol Kasprzak

Kraków 2021

Quality Assurance and Control Methods for Serial Production of Superconducting RF Cavities Assembled in Cryomodules

Karol Kasprzak

Doctor of Philosophy
Dissertation at
Institute of Nuclear Physics Polish Academy of Sciences
IFJ PAN, Kraków, Poland
by Karol Kasprzak

Supervisor 1: Prof. dr hab. Piotr Malecki
Supervisor 2: Dr hab. Dariusz Bocian

Abstract

The longest linear accelerators reach the length of a few kilometres. One of them is a part of the European X-ray Free Electron Laser (E-XFEL) infrastructure, starting from Deutsches Elektronen-Synchrotron (DESY) facility in Hamburg and ending in the next land Schleswig-Holstein. The E-XFEL total length is 1.7 km and the nominal electron beam energy is 17.5 GeV. The main elements of the E-XFEL linear accelerator are accelerating cryomodules. The E-XFEL cryomodule consists of 8 Superconducting Radio Frequency (SRF) cavities operating at the resonant frequency of 1.3 GHz.

One of the challenges of the initial phase of the E-XFEL project was the qualification tests of accelerating components. The qualification tests were performed for 800 cavities and 100 serial-production cryomodules as well as 3 pre-series cryomodules. The cryomodule tests consisted of low and high power groups of Radio Frequency measurements. The first group of measurements was performed with the use of the Vector Network Analyzer to measure the Fundamental Modes and Higher Order Modes. The second group of measurements was performed with the high power, namely with the use of the pulsed power amplifiers (klystrons). The aim of these measurements was to validate the cavities nominal parameters: the accelerating gradient and the own quality factor.

In this dissertation the quality assurance and control methods for serial production of SRF cavities assembled in cryomodules is presented. The author's contribution to this work was realized by the optimization of the testing methodology and implementation of the automated software for the E-XFEL project. The main profits from this work was assuring the repeatability of measurements by minimizing of human's errors, which resulted in keeping of the project's deadlines.

Contents

Abbreviations

AMTF	Accelerator Module Test Facility
DD	Dynamic Detuning
DESY	Deutsches Elektronen-Synchrotron
ESS	European Spallation Source
FEL	Free Electron Laser
FF	Field Flatness
FFT	Fast Fourier-Transformation
FLASH	Free-Electron Laser in Hamburg
FM	Fundamental Mode
FT	Flat-Top
HL	Heat Loads
HOM	Higher Order Mode
IFJ PAN	Institute of Nuclear Physics of the Polish Academy of Sciences
LFD	Lorentz Force Detuning
linac	linear accelerator
LLRF	Low Level Radio Frequency
MSE	Mean Square Error
MSFD	Mean Spectrum Frequency Deviation
PIP-II	Proton Improvement Plan-II
RF	Radio Frequency
SASE	Self-Amplified Spontaneous Emission
SC	Superconducting
SD	Static Detuning
SRF	Superconducting Radio Frequency
TESLA	Tera-Electronvolt Superconducting Linear Accelerator
VNA	Vector Network Analyzer
E-XFEL	European X-ray Free Electron Laser

Introduction

The longest linear accelerators reach the length of a few kilometres. One of them is a part of the European X-ray Free Electron Laser (E-XFEL) infrastructure, starting from the Deutsches Elektronen-Synchrotron (DESY) facility in Hamburg and ending in the next land Schleswig-Holstein. The E-XFEL total length is 1.7 km and the nominal electron beam energy is 17.5 GeV [1]. One of the challenges of the initial phase of the E-XFEL project was the qualification tests of accelerating components. During the E-XFEL construction phase in 2010-2016 a group of physicists and engineers from the Institute of Nuclear Physics of the Polish Academy of Sciences (IFJ PAN), Kraków, Poland, participated in two, partially overlapping, test campaigns of the serial-production accelerating components. The first one concerned measurements of Superconducting Radio Frequency (SRF) 9-cell Tera-Electronvolt Superconducting Linear Accelerator (TESLA) type cavities. The second test campaign was devoted to test the cavities assembled in the accelerating cryomodules. Each of the E-XFEL accelerating cryomodule consists of 8 TESLA type cavities.

The author participated actively in the cryomodule test campaign. During the first two years (2010-2011) the author took part in the training tests of pre-series cryomodules and in the development of the software, what was of prime importance for the cryomodule test campaign in the years 2012-2016. The tests were performed in the dedicated test infrastructure built in DESY: Accelerator Module Test Facility (AMTF). The test campaign covered: the installation of the components in the test-stands, Radio Frequency (RF) measurements at 300K, cool-down of the components to the cryogenic temperatures, and RF measurements at 2K.

This thesis presents the quality assurance and the control methods for a big set of serially produced cryomodules. These methods were developed by the author during the preparatory phase of the project (2010-2011). The author's contribution to this work was realized by *the optimization of the testing methodology and implementation of the automated software for the E-XFEL project*. The main profits from this work for the project was assuring the repeatability of measurements by minimizing of human's errors, which resulted in keeping of the project's deadlines.

In the first chapter, an overview of the E-XFEL project is presented. The second chapter briefly sets out the principles and selected topics concerning the particle acceleration with the use of the RF technology. Further, the main parameters of the cavities are described: the mode concept, the frequency, the cell shape, the quality factors, the geometric shunt impedance, and the accelerating gradient. The choice criteria of the superconducting technology for E-XFEL and their justification are discussed as well. Finally, the values of the main parameters for the E-XFEL SRF cavities are presented.

In the third chapter the measurements methodology is systematized. The infrastructure for testing of the accelerating components (cavities and cryomodules) at DESY is presented. The author focuses on the measurements of the E-XFEL cavities installed in the cryomodules (called also cryomodule measurements). However, for completeness, single cavities tests (which were performed before their assembly in the cryomodules) are also included in this thesis. The results of single cavities tests are used later as a reference for the cryomodule measurements. 800 cavities were tested under the similar conditions, when measured individually and in the cryomodules.

The whole tests procedures, for both single cavities and cryomodules, consisted of steps, which were defined by the power applied to the tested components, namely low and high power tests. The low power tests covered measurements of characteristic frequencies and amplitudes of EM field in the cavities. The high-power tests covered validation of the quality factors and the accelerating gradient. Moreover, the 3rd chapter introduces selected elements of the theory of the pulsed RF signals and clarifies the calculation of the parameter called K_T. Next, the measurement called Flat-Top, performed in order to determine the operating accelerating gradient, is described. Then, the evaluation of the thermal heat loads during normal cryomodule operation is shown.

The fourth chapter presents three software packages, which were developed and implemented by the author in order to guide and optimize the measurement procedures. In this work the author profited from the expertise of DESY, one of the leading European center for accelerator physics. The packages are related to the measurements called the Fundamental Mode (FM) spectrum and Higher Order Mode (HOM) spectra. The accelerating cavity exposed to the pulsed RF signal from the klystron requires dynamic fine adjustment of its length, which was provided by another dedicated package designed and successfully implemented by the author. It has been shown that the developed method with the use of these software packages allowed for efficient measurement and evaluation of FM and HOM spectra. Moreover, on the basis of the measurement results, the correctness of the cavity geometry compensation method in response to the high power RF pulse was demonstrated.

The fifth chapter summarizes the optimization of the testing methodology and automated software. Finally, the future plans are presented.

Chapter 1

The E-XFEL project overview

The European X-ray Free Electron Laser (E-XFEL) placed in Hamburg, Germany, is a research facility constructed to provide "ultrashort X-ray flashes with brilliance of 10^9 times higher than conventional X-ray radiation sources" [2]. The comparison to the existing infrastructures is presented in the Figure 1.1. The circular type electron accelerators (e.g. Petra synchrotron at DESY) have limitations in delivery of high energy and high intensity beam, mainly due to the bremsstrahlung. In order to achieve the higher electron energies either the circular accelerator with higher radius or a linear accelerator is needed. The high energy and high intensity electron beams are required to achieve the final product: high X-ray radiation. The linear accelerator was chosen for E-XFEL and for its demonstrator called the Free-Electron Laser in Hamburg (FLASH).
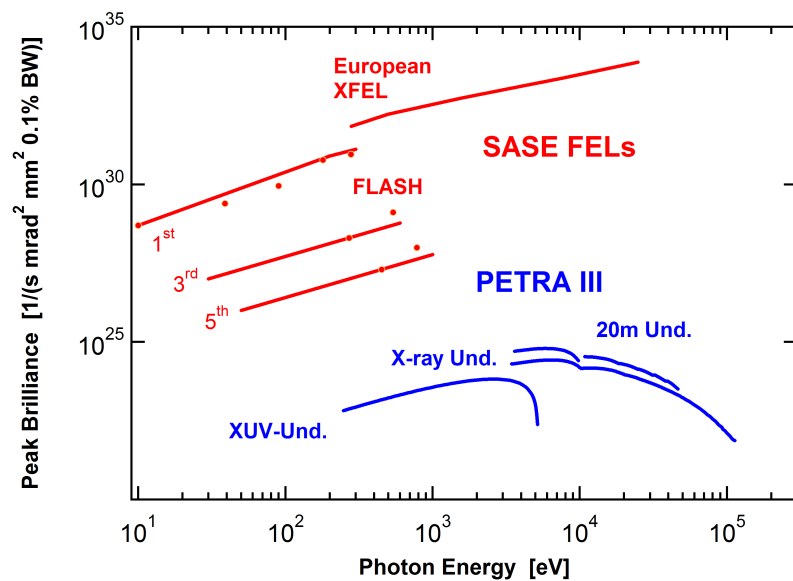

Figure 1.1: Comparison of the E-XFEL brilliance to other facilities at DESY: FLASH and Petra [4].
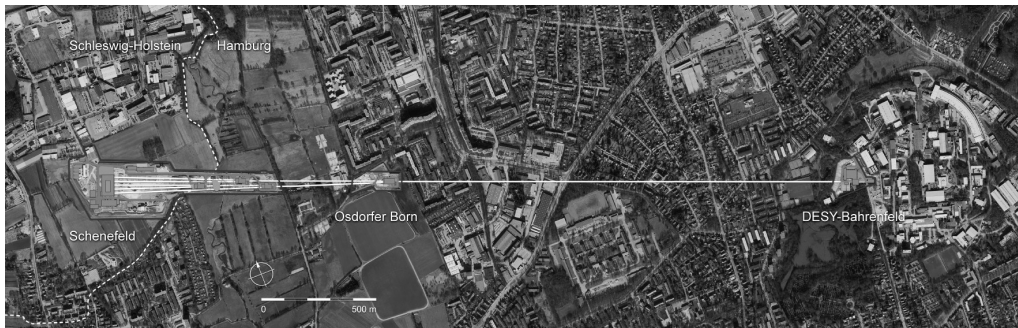
Figure 1.2: The E-XFEL tunnel facility [1].

The E-XFEL (see Figure 1.2) injector is located in DESY-Bahrenfeld. This part of infrastructure produces the beam of electrons with the use of the RF gun, in which an electrode is exposed to a UV laser pulse. In consequence the electrons are ejected from electrode surface, compressed and pre-accelerated [2]. Further, the electrons are accelerated in the main part of E-XFEL - linear accelerator (linac), which is installed in the tunnel from DESY-Bahrenfeld to Osdorfer Born. The E-XFEL accelerator consists nominally of 100 RF (1.3 GHz) accelerating cryomodules [2]. They are used to ramp the energy of electrons to its nominal value of 17.5 GeV. The cryomodules are the major part of the E-XFEL and this dissertation is focused on their testing. The next section of E-XFEL contains devices to produce the X-ray radiation with the use of the accelerated electrons. The electrons are wiggling in the specific component called undulator (Fig. 1.3), which provides the sinusoidal magnetic field so that the FEL process can take place [3]. During this operation the Röntgen radiation is produced and delivered to the several experimental station (located in Schenefeld, Schleswig-Holstein). The whole infrastructure, in which a light is produced from electrons with the use of the undulators, is called the Free Electron Laser (FEL) [5].

In the classical laser some radiation feed is needed to stimulate the emission of photons, which are amplified with use of mirrors [2]. In the case of FEL, the electron bunch passes the undulator's magnetic field and emits photons which are travelling with the speed of light, faster then the bunch. Matching the electron beam parameters with field parameters of undulators one may reach resonant conditions allowing for spontaneous self-amplification (SASE) of the photon bursts [6].

To summarize, the E-XFEL infrastructure combines features of a laser and a microscope [7]. As a laser it emits monochromatic, coherent and directional radiation. As a microscope, the X-ray wavelengths allows to analyse the structure of objects down to atomic resolutions. Therefore E-XFEL provides excellent research opportunities for scientists in physics, chemistry, materials science and biology [2].
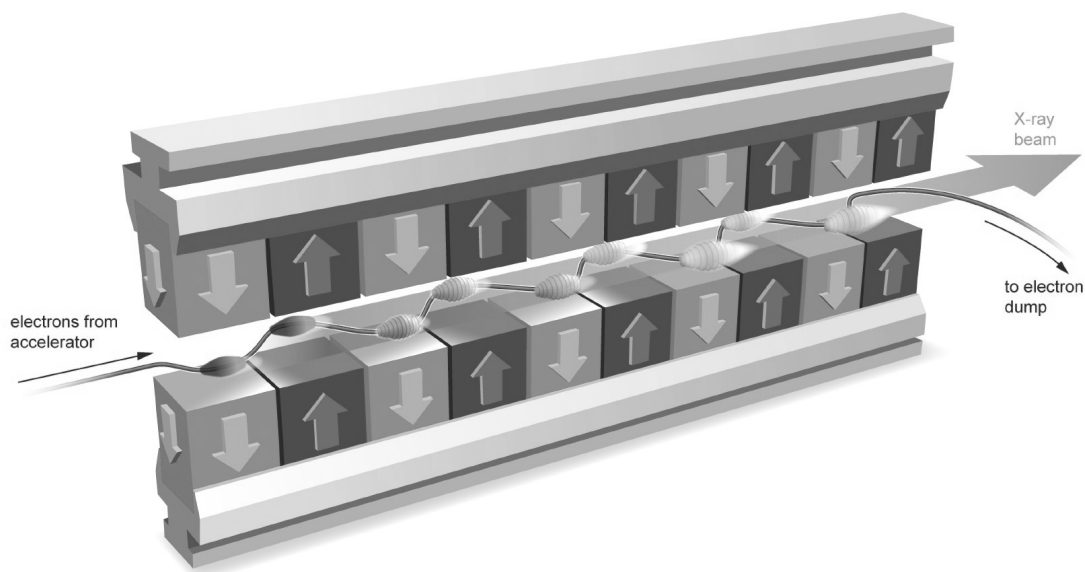
Figure 1.3: SASE principle in the undulator [1].

The main areas of application of the E-XFEL light product are given by the names of experimental stations proposed for the E-XFEL [2]:

- Femtosecond X-ray Experiments : time examination of the dynamics of solids, liquids, gases

- Single Particle & Biomolecules : visualization of single particles, clusters and biomolecules

- Small Quantum Systems : tests of atoms, ions, molecules and clusters under intense fields

- Spectroscopy & Coherent scattering : measurements of biological objects using soft X-rays

- Materials Imaging & Dynamics : experiments on nanodevices and their dynamics

- High Energy Density Science : examination of matter under hard X-ray

Chapter 2

SRF linear accelerator for the E-XFEL project

In this chapter some basic information on linear accelerators of particles is presented. The main emphasis is placed on devices which operate with sinusoidally varying RF electromagnetic fields. Such fields in free space are characterized by the vectors of electric **E** and magnetic **B** fields perpendicular to the direction of the wave's propagation. They are called TEM - transverse electromagnetic type of the field. In order to use TEM for the acceleration of a charged particle, one has to "tailor" the field to have the electric field component oriented towards the particle's direction of movement (see equation (2.1)). The TEM field formation is possible in waveguides with conductive boundaries which eventually evolved into resonators. The E-XFEL superconducting cavities, originally developed at DESY for the TESLA project [8], are excellent examples of such resonators.

2.1 Particle acceleration using resonant cavities

The principle of acceleration is described by the Lorentz force. A particle with the charge q moving with some velocity **v** in the electromagnetic field (**E**, **B**), experiences the force **F** [6]:

$$\mathbf{F} = q(\mathbf{E} + \mathbf{v} \times \mathbf{B}) \tag{2.1}$$

The magnetic field component **B** acts on a charged particle with the force **F** (eq.(2.1)) which is perpendicular to the direction of the particle's velocity **v** [9]. This feature is used for "optical" treatments (focusing, defocusing, trajectory control) of groups of charged particles called beams.

The maximal energy gain $\Delta \mathbf{W}$ by the charged particle, i.e. the work done by the $\mathbf{E}$ field component when the particle moves from point p_1 to point p_2, can be expressed as:

$$\Delta \mathbf{W} = \int_{p_1}^{p_2} \mathbf{F} dl = q \int_{p_1}^{p_2} \mathbf{E} dl = qV_{acc} \tag{2.2}$$

where V_{acc} is the accelerating voltage.

For a time-dependent field, propagated in complex accelerating structures, the analysis and determination of the V_{acc} becomes complicated [9-13]. In the following section, the explanation of the basic principles of operation of such structures with some emphasis on quantities and parameters relevant for the main subject of this work is provided. Many of the linear accelerator structures have been developed and built, starting from the pioneer drift tube linacs. The theory and implementation of the recent special waveguides, such as resonating cavities, have progressed considerably, particularly for the electron machines.

Inside a waveguide (empty space surrounded by e.g. rectangular conducting walls), the fields are described by the Maxwell equations:

$$\nabla \times \mathbf{B} - \frac{1}{c^2}\frac{\delta}{\delta t}\mathbf{E} = 0 \qquad \nabla \cdot \mathbf{B} = 0 \tag{2.3}$$

$$\nabla \times \mathbf{E} + \frac{\delta}{\delta t}\mathbf{B} = 0 \qquad \nabla \cdot \mathbf{E} = 0 \tag{2.4}$$

where c is the speed of light in vacuum. From the Maxwell equations one can obtain the *wave equations* (four dimensional Laplace equations) separately for the electric and magnetic field components:

$$\nabla^2 \mathbf{E} - \frac{1}{c^2}\frac{d^2\mathbf{E}}{dt^2} = 0 \tag{2.5}$$

$$\nabla^2 \mathbf{B} - \frac{1}{c^2}\frac{d^2\mathbf{B}}{dt^2} = 0 \tag{2.6}$$

It is noteworthy that all equations describing the both fields are linear. So, any two solutions can be linearly superposed. Also, superposition at different frequencies is possible, which enables the application of Fourier transforms. The Fourier transforms are very useful tools allowing to describe various solutions either in the frequency or in the time domain.

A good insight into the phenomenon of the electromagnetic (EM) wave propagation along, e.g. the waveguide, might be obtained while considering the superposition of two plane waves (being simple solutions of the above wave equations) [10]. Both are polarized in y direction and are propagating in x-z plane at an angle $\pm\phi$ with respect to the axial direction z (for the purpose of simplicity, the rectangular waveguide is considered). This is equivalent to the consideration of an oblique incidence of a wave (polarized in y direction) on perfectly conducting walls of the waveguide. The direct and reflected waves will interfere in the same way. In both cases, the resulting wave pattern is travelling in z direction and forming a standing wave pattern in the x direction. That is easily demonstrated with

the following equations describing the superposition of two plane waves travelling in $\pm\phi$ directions, oscillating at frequency ω:

$$E_{y^+} \propto sin(\omega t - k_z z + k_\perp x) \tag{2.7}$$

$$E_{y^-} \propto sin(\omega t - k_z z - k_\perp x) \tag{2.8}$$

$$E_{y^+} + E_{y^-} = 2sin(\omega t - k_z z)cos(k_\perp) \tag{2.9}$$

In the above equations symbols $k_\perp$ and k_z are the components of $\vec{k}$, the wave vector, which points to the direction of the wave propagation. Its length measures the phase shift per unit length in this direction.

$$k_z = kcos(\phi) \qquad k_\perp = ksin(\phi) \tag{2.10}$$

$$k = \frac{2\pi}{\lambda} = \frac{\omega}{c} \tag{2.11}$$

It is important to observe, that the distance between two adjacent wave crests in the z-direction (propagation direction) is longer than the actual wavelength λ. It means that the wave moves into this direction with the phase velocity $v_{\phi,z}$ greater than the velocity of light c:

$$v_{\phi,z} = \frac{\omega}{k_z} = \frac{c}{cos(\phi)} \tag{2.12}$$

There are many positions of reflecting walls for which forming the standing wave pattern is possible, as the equation $cos(k_\perp) = 0$ has many solutions. The solutions correspond to a different number of half-waves in the transverse direction. Each one represents a different waveguide mode. Our simplified example, according to an effective nomenclature, refers to the TE_{n0} mode. For example, a traverse polarization direction $k_\perp$ has been selected. More generally, TE_{mn} or TM_{mn} symbols for a rectangular waveguide refer to TE or TM fields, where m and n are the numbers of half waves in the x and y direction, respectively. In case of cavity modes, a third subscript is added, indicating the number of half wavelengths in the propagation direction. When these modes describe the configuration of electromagnetic fields in the cavity, they are called cavity modes.

More realistic considerations refer to circular (or cylindrical) waveguides. Many RF cavities are based on the simple cylindrical shape of a metallic cavity with conducting walls placed at z=0 and z=L (see Fig.2.1). Within perfect conducting walls, electric fields parallel to the metallic surface vanish. Magnetic fields perpendicular to a metallic surface vanish as well (from Maxwell equations we obtain: $\mathbf{n} \cdot \mathbf{B} = 0$, $\mathbf{n} \times \mathbf{E} = 0$).

To accelerate particles, the EM waves have to be confined to e.g. a cylindrical cavity in order to generate an electric field along the direction (z direction) of the particle motion. The wave equation in the cylindrical coordinates for E_z can be written as:

$$\frac{\partial^2 E_z}{\partial z^2} + \frac{1}{r}\frac{\partial}{\partial r}\left(r\frac{\partial E_z}{\partial r}\right) + \frac{1}{r^2}\frac{\partial^2 E_z}{\partial \phi^2} - \frac{1}{c^2}\frac{\partial^2 E_z}{\partial t^2} = 0 \tag{2.13}$$
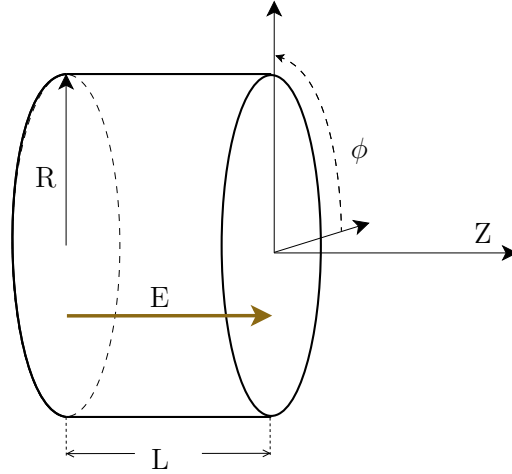
Figure 2.1: The cylindrical pillbox RF cavity model.

This wave equation has an infinite number of solutions. One may show (e.g. [9, 15]), how the above mentioned boundary conditions ($\mathbf{n}\cdot\mathbf{B} = 0$, $\mathbf{n}\times\mathbf{E} = 0$), practically related to the cavity geometry, determine the spectra of operating frequencies of a cylindrical cavity. The simplest example applies in the following: azimuthally symmetric, standing wave:

$$E_z(r, z, t) = E_0 R(r) cos(\omega t) \tag{2.14}$$

where the R(r) is a function dependent on r. Applying (2.14) to (2.13) gives the equation for R(r):

$$\frac{\mathrm{d}^2 R}{\mathrm{d}x^2} + \frac{1}{x}\frac{\mathrm{d}R}{\mathrm{d}x} + R = 0 \tag{2.15}$$

where $x = \omega r/c$ and the solution for the longitudinal field is the zero order Bessel function $J_0(\omega r/c)$:

$$E_z = E_0 J_0(\omega r/c) cos(\omega t) \tag{2.16}$$

One of the boundary conditions says: E_z must vanish at the cavity radius, $E_z(r = R) = 0$. It can be only satisfied if the Bessel function equals zero i.e. $J_0(\omega_c R/c) = 0$. The first zero of J_0 is at 2.405, which means that

$$\omega_c = 2.405c/R \tag{2.17}$$

and that for a given radius R there is only a single frequency satisfying the boundary condition.

Continuing that example one can apply the Ampere's law to find a magnetic field raised by the E_Z:

$$\oint \vec{B} \cdot d\vec{l} = \mu_0 \varepsilon_0 \int_S \frac{\partial \vec{E}}{\partial t} \cdot d\vec{S} \tag{2.18}$$

where:

- μ_0 is the permeability of vacuum,

- ε_0 is the permittivity of vacuum.

One may find that the corresponding magnetic field is:

$$B_\theta = -(E_0/c)J_1(k_r)sin(\omega t) \tag{2.19}$$

where $k_r = 2.405/R$. Equations 2.16 and 2.19 form one particular solution of normal modes of a cylindrical cavity's oscillation. This is a TM_{010} - Transverse Magnetic mode because the axial magnetic component B_z is zero. For cylindrical cavities, subscripts mnp in the symbol TM_{mnp} mean (and also for TE_{mnp}):

- m full-period variation in θ

- n zeros of the axial field component in radial direction

- p half-period variations in z

The Transverse Magnetic are the most frequently used modes in RF cavities for accelerating of a beam. The TM_{010} is the mode with the lowest frequency among all the modes. The mode with the lowest frequency is called the Fundamental Mode (FM). TM_{010} has the maximum of an electric field component on the Z axis, and the magnetic field is rotating around electric component with no effect on particles in the centre. Other modes are called Higher Order Modes (HOMs). One may also find the nomenclature: monopole mode for m=0, dipole mode for m=1, quadrupole mode for m=2, etc. Some of them are detrimental for the beam and, for example, HOMs increase the thermal load or cause the loss of the beam. Their excitation may be overcome, for example, by using HOM couplers (antennae) in order to extract them from the cavity.

2.2 Multicell cavity structure

There are several different shapes of the standing wave accelerating cavities [10, 17, 18]. For the TESLA type cavities, an elliptic geometry was chosen because such geometry allows for the effective reduction of the multipacting process. The multipacting is a serious limitation for cavities, especially those working at high accelerating gradients. The multipacting is an electron discharge due to the interaction with the cavity walls, appearing when electrons are emitted synchronously with the RF field and multiply at the impact with the cavity walls.

Figure 2.2: The E-XFEL type cavity [16].

It is typical that the accelerating cavities are connected together in a line (string), so that the RF cavity consists of many "cells". The E-XFEL accelerating cavity consists of 9-elliptical-cells (9 cavities) connected in a string (see Figure 2.2). It is a result of R&D on costs and field effect, performed for predecessor project called TESLA [8]. The technology developed for TESLA project was adopted and used in E-XFEL. In order to reduce the costs of the project, the number of cells in a cavity should be as high as possible, because the beam is not accelerated in the end tubes and between the cavities. On the other hand, there is a limit of the maximum number of cells. It is a field homogeneity, which deteriorates with the increasing number of cells [4]. The Fundamental Mode (FM) should have constant distribution through all the cells in order to maximize the acceleration. Finally, the 9 cell RF cavity was the optimum choice taking into account the optimization of costs and field effects. The consequence of connecting coupled cavities in a string is a different standing wave pattern.

The 9-cell E-XFEL RF cavity structure hosts nine FMs (of TM_{010}) in the range 1.27 - 1.3GHz. It is known from theoretical consideration that, "n coupled resonators can oscillate in n modes (frequencies) for each resonance field pattern being an eigenvector of a single (uncoupled) cell" [17]. For the multicell standing wave structures [6], their names denote phase advance (shift) of the electrical field component on the beam axis within each cell. For the 9 cell E-XFEL cavity at TM_{010} Fundamental Modes are called $\pi, 8\pi/9, ..., \pi/9$ mode. Actually there are nine modes within the Fundamental Mode (TM_{010}). The dispersion relation of the FM frequencies and HOMs is discussed later in this dissertation (see Chapter 3: Figure 3.8). For the E-XFEL operation π mode of the TM_{010} is used to accelerate relativistic particles, so the bunch passes the cavity during a half of the RF period.

2.3   Cavity equipment and E-XFEL cryomodule

The cavities are equipped with a set of components that are required for their proper operation. The list below shows the E-XFEL cavity equipment (see Figure 2.3):

1. The input power coupler - a coupler used to deliver power to the cavity,

2. The HOM couplers - each of the E-XFEL cavity is equipped with 2 couplers. The E-XFEL HOM couplers are installed inside the cans, at both ends of the cavity. They are used for HOMs extraction from the cavity. The HOM coupler is equipped with a part that blocks extraction of the operating frequency (rejection filter),

3. The pickup probe - a weakly coupled antenna used for EM field monitoring,

4. The helium tank - a container filled with a liquid helium in which the cavity is immersed,

5. The beam pipe - two pipes connected to the end-cells,

6. The tuning system - a step motor and two piezoelectric devices (shortly named piezos) used for the E-XFEL cavity - showed in Figure 2.4. The step motor and piezos are used to deform the length of the whole RF cavity in order to adjust the cavity to the resonant frequency. Piezos are transducers, which generate a voltage when they are deformed. The opposite effect also occurs: under external voltage, the piezoelectric elements are deformed. Each piezo can work as a sensor or an actuator.
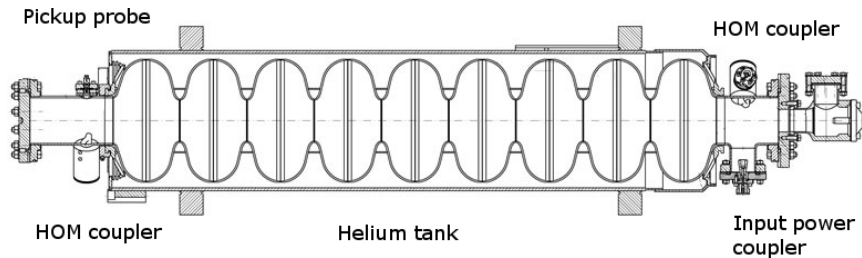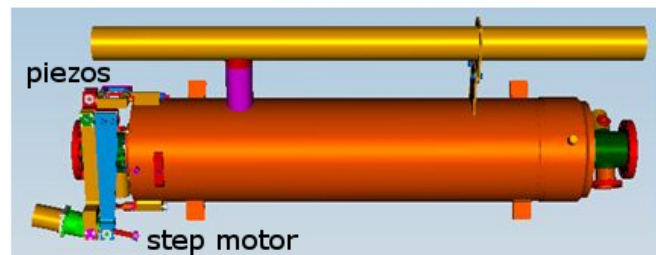

Figure 2.3: Side view of the E-XFEL cavity [1].

Figure 2.4: The E-XFEL cavity in a helium tank (courtesy of N.Ohuchi).

The basic element of the E-XFEL linear accelerator is the accelerating cryomodule. The E-XFEL accelerating cryomodule consists of 8 cavities connected in a string, 2 dipole magnets, one quadrupole magnet, a Beam Position Monitor (BPM) and a set of cooling pipes (see Figure 2.5). The set of 3 magnets is used for the beam position correction and beam compression. Each module is equipped with the sets of pipes, which are used for the cooling of the cryomodule. The energy is applied by the klystrons to the E-XFEL cavities installed in the cryomodules. A single klystron (RF station) supplies 4 cryomodules (32 RF cavities) using an asymmetric power distribution in waveguides [19].
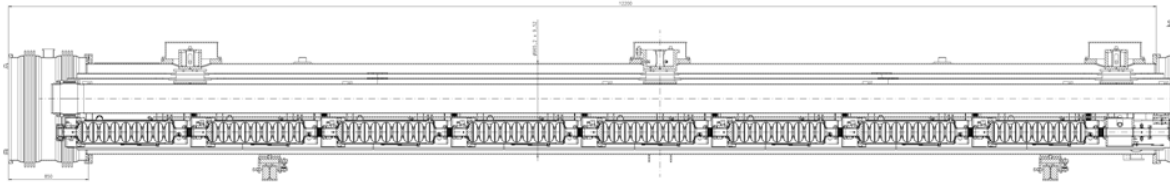

Figure 2.5:   The E-XFEL cryomodule with 8 RF cavities.

2.4   Cavity operation

Before getting into the details of the pulsed mode of the E-XFEL cavity operations, the basic aspects of an RF linear accelerator are briefly discussed:

- acceleration requires that particles arrive bunched in time,

- the cell length (L) in a multicell structure must be related to the RF wavelength (λ) and $\beta = v/c$, which is a particle velocity (v) relative to the speed of light (c): $L = \frac{1}{2}\beta \cdot \lambda$,

The acceleration of a bunched beam can be realized with the use of two methods: with the use of a pulse or Continuous Wave (CW) mode. The pulsed method is used for the E-XFEL. In the pulsed method (see Figure 2.6), the energy is applied to the cavity only during the pulse and the cavity behaviour is divided into 3 phases:

1. During the *filling time*, the EM wave is coupled to the cavity so that the energy in the cavity increases. For E-XFEL, the duration of the filling time is 730 μs.

2. During the *flat-top time*, bunches are accelerated. Up to 2700 bunches are accelerated in the E-XFEL during a single pulse [1]. Due to the fact that the work is performed on each bunch, the energy from the pulse is no more increasing in the cavity. In the simplified description, we assume that it is "flat". For E-XFEL, the duration of the flat-top is 650 μs.

3. During the *decay time*, the energy stored in the cavity is dissipated and the source of the EM wave is off.
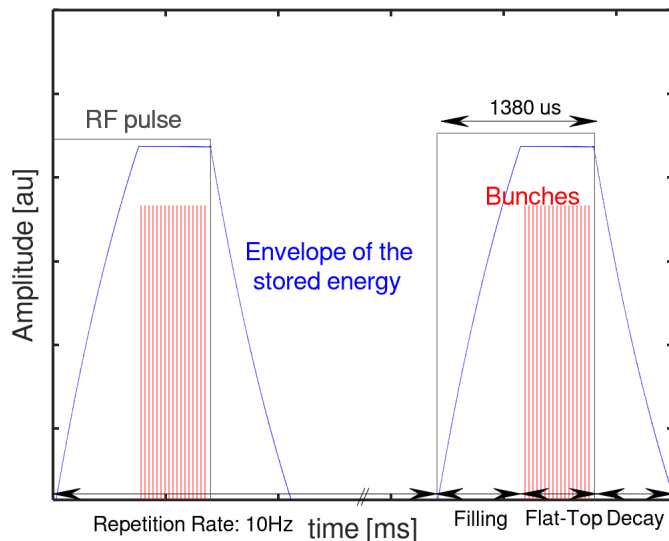
Figure 2.6: Schematic drawing of a pulsed method.

Between pulses no bunch is accelerated. The repetition rate defines how often the cavity is supplied with the EM wave pulse (for the E-XFEL operation was set to 10 Hz). In the Continuous Wave method, the cavities are constantly supplied by the EM wave source and bunched beam is accelerated without the time regime dictated by the RF pulse, but satisfying the requirement of the π mode synchronization with the bunched beam.

For the E-XFEL pulsed method, the duty cycle is 0.65%. For the CW method, the duty cycle may even reach 100%. The pulse method with the use of klystrons (pulsed power amplifiers) was chosen for the E-XFEL cavity operation. It is planned to replace the klystrons with the CW power amplifiers (Inductive Output Tubes) during the upgrade of E-XFEL [20].

2.5 Cavity parameters

2.5.1 Quality factor

The walls of the cavity are not perfectly conducting and the magnetic component of the EM wave causes electric current flow in the walls [10]. These currents cause the energy transfer by the heat dissipation to the surroundings. This is why the accelerating cavity as a resonator is characterized by a dimensionless quantity called the own quality factor (Q_0). One can also find the name "unloaded" or "intrinsic" quality factor [21]:

$$Q_0 = \frac{U\omega_0}{P_c} \tag{2.20}$$

where Q_0 is a parameter characterizing the power dissipation (P_c) through the cavity walls in relation to the energy stored in the cavity (U). It is defined for each cavity mode oscillating with the angular frequency $\omega_0 = 2\pi f_0$ (f_0 is the resonant frequency of a mode). Q_0 is one of the quality factors which are explained in next sections of this chapter. Numerically, the typical own quality factor (Q_0) is of the order of 10^4 for normal-conducting structures and 10^{10} for superconducting cavities. The above and following descriptions are also relevant for the multicell resonators. Thus, in this dissertation, the quality factors and the stored energy describe the 9-cell E-XFEL cavity.

In order to increase the Q_0, an extensive material study aiming at decreasing of heat dissipation caused by current flow in the cavity walls was performed. This is why the Superconducting (SC) materials are used. Superconductivity is a phenomena observed in certain classes of materials and demonstrated among others properties a negligible electrical resistance below a transition temperature [22, 23]. Such temperature together with the maximum current density and maximum magnetic field, form a critical surface, which should not be exceeded to maintain the superconducting state in the material. The quench takes place when the critical surface is exceeded by any of the 3 parameters (temperature, magnetic field, current density) and then the superconductivity is lost, namely the element becomes the normal resistive.

These considerations justify the choice of the material for the E-XFEL cavities. Finally the pure niobium was selected due to its highest critical temperature, the highest critical field and relatively simple production process.

Apart from the negligible power dissipation through the SC cavity walls also less power is needed to achieve the same EM field amplitudes for SC cavities. These two aspects lead to the reduction of the operational costs of the accelerator, especially to the price of high power amplifiers, which constitutes the main contribution to the equipment budget.

However, there are a few limiting factors of the Superconducting Radio Frequency (SRF) technology [6, 10], e.g.:

1. Low accelerating fields - the magnetic field must stay below the critical field of the superconductor (thus max. $|E_{acc}| \sim 30MV/m$); for the normal-conducting structures the fields can be higher (max. $|E_{acc}| \sim 100MV/m$).

2. Field emission - the high electric field can lead to electrons quantum tunnelling out of the cavity wall creating a field emitted current. The emitted electrons absorbs some of the stored energy and may: be synchronized with the RF and further accelerated through the beam line (dark current) or may hit the cavity walls, which is observed by the X-ray radiation (measured by gamma detectors).

3. Costs of a cryogenic installation.

Finally, the choice of the technology depends on the analysis of the project requirements and costs of construction and operation.

2.5.2 Loaded quality factor

The next parameter, which characterizes the cavity with the input coupler is called the external quality factor (Q_{ext}), where P_{ext} is the power leaking from the cavity through the input coupler.

$$Q_{ext} = \frac{U\,\omega_0}{P_{ext}} \tag{2.21}$$

There are also other quality factors, which characterize the power leaking from the cavity through remaining supporting structures (couplers, pickups). Q_{trans} is related with the transmitted power P_{trans} (emerging from the pickup probe). Q_{HOM1} (or Q_{HOM2}) is related with the power P_{HOM1} (or P_{HOM2}) emerging from HOM couplers:

$$Q_{trans} = \frac{U\,\omega_0}{P_{trans}} \tag{2.22}$$

$$Q_{HOM1} = \frac{U\,\omega_0}{P_{HOM1}} \tag{2.23}$$

$$Q_{HOM2} = \frac{U\,\omega_0}{P_{HOM2}} \tag{2.24}$$

The quality factors for pickup (Q_{trans}) and HOMs ($Q_{HOM1}\,and\,Q_{HOM2}$) for the π mode (operating frequency) are higher than the Q_0. As a result the stored energy is not transferred outside of the cavity for the operating mode. In case of the SRF cavities, the Q_{ext} vary between 10^5 and 10^7 [25].

The equation, which combines the quality factors is:

$$\frac{1}{Q_{load}} = \frac{1}{Q_{ext}} + \frac{1}{Q_0} + \frac{1}{Q_{trans}} + \frac{1}{Q_{HOM1}} + \frac{1}{Q_{HOM2}} \tag{2.25}$$

where Q_{load} is the loaded quality factor, which relates the energy stored in the cavity to the power dissipated (P_{load}) via all supporting structures and cavity walls:

$$Q_{load} = \frac{U\omega_0}{P_{load}} \tag{2.26}$$

Q_{load} defines also the time (and the number of the cycles) it takes to dissipate the energy stored in the cavity through the walls and all its structures. Thus the loaded quality factor is obtained from the slope of the stored energy decay (from the *transmitted* power emerging from the pickup probe) in the cavity when the RF source is off (see Figure 2.7):

$$Q_{load} = 2\pi f_0 \tau \tag{2.27}$$

where τ is the decay time.
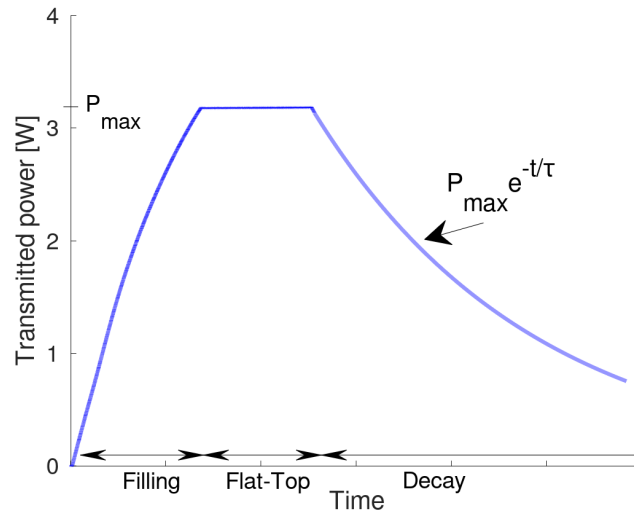
Figure 2.7: Transmitted power emerging from the pickup probe during the RF pulse.

The Q_{load} is also defined in the frequency domain (see Figure 2.8):

$$Q_{load} = \frac{f_0}{f_{3\_2} - f_{3\_1}} \tag{2.28}$$

$f_{3\_2} - f_{3\_1}$ is a width of a resonance curve at a half of the maximum. From equations (2.22) and (2.23) one may see that the decay time and width of the resonance curve are related:

$$f_{3\_2} - f_{3\_1} = \frac{1}{2\pi\tau} \tag{2.29}$$

Figure 2.8: The stored energy measured as a function of the EM wave frequency.

2.5.3 Geometric Shunt Impedance

Another parameter that is characterizing the accelerating voltage and the power dissipation in the cavity walls is the shunt impedance:

$$R = \frac{|V_{acc}|^2}{P_c} \tag{2.30}$$

When the R is divided by the own quality factor Q_0 for a given mode, a geometric shunt impedance (called R over Q) [17, 21] is given:

$$R/Q = \frac{|V_{acc}|^2}{U\,\omega_0} \tag{2.31}$$

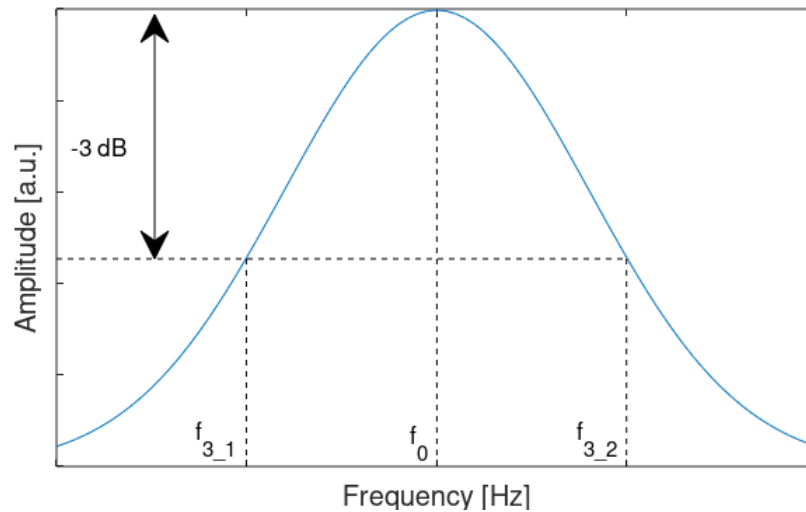The indexation in Q_0 is skipped intentionally. Sometimes other definition of R and R/Q divided by "2" are used. Here, a common linac definition is used [25, 26]. The values of R/Q for modes of E-XFEL were calculated numerically [27]. The geometric shunt impedance is a parameter equal to the ratio of the square of the accelerating voltage to a given stored energy of a cavity mode. R/Q is independent of the power dissipation in the cavity walls (Pc) and it depends on the cavity geometry.

Because the accelerating voltage (V_{acc}) determines the particle's energy change (see equation (2.2)), R/Q defines "how effective is the beam-cavity exchange of the energy" [28]. For the operating mode, the highest R/Q is desired in order to increase the energy transfer to the beam. In case of HOMs, the aim is opposite: to minimize its value. The relativistic beam, which passes the cavity, excites different HOMs, for which the beam is travelling along the E component. The superposition of the excited HOMs creates wakefields. These wakefields are commonly described as parasitic, because these HOMs are responsible for: slowing down of particles within the bunch, have an influence on the following bunches and cause the increase of the power dissipation [8]. The power dissipation increase is an important limiting factor for the superconducting cavities.

One may describe wakefields in the frequency domain [14, 27-28]. In this approach, the current of the periodical bunched beam is described by the infinite number of "sinusoidal beam currents". Thus, the total power induced by the "beams" on the mode is described as follows [28]:

$$P_n = \frac{1}{2}\sum_{k=0}^{\infty} Z_n(\omega_K)\,I_k^2 \tag{2.32}$$

where k is the index of one "sinusoidal beam" with angular frequency ($\omega_k = 2\pi f_k$). $Z_n(\omega_K)$ is a beam impedance defined as:

$$Z_n(\omega_K) = \frac{(R/Q)_n\,Q_{load,n}}{1 + jQ_{load,n}\left(\frac{\omega_k}{\omega_n} - \frac{\omega_n}{\omega_k}\right)} \tag{2.33}$$

The indexation n is added to the $R/Q, Q_{load}$ and ω in order to indicate that values represents the n-th cavity mode. j is the imaginary unit.

In order to decrease the power induced by the beam, the "beam" impedances must be lowered, i.e. one should separate the "sinusoidal beams" and the mode resonance by rearrangement of the time structure of the group of bunches. The second option to decrease the induced power is to adjust cells shapes in order to decrease the R/Q. Furthermore, in order to improve the HOMs energy transfer out of the cavity, the HOM couplers are used. This leads to the decrease in the loaded Q of each mode [6, 10, 26, 28].

2.5.4   Accelerating gradient

When a particle is travelling without significant velocity change on the cavity axis, the average accelerating electric field (E_{acc}) is defined as [21]:

$$E_{acc} = \frac{|V_{acc}|}{d} \tag{2.34}$$

where d is the cavity length. E_{acc} is also called shortly the gradient [9]. E_{acc} is also an important figure of merit, which characterizes the cavity performance. E_{acc} is obtained from the power measurement from the pickup probe. This subject is discussed in details in chapter 3.2.3. The accelerating voltage (V_{acc}) may be calculated from the E_{acc}.

Due to the fact that the electrical length of the E-XFEL 9-cell cavity (d) is 1.038 m, the accelerating voltage and accelerating gradient are used in this dissertation interchangeably. The E-XFEL nominal accelerating gradient is 23.6 MV/m [2].

2.6   SRF E-XFEL cavity - frequency choice

The accelerating cavities are operating in the Radio Frequencies (microwaves). The Radio Frequencies (RF) were chosen because of the experience with the high power amplifiers for the radar purposes, which worked in these frequency ranges and that the size of the cavity is reasonable for the industrial production.

The choice of each RF cavity exact size and operation frequency is a result of the optimization of the project costs and technology restrictions. Due to the fact that the E-XFEL accelerator is a linear machine it indicates that the frequency should be as high as possible to reduce the costs (the length of the accelerating cavity is in the inverse proportion to the frequency). Smaller diameters of the cavities cause technical problems with the cavity's geometry adjustment. Moreover, the wakefields cause the beam spread increase with the square of the frequency in the longitudinal direction and with the cube of the frequency in the transverse direction. Besides, the cavity wall resistance depends strongly ($\approx f^2$) on the microwave frequency [2, 8, 21, 28]. Originally 1-2 GHz [30] was planned in order to have a cavity length between 0.5-1 m. The optimum frequency was 1.5 GHz, but the reason of 1.3 GHz choice was the power amplifiers (klystrons) availability.

In summary, the E-XFEL cavities accelerate the electrons with the use of 1.3 GHz EM standing wave and with π mode of the $TM010$.

2.7 E-XFEL cavities and cryomodules summary

The major parameters of the E-XFEL cavities [2, 31] are listed in Table 2.1.

$Type\,of\,the\,accelerating\,structure$	$Standing\,wave$
$Accelerating\,mode$	$TM010,\,\pi-mode$
$Material$	$Niobium$
$Cavity\,operating\,frequency$	$1.3\,GHz$
$Cavity\,own\,quality\,factor\,Q_0\,for\,\pi\,mode$	$>10^{10}$
$Geometric\,shunt\,impedance\,R/Q\,for\,\pi\,mode$	$1036\,\Omega$
$Q_{ext}\,of\,the\,input\,power\,coupler\,for\,\pi\,mode$	$4.6\,\times\,10^6$
$Q_{ext}\,possible\,changes\,for\,\pi\,mode$	$1.5*10^6\,-\,10^7$
$Number\,of\,HOM\,couplers$	2
$Tuning\,range$	$\sim\,600\,kHz$
$Pulse\,length$	$1380\,\mu s$
$Flat-Top\,time$	$650\,\mu s$
$Repetition\,rate$	$10\,Hz$
$Operating\,temperature$	$2\,K$
$Cavity\,length$	$1.038\,m$
$Nominal\,accelerating\,gradient\,E_{acc}$	$23.6\,MV/m$

Table 2.1: The E-XFEL RF parameters.

The external quality factor varies when one tries to maximize the power coupling between the RF source and the cavity.

Chapter 3

The cavity and the cryomodule measurements

This dissertation focuses on measurements of the E-XFEL cavities installed in the cryomodules (called also cryomodule measurements). However, the single cavities test campaign (before cavity assembly in the cryomodules) is also discussed. The results of the single cavity test campaign are used as a reference data during the cryomodule test campaign.

In this chapter the basic description of the serial-production workflow of the E-XFEL cavities and cryomodules is presented with a focus on the RF measurements of these accelerating components. The RF measurements are split into two groups called low and high power. The low power measurements have been performed with the use of the Vector Network Analyzer (VNA). The frequencies and the loaded quality factors of cavity modes were measured through the external connection of cavity antennae (input power coupler, pickup probe and HOM couplers). The high power measurements have been performed in order to test the own quality factor and the accelerating gradient, for the cavities under the normal working conditions (pulsed operation, in the cryogenic temperatures, but without any beam). During the high power measurements, the cavities were supplied from the RF generators and high power RF amplifiers. The signals from the cavities were monitored with use of the power meters [32].

3.1   E-XFEL cavities and cryomodule production

The serial-production of the E-XFEL accelerating components, namely: the SRF cavities and cryomodules, was done in collaboration with a number of distributed European Technological Facilities and Industry [33, 34]. The production of cavities was carried out by two companies: RI (Germany) and ZANON (Italy) [35]. The RF measurements were performed in Accelerator Module Test Facility (AMTF) in Deutsches Elektronen-Synchrotron (DESY), Hamburg [36]. The layout of AMTF is presented in Figure 3.1 .
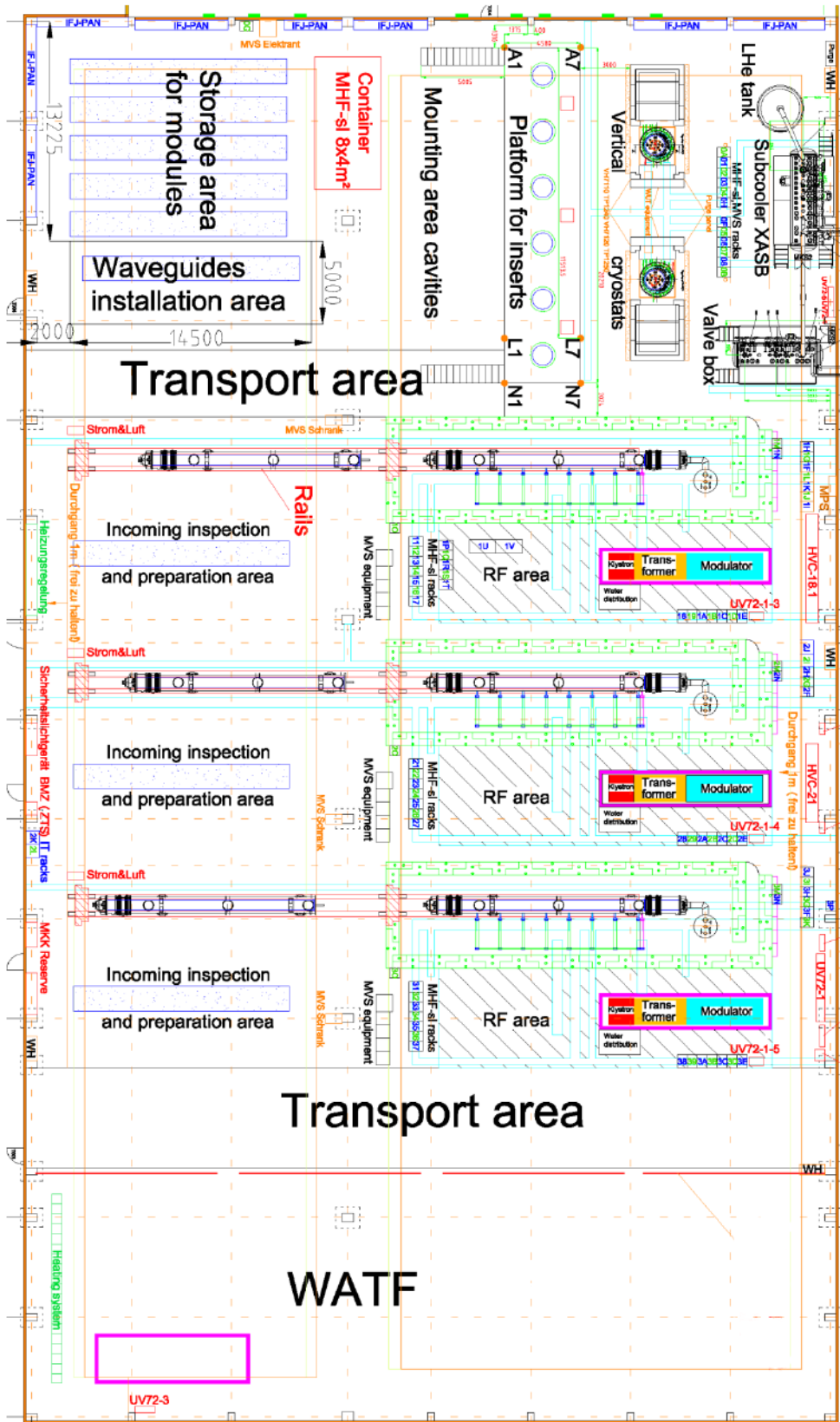
Figure 3.1: The AMTF hall layout [38].

The AMTF infrastructure was equipped with 2 vertical test-benches for qualification testing of SRF cavities. Up to 4 cavities were measured at once in each of the vertical test-bench. After the qualification tests, the cavities were transported to CEA, Paris-Saclay, in order to be assembled in the cryomodule. The cryomodules with the cavities assembled were transported back to DESY. The cavities in the cryomodules were tested again in AMTF in a new configuration, with the use of 3 test-stands for testing of cryomodules.

3.2 The E-XFEL cavities test campaign

Each single cavity was transported from manufacturers to DESY, where in AMTF basic visual incoming inspection was done (see workflow in Figure 3.2). Further, the cavities were mounted on dedicated supports called inserts, where vacuum connections and related preparations at the room temperature were performed. Vacuum connections were tested for the leak-tightness to ensure that the measurements will be done in a predetermined vacuum.

Then, the Fundamental Mode (FM) spectrum was measured and the HOM coupler rejection filters were mechanically tuned. As a result of this tuning, the undesirable extraction of the FM π mode through the HOM couplers is minimized [40, 47].

After these operations, the inserts with mounted cavities were transported to the vertical cryostats, where the cavities were cooled down to 2K. Under the cold conditions the FM spectrum was measured again. Next, the dependence of the own quality factor versus gradient, namely $Q_0 vs E_{acc}$, was measured.

The HOM spectra test finalizes the measurement procedure at 2K in vertical cryostat in the AMTF. Further, the cavities were warmed up and dismounted from the inserts. The FM spectrum was then measured again as an outgoing inspection. Finally, the cavities that fulfilled the $Q_0 vs E_{acc}$ and the HOM spectra test were sent to CEA, Paris-Saclay to be assembled in the cryomodules. Otherwise, the re-treatment at DESY was done and the qualification process was repeated. The treatment means cleaning of the inner surface of the cavity (mechanical or chemical) or/and the cavity exposure to the high temperature (for more information see [35]).

Reception of the cavity

Incoming inspection

Assembly

Preparation of the cavity

FM spectrum measurement and HOM coupler tuning

Cool down

Measurement at 2K (FM spectrum, Q vs E, HOM spectra)

Warm up

Disassembly

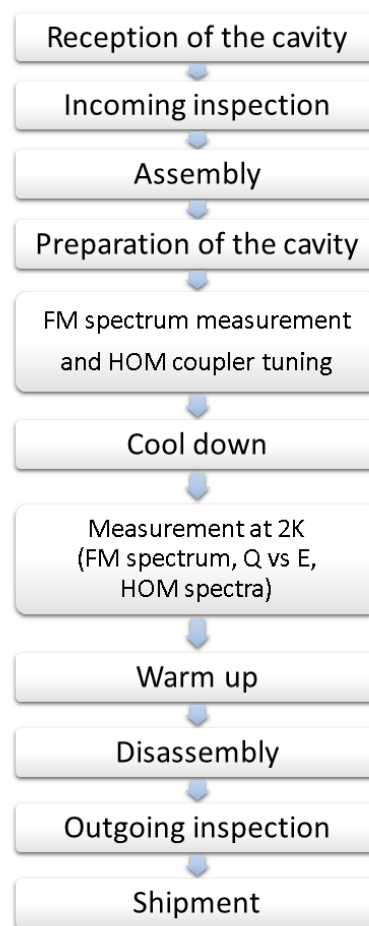Outgoing inspection

Shipment

Figure 3.2: E-XFEL single cavity quality control workflow in AMTF.

3.2.1   Field Flatness tuning and Fundamental Mode spectrum measurement

During the cavity's manufacture, the profile of EM field for the whole 9-cell structure was measured. This profile is a graph showing the amplitude of EM field variations along the beam axis of the cavity. This profile is measured with the use of the perturbation method [21, 37]: the EM field oscillating at the frequency of π mode is perturbed by pulling a small bead (dielectric or metallic) with a non-conducting wire on the beam axis of the RF cavity (see Figure 3.3).
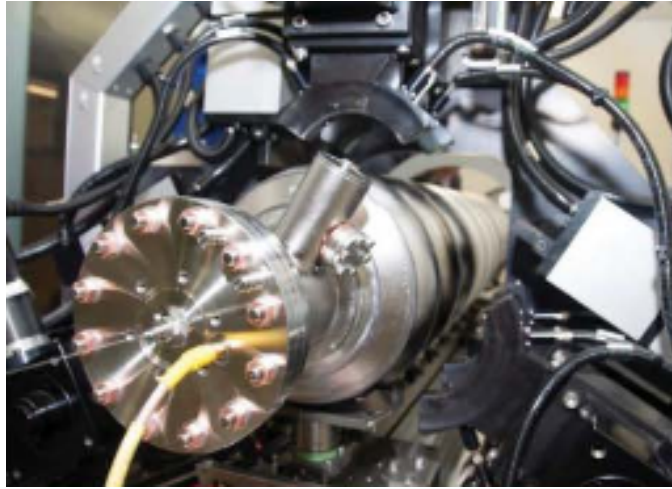

Figure 3.3: A wire for the field profile measurement and the tuning machine for the field flatness tuning (Courtesy W. Singer).

The bead inside of the cavity causes the resonant frequency deviation ($\Delta\omega$). This change of the angular resonant frequency (ω_0) by $\Delta\omega$ is proportional to the square of the E field component on the beam axis (E_z) [39], where B_z component for TM_{010} on the beam axis is zero:

$$\frac{\Delta\omega}{\omega_0} \propto E_z^2 \tag{3.1}$$

Thereby, the distribution of the E_z (beam axis) component of the EM field is obtained by correlating the bead position with the resonant frequency distortion of each of the 9 cells of the accelerating structure. An example of a field profile is shown in Figure 3.4.

The EM field profile measurement is accompanied by the field flatness (FF) tuning of the whole 9-cell structure. FF tuning is an iterative process of each cell's shape adjustment. It is a process aimed at both: setting the π mode frequency to the desired one (for the E-XFEL cavity at the room temperature $\approx 1.29775\,GHz$) and adjustment of the electric field profile of the π mode in the multicell cavity on the beam axis to be equal in each cell (see Figure 3.4) [2, 40]. It stems from the fact that with the cells shape adjustment the resonant frequencies of the whole 9-cell structure change as well.
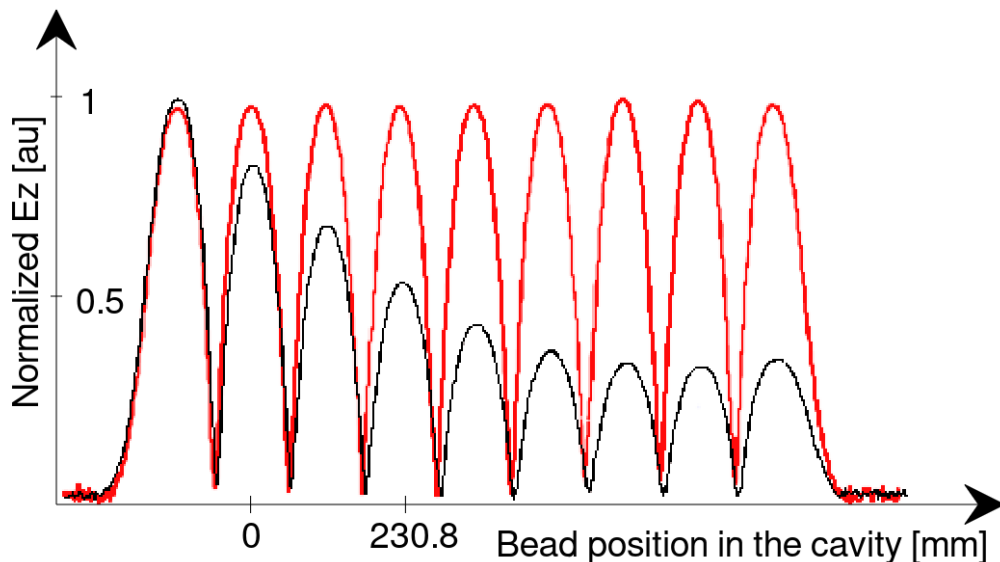
Figure 3.4: Normalized electric field component on the beam axis measured as a function of the bead position in the cavity, measured for the π mode: before (black) and after (red) the field flatness tuning.

The tuning of the π mode frequency to the value of 1.29775 GHz at room temperature results from the observation that after cool-down the π mode frequency shifts to about 1.2997 GHz and then the final fine adjustment to the 1.3 GHz will be easily completed by step motors, equipment added to cavities at the cryomodule assembly.

The FF tuning is performed by pushing and stretching of each individual cell of the cavity by the tuning machine (see Figure 3.3). The tuning result reflects in the Field Flatness parameter. The FF corresponds to the electric field profile at the π mode frequency on the beam axis and is defined in three ways [39-42]. In this thesis the FF equals to the ratio of minimum to the maximum amplitude in the profile in percent ($|E_{min}/E_{max}|*100\%$). The flat profile of the electric component maximizes the accelerating voltage in the multicell cavity, so the energy transmitted to the beam (during accelerator operation) would be the highest possible one.

To continue the subject, the measurements of a set of resonant frequencies (modes) characteristic of the n-coupled structure of the n-cell accelerating cavities forming so called the "Fundamental Mode (FM) spectrum" is described. The FM spectrum measurements are done also during the previously described EM field profile measurement and FF tuning, but they are also routinely repeated at various stages of the cavities and cryomodules tests. The RF waves are delivered to the cavity through the input power coupler and stored energy is monitored through the pickup probe with the use of the Vector Network Analyzer (VNA). The VNA is a particularly useful device and contains both its own source of the RF signal and multiple receivers. It can measure not only the amplitude but also the phase of the received signal. The RF results are described using i.a. so called the S (Scattering) parameters [10]. The S parameters are the ratios of incident to reflected or

to transmitted voltages. S-parameter is described as S_{ij}: "incident at port j and detected at port i". Reflection is when i = j. Here, the S parameters are presented on the VNA in terms of *power gain (or loss)* ratios [44, 45]. The power gain (loss) is shown in the frequency domain, which simplifies understanding of the behaviour of RF devices.
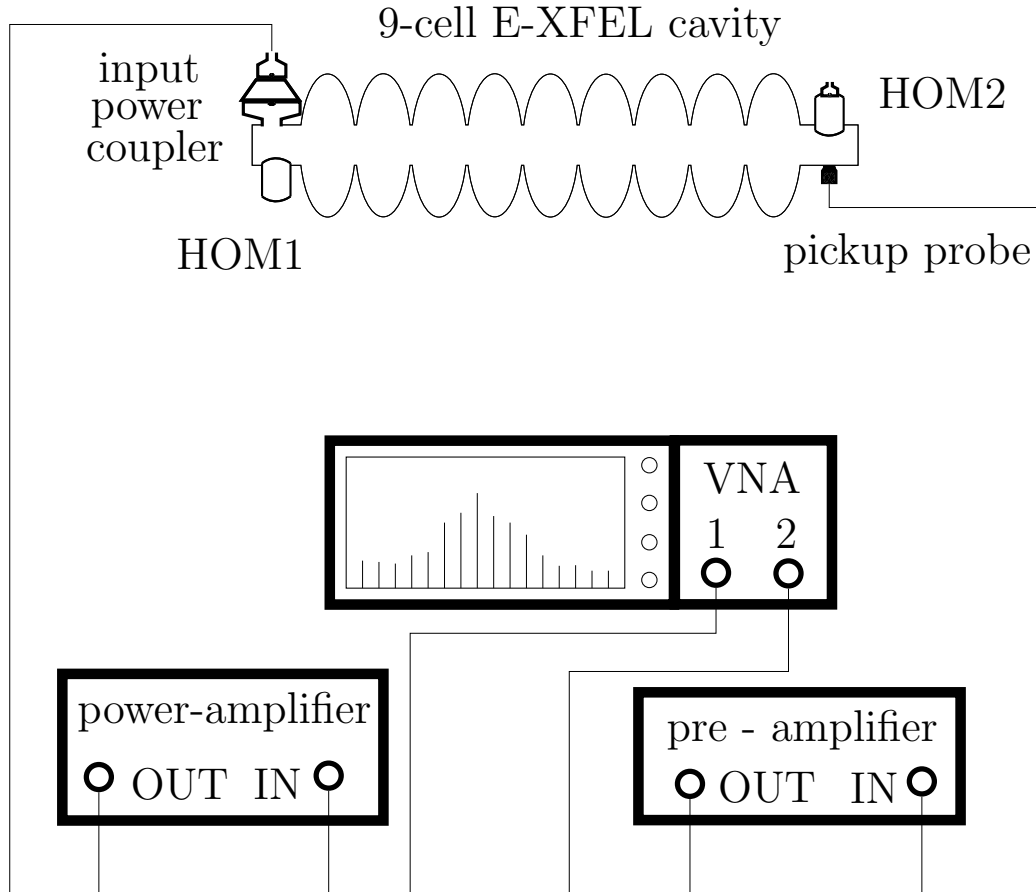

Figure 3.5: Test setup for the FM spectrum measurement.

The Fundamental Mode spectrum is measured by S_{21}. The S_{21} is a forward transmission coefficient from port 1 to port 2. In order to measure the resonant frequencies of the π mode and other modes of the E-XFEL cavity, the S_{21} is measured as a ratio of applied RF stimulus of the input coupler to the power emerging from the pickup (see Figure 3.5). In selected cases the RF amplifiers (power or/and pre-amplifier) are added in order to compensate the attenuation in the tested cavity, antennae and cables [46].

In the Figure 3.6 a typical response of the E-XFEL cavity to the RF stimulus in the range of 1.27 - 1.30 GHz provided by the VNA is presented. The modes π, $8\pi/9$, ... , $\pi/9$ of the Fundamental Mode correspond to the 9 maxima in the plot (for details see: Section 2.2 Multicell cavity structure). The π mode is the resonance with the highest frequency in the TM_{010}, while $\pi/9$ is the lowest one. To perform the field profile measurement, one place the marker on the VNA screen on the peak corresponding to the π mode (e.g. Marker 2 in Figure 3.6), follow its frequency change (it is one of the VNA functionalities), and finally correlate the frequency deviation with the bead position in the cavity [21].
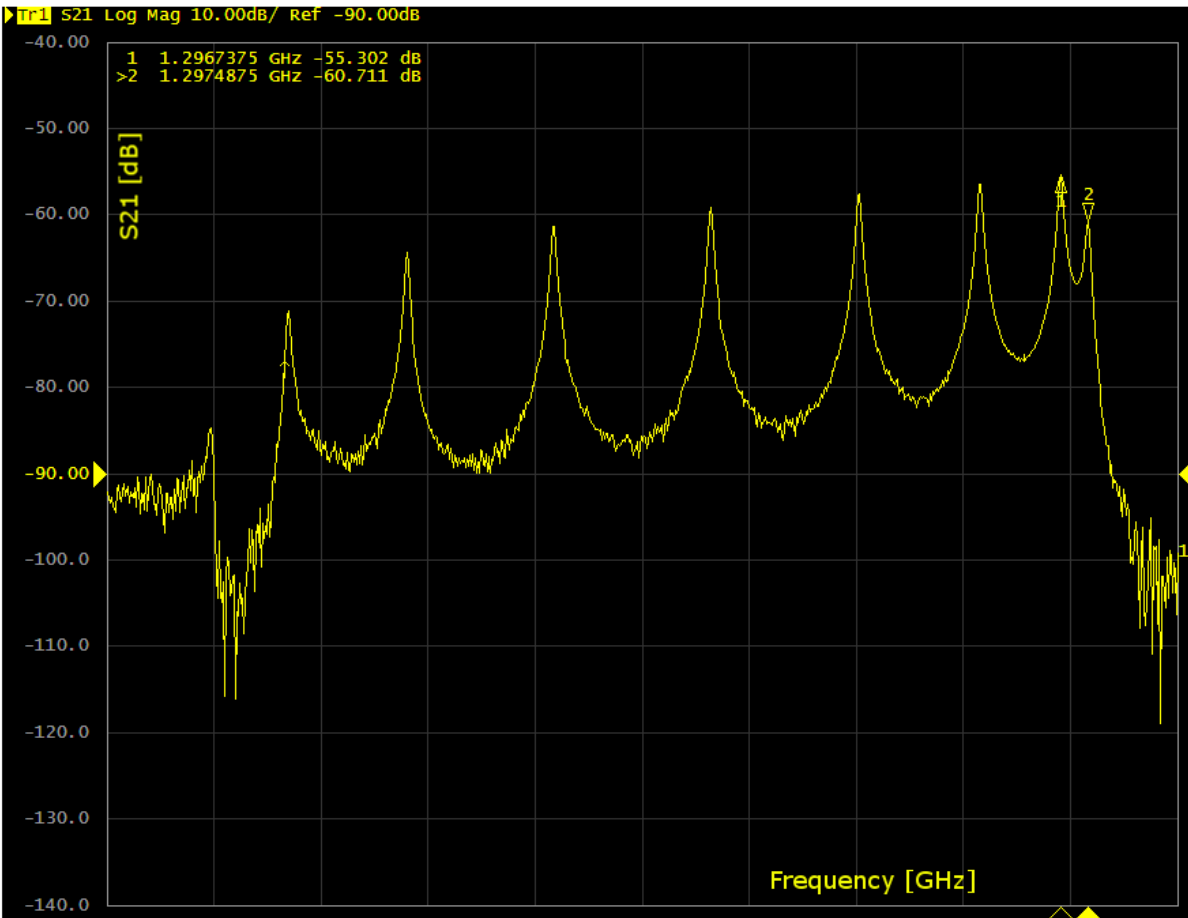

Figure 3.6: Typical FM spectrum at the room temperature in VNA.

After the field profile measurement and the FF tuning, the frequencies of the FM were recorded, with the use of the VNA test setup. The first FM spectrum measurement, just after the Field Flatness tuning is the special one. The frequencies recorded during this measurement were stored to the database and are used as the reference for each of following FM measurements - especially for the test of cavities assembled in the cryomodules. The recorded frequencies are characterizing parameters of each single cavity.

It was demonstrated by the experiment done at DESY that the validation of the FF is possible at any time by comparing the actual FM spectrum measurement to those values stored just after the FF tuning (reference frequencies) [40, 41]. During the DESY experiment, each individual cell of the cavity was deformed, while changes of the field flatness for the π mode and the changes of frequencies within Fundamental Mode were recorded and correlated.

Thereby, the measurement of the FM frequencies was used to determine the FF for cases when it is not possible to access the interior of the cavity to perform the field profile measurement with bead pulling, i.e. during the cryomodule measurements in AMTF. The cavity antennae were accessible always by external connectors, so the measurement with the VNA was possible (also later during the cryomodule qualification tests). Therefore, the FM spectrum measurements were repeated several times, when required, in order to assure that no accidental activity influenced the field profile by changing of the cavity geometry. In consequence, the Fundamental Mode frequencies express the stability of the multi-cell structure in the long production process.

3.2.2   Successive Fundamental Mode spectrum measurement

Here we present the method of the FF stability estimation by comparison of two FM spectra measurements. This method is based on the above described experimental observation that the stability of the FF is related to the stability of the FM spectrum [40]. So, every time we need to check the FF we measure frequencies of the FM spectrum (denoted in following formulae as f_i^{mes}) and compare them with the reference spectrum recorded for each cavity in the database. Technically, we construct the relative spectrum calculated with the following formula:

$$R_i = \frac{f_i^{ref}}{f_i^{mes}} - \frac{f_N^{ref}}{f_N^{mes}} \tag{3.2}$$

where f_i^{ref} is i reference frequency recalled from the database. This frequency was measured and recorded during the FF tuning. f_i^{mes} is i frequency for $i\pi/N$ mode measured during the test, where $i \in\, <1, N>$ and N is the number of cells in a cavity (for E-XFEL N=9).

It is assumed that R_i is linear with respect to i. The linear regression line is shown in the Figure 3.7, for which one calculates the Mean Square Error (MSE):

$$MSE = \frac{1}{N} \sum_{i=1}^{N} (R_i - L_i)^2 \tag{3.3}$$

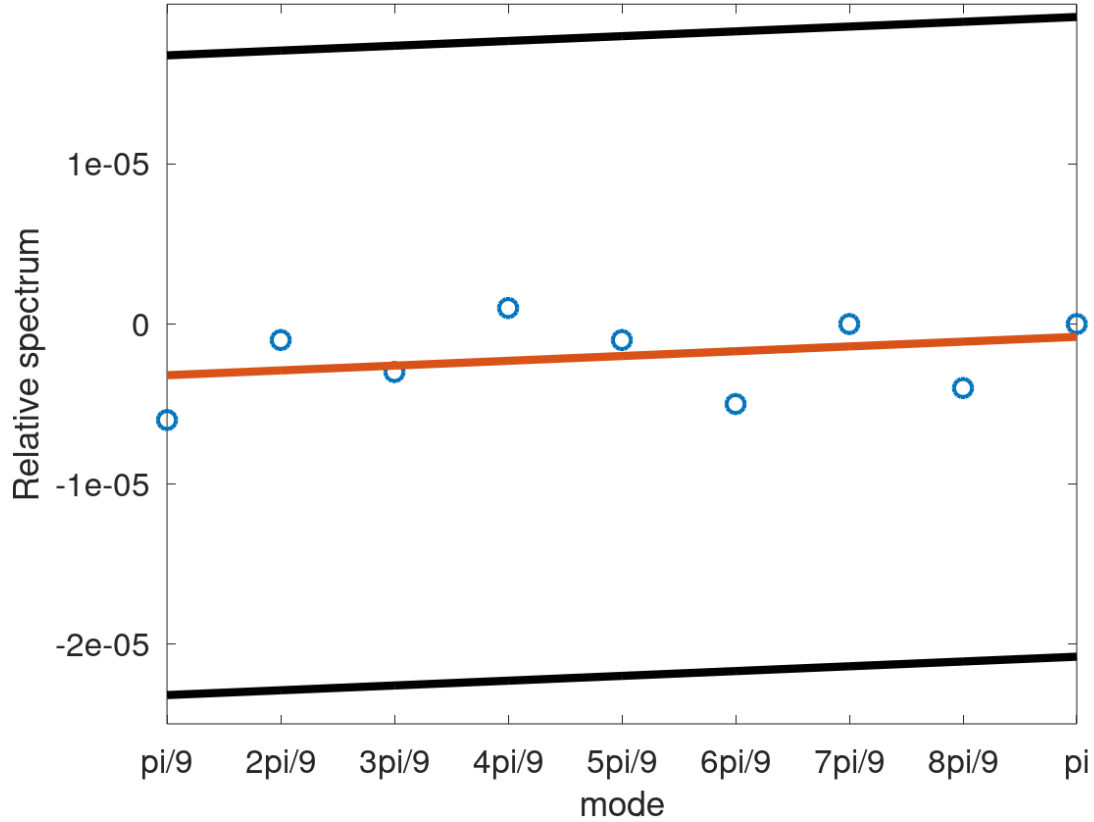where L_i are points from the fitted line.

Figure 3.7: Relative spectrum for a single E-XFEL cavity measurement for each mode (blue circles) and its linear approximation (red). The acceptance criteria is marked by the 2 black lines.

Finally, the estimation of the Field Flatness is given by the Mean Spectrum Frequency Deviation (MSFD) [40, 47], which was specified by the MSE for the E-XFEL operating frequency:

$$MSFD = 1.3 \ GHz * \sqrt{MSE} \tag{3.4}$$

The acceptance criteria was:

$$MSFD < 10 \ kHz \tag{3.5}$$

for which the FF was better than 90% [40, 46]. The correlation between MSFD and the FF were proven experimentally at DESY [41], as mentioned above.
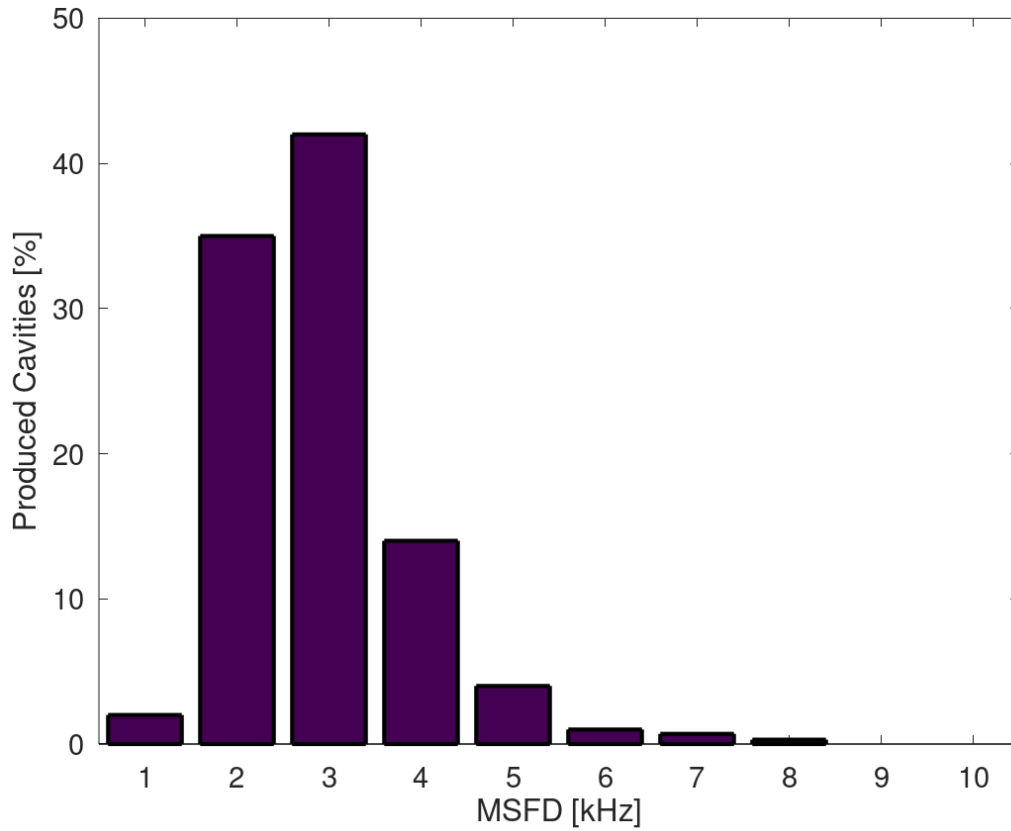
Figure 3.8: The Mean Spectrum Frequency Deviation [MSFD] for the E-XFEL cavities [48].

In Figure 3.8 the distribution of the Mean Spectrum Frequency Deviation shows that all of the E-XFEL cavities fulfilled the acceptance criteria [48].

3.2.3 $Q_0 vs E_{acc}$ measurement

The $Q_0 vs E_{acc}$ is the main measurement performed in order to characterize the single SRF cavity at 2K and to determine the cavity limitations and behaviour [50]. From the Q_0 the heat dissipation through the cavity walls is calculated. The E_{acc} represents the energy that is stored in the cavity without the quench.

In order to discuss the subject of the measurement procedure, some basic nomenclature, which will be used in this section, is described below. The RF power flowing into the cavity through the input coupler is called *forward power* (P_{for}). The power returning from the input coupler is named *reflected power* (P_{refl}) and the power emerging from the pickup probe is called *transmitted power* (P_{trans}). The power emerging from the HOM coupler are named after the HOM couplers (P_{HOM1} and P_{HOM2}). These names are also shown in Figure 3.9, where the test setup is presented.
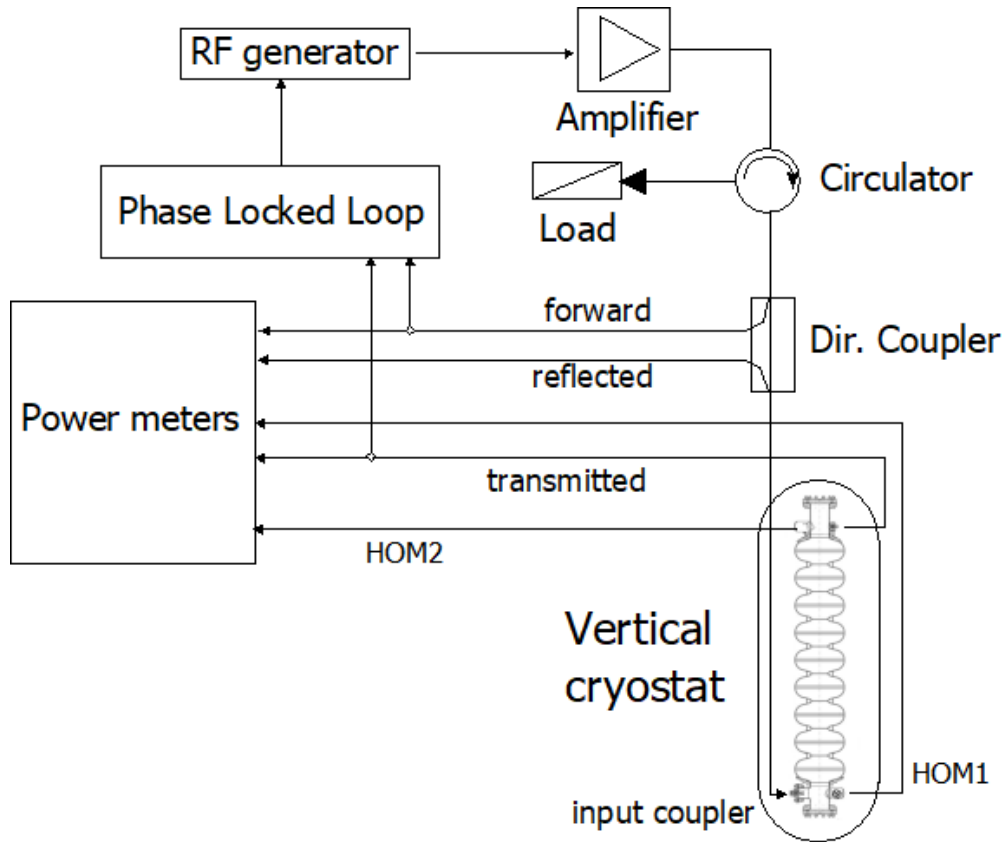

Figure 3.9: The $Q_0 vs E_{acc}$ measurement test setup.

During the $Q_0 vs E_{acc}$ measurement the cavity is powered through the input coupler - with the use of the RF signal generator and the high power amplifier. The reflected signal is transferred across the circulator to the load, where the RF reflected energy is dissipated. The RF circulator is a three-port device used to control the direction of RF wave flow, so that the reflected wave does not damage the RF amplifier. A small amount of the RF power is also coupled through the directional coupler in order to monitor the *forward* and *reflected* power with the use of the power meters.

The cavity behaviour is analysed with the use of the *transmitted* signals: the power or the voltage emerging from the pickup probe. The transmitted voltage (V_{acc}) in time domain is represented by the slow varying amplitude ($V_{ampl}(t)$) and slow varying phase difference ($\psi(t)$) between the transmitted voltage and the voltage from the generator. It is defined as:

$$V_{acc}(t) = V_{ampl}(t) \, cos(\omega_0 + \psi(t)) \tag{3.6}$$

where $\omega_0 = 2\pi f_0$, f_0 is the *input* (RF generator) frequency ($\approx 1.3 GHz$).

The *transmitted* voltage is measured with some analog-to-digital converters and *transmitted* power is measured with the use of the calibrated power meters. Thereby, the calibration of the voltage is possible ($V_{ampl}^2 \propto P_{trans}$). In the same way the relation between the voltage and power of the *forward* and the *reflected* signals is described.

The $Q_0 vs E_{acc}$ measurement procedure starts from the search of the resonant frequency of the π mode. The search starts from the frequency recorded during the FM spectrum measurement at 2K. The frequency search is performed within 1 kHz, which is the accuracy of the FM spectrum measurement. The 10 second RF pulses are applied with a constant power and different frequency to the cavity, while the response on the *transmitted* power is measured. The frequency, for which the highest *transmitted* power was measured, is set in the RF generator. Next, the cavity's resonant frequency is kept stable with the use of the Phase Locked Loop (PLL) system, keeping the transmitted and forward voltages phase difference in lock step [49].

The $Q_0 vs E_{acc}$ measurement is the *high power test* of the single cavity. During the $Q_0 vs E_{acc}$ measurement, the *forward* power pulse is applied to the cavity and is ramped (up to 200W). At each *forward* power step the Q_0 and the E_{acc} are calculated by analysing and measuring signals: the signal transferred to the input power coupler, the signal reflected from the input power coupler and the signal transmitted through the pickup probe [49-50].

The calculations for each point starts with the calculation of the coupling strength (β_{ext}) of the input coupler to the cavity, defined as:

$$\beta_{ext} = \frac{Q_0}{Q_{ext}} = \frac{P_{ext}}{P_c} = \frac{P_{ext}}{P_{for} - P_{refl} - P_{trans}} \tag{3.7}$$

where P_c is the power dissipated through the cavity walls and P_{ext} is the power leaking through the input coupler.

The coupling strength may be calculated in 3 different ways [17, 21]. In this work, one method was chosen, in which the characteristic points (see Figure 3.10) of the reflected signal are measured and then used to calculate β_{ext}^*. The β_{ext}^* is a coupling strength, where losses of the transmitted power are not taken into account:

$$\beta_{ext}^* = \frac{P_e}{P_i - P_r} \tag{3.8}$$

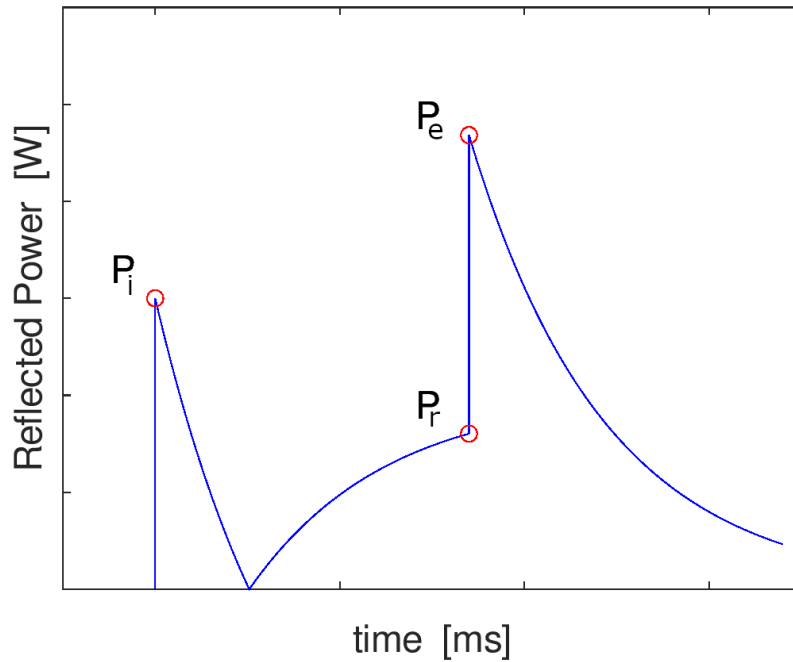Figure 3.10: The reflected power with marked values used to calculate β_{ext}^*.

The P_e, P_i and P_r are the characteristic values of the *reflected* power at the beginning and end of the *forward* power pulse (see Figures 3.10 and 3.11). The β_{ext} is then calculated with use of β_{ext}^*:

$$\beta_{ext} = \beta_{ext}^*(1 + \frac{P_{trans}}{P_c}) \tag{3.9}$$

For the E-XFEL cavities $\frac{P_{trans}}{P_c} < 9\%$. For nominal E-XFEL gradient P_{trans} is $\approx 3.7W$. P_{trans} and P_c corresponds here to their values just before the RF pulse is turned off.
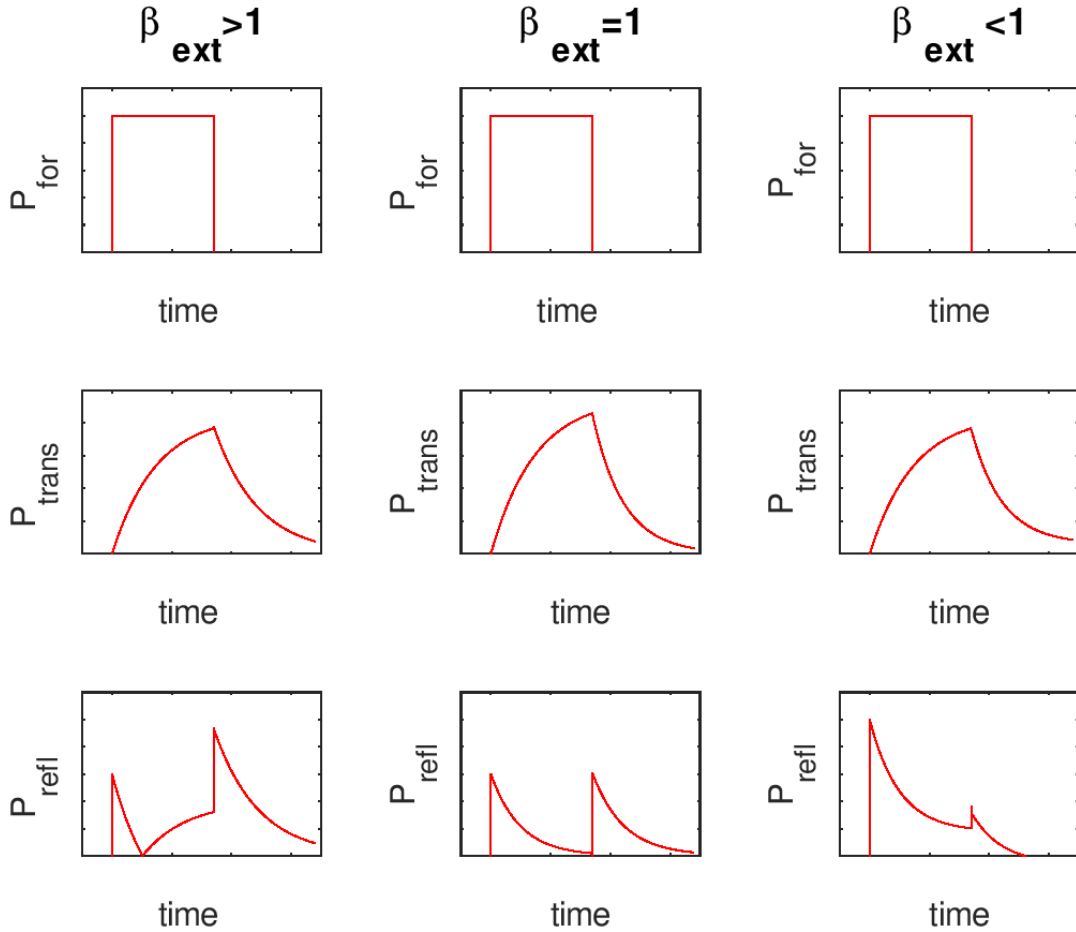
Figure 3.11: Rectangular forward power (P_{for}) and the dependence of the reflected power (P_{refl}) on the β_{ext}. The transmitted power (P_{trans}) is presented as well.

In general, there are 3 different shapes of the *reflected* power signal. This shape depends on the coupling strength (β_{ext}). The pulsed rectangular *forward* power signal is required to calculate β_{ext}.

During the $Q_0 vs. E_{acc}$ measurement, with the successive *forward* power steps, β_{ext} decreases from 2-5 to the values below 0.3. The $\beta_{ext} = 1$, called the critical coupling, minimizes the reflections and it minimizes the measurement error of powers. As a consequence, the measurement error ranges are $\frac{\Delta E_{acc}}{E_{acc}} = 5 \div 10\%$ and $\frac{\Delta Q_0}{Q_0} = 10 \div 20\%$ [17, 50, 52].

After the β_{ext} calculation, the loaded quality factor is obtained from the exponential drop of the *transmitted* power (see equation (2.27)). The power dissipated in the cavity walls (P_c), Q_0 and E_{acc} are calculated as following [51]:

$$P_c = \frac{4\,\beta_{ext}^*\,P_{for}}{(1+\beta_{ext}^*)^2} - P_{trans} \tag{3.10}$$

$$Q_0 = Q_{load}(1 + \beta_{ext}^*\,(1 + \frac{P_{trans}}{P_c}) + \frac{P_{trans}}{P_c}) \tag{3.11}$$

$$E_{acc} = \frac{\sqrt{R/Q\,P_c\,Q_0}}{L} \tag{3.12}$$

where L is the 9-cell cavity length and R/Q is the geometric shunt impedance.

After obtaining the first point on the Q_0 and E_{acc} dependence, the further calculations are performed with the help of the proportional factor, called K_T. This factor allows to calculate further points for the $Q_0 vs E_{acc}$ dependence regardless of the losses in the input power coupler and regardless of the coupling. K_T is calculated from the power emerging from the pickup probe (*transmitted* power):

$$K_T = \frac{E_{acc}}{\sqrt{P_{trans}}} \tag{3.13}$$

K_T for the E-XFEL cavities is in the range of $1.38 * 10^7 \div 2.17 * 10^7 \frac{MV/m}{\sqrt{W}}$. The factor K_T, determined during the cavity test campaign, becomes an another important parameter of each cavity. It is recorded for the future cryomodule test campaign, described in section 3.3.4.

In the following power steps, the E_{acc} is calculated with use of the equation (3.13) from the *transmitted* power and with the use of the previously calculated K_T. Q_0 is obtained from the equation 3.12 as:

$$Q_0 = \frac{(E_{acc}\,L)^2}{R/Q\,P_c} \tag{3.14}$$

where P_c is calculated with the use of equation 3.10. For each power step, the values of: Q_0, K_T, powers, gradient and power plots were stored in the database.

This procedure is repeated in a loop until reaching the cavity or the infrastructure limit. The AMTF infrastructure is mainly limited by the maximum *forward* power, namely by the power amplifier. The maximum accelerating gradient of tested cavities was limited by: the cavity quench, the high field emission, the forward power limit or the HOM coupler.

Number of forward power steps allowed to draw the $Q_0 vs E_{acc}$ curve, which was used as a tool for detection of cavity imperfections. An example of the $Q_0 vs E_{acc}$ curve for a single E-XFEL cavity in presented in Figure 3.12. Ideally, the Q_0 should be constant for each E_{acc} until the cavity quenches. Some drop of Q_0 for increasing gradient is always observed due to the Field Emission. The multipacting for the E-XFEL cavities was observed in the range 18-22 MV/m causing strong Q_0 drop e.g. below 10^{10}. The multipacting was conditioned by applying the RF pulses to the cavity for $10 - 30$ minutes. After the conditioning Q_0 went back the value corresponding to the $Q_0 vs E_{acc}$ curve.
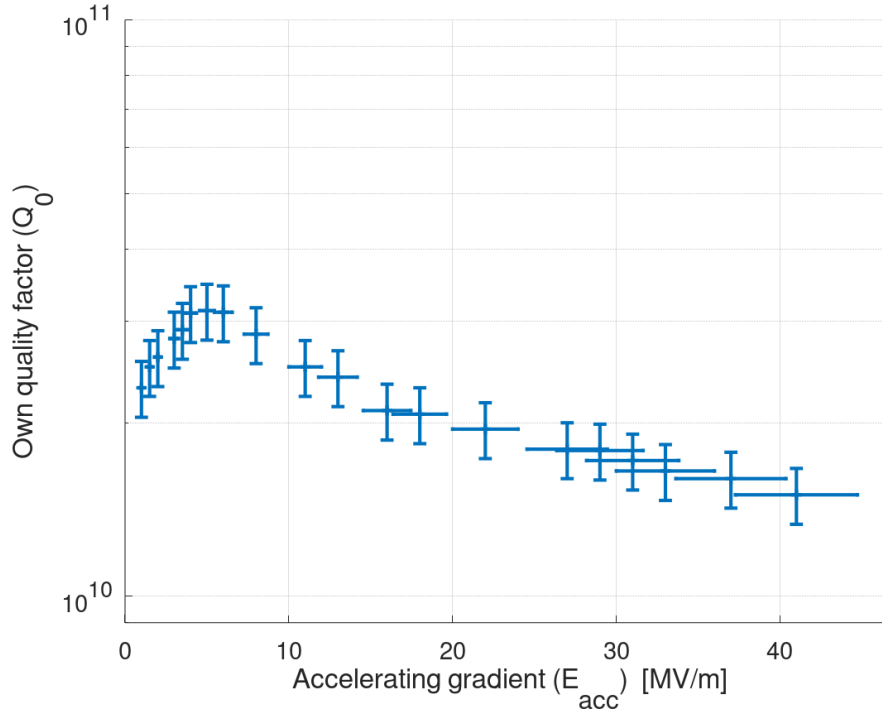

Figure 3.12: An example $Q_0 vs E_{acc}$ curve stored for a single E-XFEL cavity.

Finally, when the whole $Q_0 vs E_{acc}$ curve was drawn, the usable gradient was determined. The usable gradient was the greatest gradient for which $Q_0 > 10^{10}$ and for which the X-ray threshold (indication of the field emission) was not exceeded at any of the detectors. The measurement of the X-ray was done at the top and bottom of the cavity. The thresholds were $0.01 \, mGy/min$ and $0.12 \, mGy/min$ respectively. The cavities that did not fulfil the usable gradient ($E_{acc} < 20 \, MV/m$) were treated at DESY and measured again [21, 35, 50]. Thus, 1241 qualification tests for 800 cavities were performed.

3.2.4 The Higher Order Modes spectra measurement

The aim of the HOM spectra measurement was to determine the loaded quality factors and the frequencies of: the first two groups of dipole modes (TE_{111} and TM_{110}) and the second group of monopole modes (TM_{011}). The test setup for the HOM spectra measurement is presented in Figure 3.13. The Q_{load_HOM} was calculated from the resonance curve in the frequency domain with use of the equation (2.28). The indexation HOM is added to the Q_{load} in order to indicate that the results of the measurement represents the frequency of the HOM mode and to indicate that the measurement is performed throughout the HOM couplers.

After the HOM spectra measurement, it was checked that parasitic modes will be effectively dumped and wakefield excitation will be limited in the future while the accelerator is running [54]. The monopole mode (TM011) causes the growth of thermal losses [56-57]. The TE111 and TM110 dipole modes cause the emittance growth, especially when the beam is not centred to the axis of the cavity.

The indication of effective dumping of HOM is the low Q_{load_HOM}, which is a result of the optimized HOM energy extraction with the use of HOM couplers. The better coupling though the HOM coupler is provided through the increase of amplitudes of HOMs in the end cells and decreased inside of the cavity. The opposite decomposition of amplitudes is called the HOM trapping. Thus, end-half-cells dimensions are different than the inner-half-cells. This is why, sometimes, in order to lower the loaded quality factors of HOMs, an additional cells adjustment was done during the FF tuning [55]. Despite this asymmetry, the Field Flatness quality for the π mode is still kept.
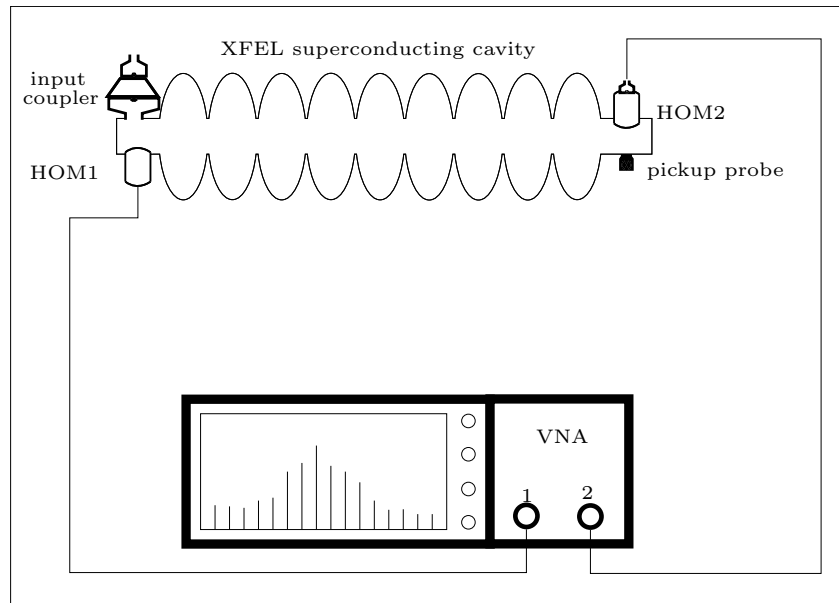

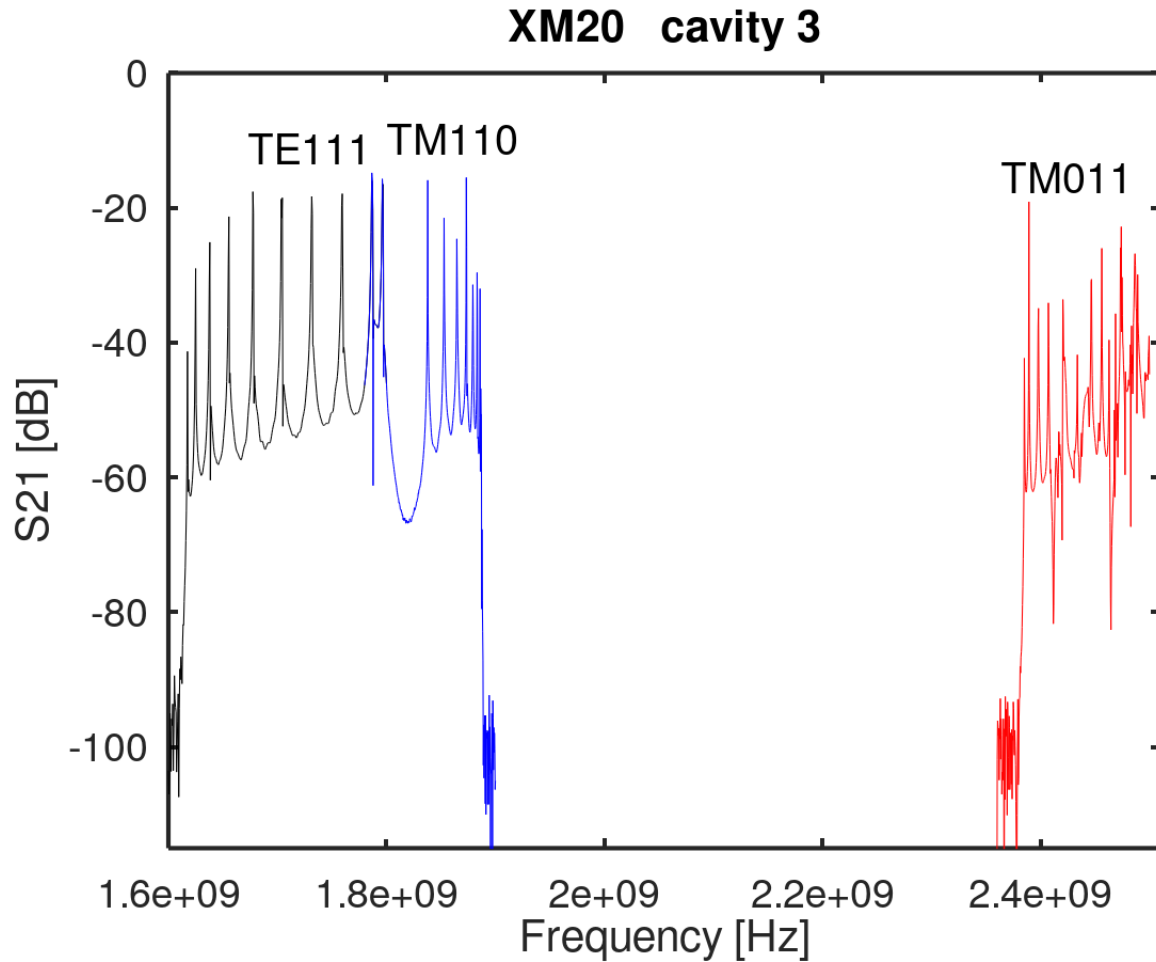Figure 3.13: The test setup for the HOM spectra measurement.

Figure 3.14: Measured HOMs view in a VNA band 1.60-2.55 GHz for the test setup presented in Figure 3.13.

The three mentioned group of modes are plotted in Figure 3.14. For group of the monopole modes, nine frequencies and nine Q_{load_HOM} were measured. For groups of dipole modes, 9 pairs (18 freq. and 18 Q_{load_HOM}) were measured, because each dipole mode is represented by two close (difference less than 1 MHz) resonances. Due to the manufacturing process inaccuracy the cavities are not ideally symmetric around the beam axis. Inside of the asymmetric cavity the excited dipole modes are split into two components representing a single HOM [59].

The HOMs with the higher frequencies, i.e. above so called cut off frequency of the beam pipe (see Chapter 2.3), were not measured [56]. Beam pipe size defines the cut off frequency of the travelling modes. In E-XFEL, the suppression of travelling wave HOMs is mainly provided by the HOM dumpers (absorbers) connected to the beam pipes between the cryomodules in the accelerator tunnel [2].

During the operation of accelerator, when the particles moving practically with the speed of light, the modes synchronized with the beam are essential for the beam-HOM interaction. A synchronous condition with a relativistic particle is presented with a black solid line on the Brillouin diagram in Figure 3.15. The Brillouin diagram is a dispersion relation of the resonance frequencies of RF cavity modes (in multicell resonant RF cavities) over phase advance of the electric field on the beam axis in the cavity (see Figure 3.15). Only resonances, which have the frequencies closest to intersections of mode dispersion lines with the black line are important for the beam-HOM interaction. These modes were chosen to be validated during the measurements [27]. For these modes the maximum possible loaded quality factor was studied and simulated (for example by Baboli [56]) showing that neither the beam is deflected, nor emittance grows [55].
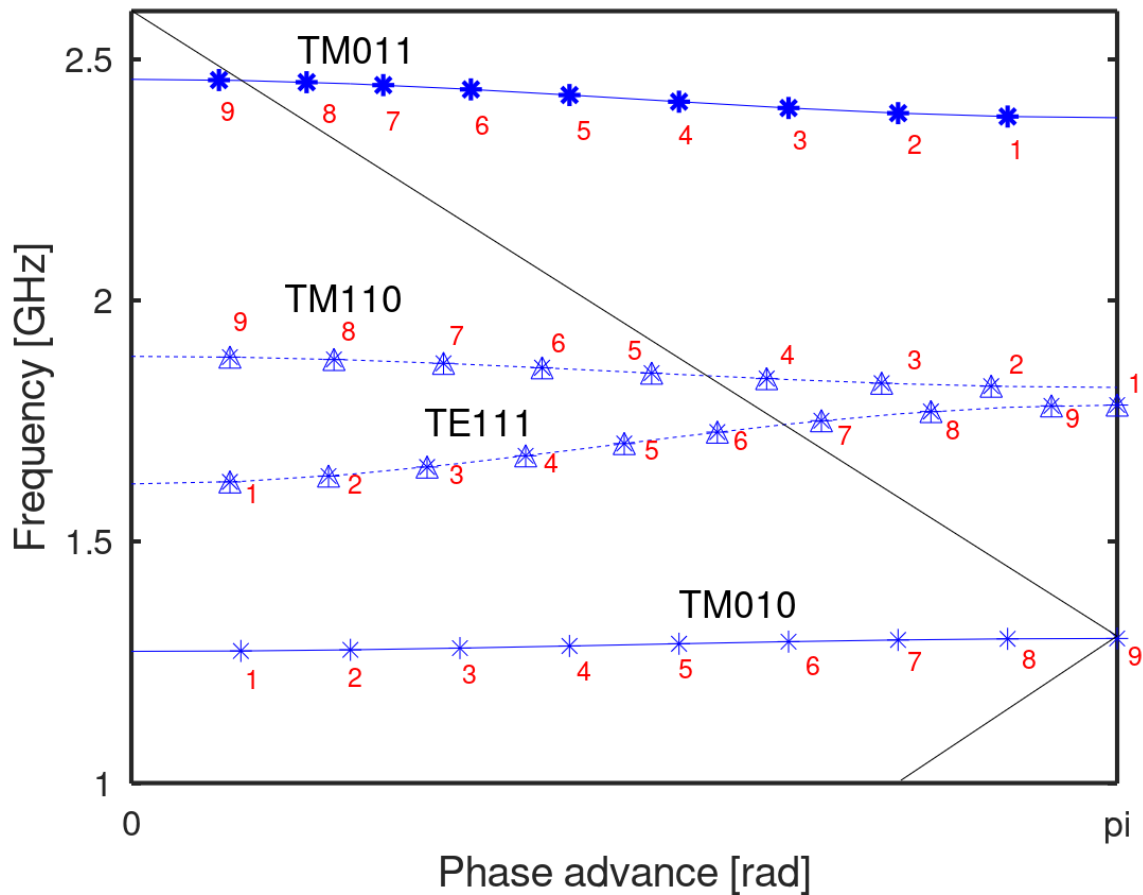

Figure 3.15: Dispersion curves for measured HOMs (solid blue lines are monopole modes, dashed blue lines are dipole modes). FM (TM_{010}) is presented as well. A synchronous condition with a relativistic beam is presented with a black line. Measured resonances are numbered (red) and marked with $\triangle$ and $*$.

The maximum $Q_{load\_HOM} < 2 * 10^5$ for the following resonances was defined:

- TE_{111} - resonance 6 and 7

- TM_{110} - resonance 4 and 5

- TM_{011} - resonance 9

The resonances were numbered from the modes with the smallest frequencies to these with the highest (see red numbers in Figure 3.15). In order to check the dispersion relation (frequencies), other resonances in the HOMs were measured as well. In Figure 3.16 an example is presented for the cavity 3 in the cryomodule XM35.
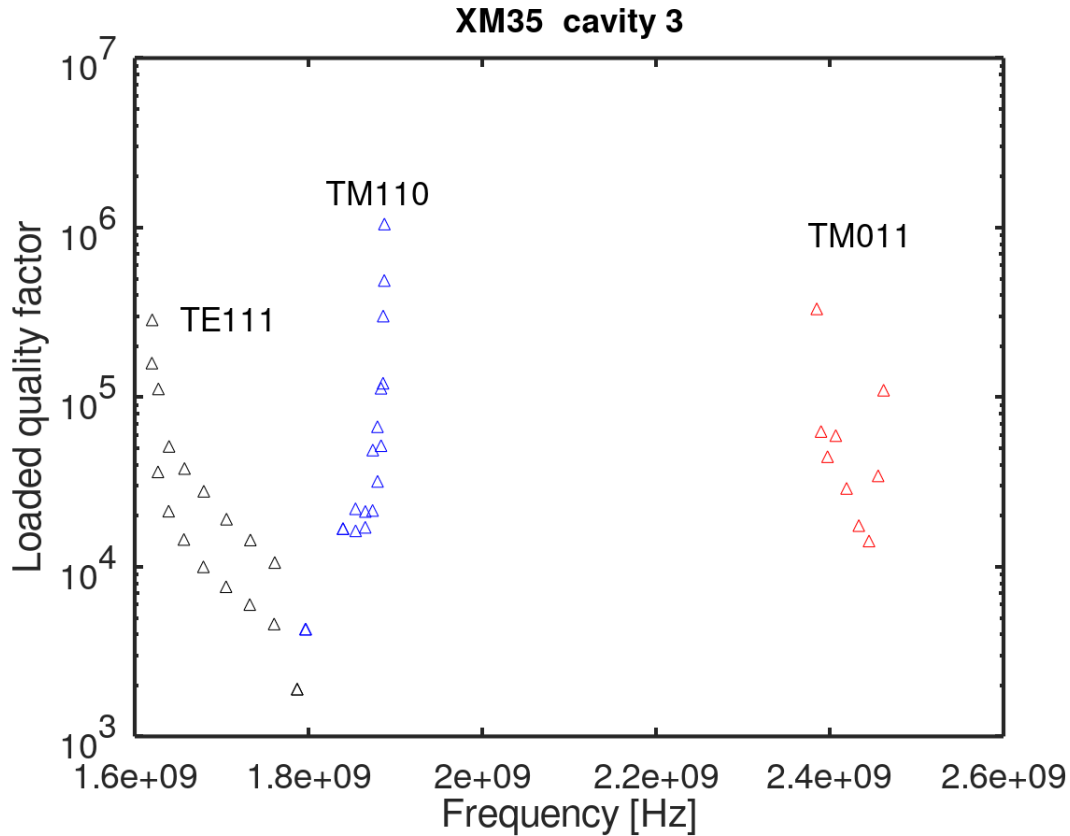

Figure 3.16: Values of the loaded Quality factors for HOMs measured with the use of the test setup presented in Figure 3.13.

Finally, the cavities that did not fulfil the acceptance criteria were tuned at DESY and measured again. Otherwise, the cavities were accepted to be assembled in the cryomodule.

3.3   The E-XFEL cryomodule test campaign

The assembly of the E-XFEL cryomodules was performed in CEA, Paris-Saclay. The 8 E-XFEL cavities with magnets package were connected under clean room conditions. The cavities were equipped with movable input power couplers, which enable to power them with the short ($\sim 1.4ms$) and high power ($\sim 250kW$) RF pulses. Each cavity was also equipped with step motor and piezos.

Next, the string of 8 cavities and magnets package was inserted into vacuum vessel, which was equipped into thermal radiation shields and internal connections for helium supply. The whole system is called cryomodule. Finally, the cryomodule was transported to DESY.

After arrival of the cryomodule to AMTF, first, the visual incoming inspection was performed (see Figure 3.17). Then, the FM spectrum at 300K was measured for each of 8 cavities. During the cryomodule test campaign the interior of the cavity was not accessible. Thus, the validation of the Field Flatness was possible only by comparing the measured resonant frequencies of the FM to the reference values stored just after the FF tuning. The reference frequencies for the FF estimation were recalled from the database (for details see Section 3.2.2) for each cavity individually.

The access to the cavity antennae was required to perform the test. The pickup probe connections were accessible from the bottom of the cryomodule by the external flanges. The input power coupler was accessible with the use of adapters. In Figure 3.18 one may see the green adapters. After the measurement, the adapters were disassembled.

Next, the cryomodule was installed on movable support in order to drive the module on rails to the concrete shielding (test-stand) - see Figure 3.1. Inside of the test-bench the cryomodule was connected to cryogenic installations. Then, the test-stand's waveguides were connected to the cryomodule, and various vacuum connections were performed. In Figure 3.18, the cryomodule XM-2 connected to the test-stand in AMTF is shown.
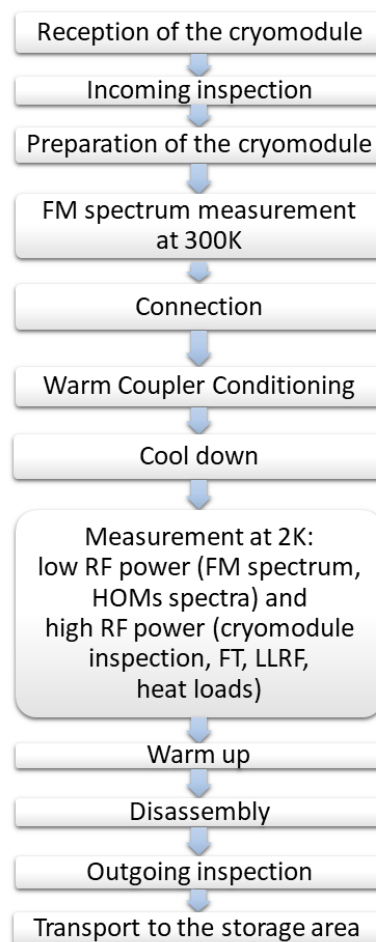
Figure 3.17: E-XFEL accelerating cryomodule quality control workflow in AMTF.

When all connections of the cryomodule to the test-stand were done, the input power couplers were conditioned (Warm Coupler Conditioning). It was a process of applying RF pulses to the input power coupler starting from the short pulse (e.g. 20 μs) and ramping pulse until reaching the maximum power. The process was repeated with different pulse lengths (e.g. 50, 100, 200 ... μs) until, reaching the maximum length of the RF pulse (1300 μs). The objective of the conditioning was to clean the couplers from the impurities.
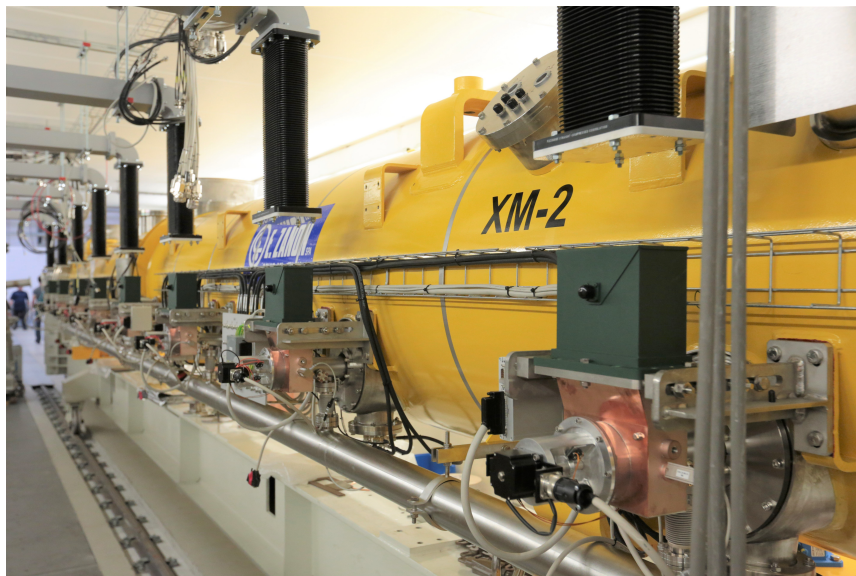

Figure 3.18: One of the E-XFEL cryomodules in the test-stand for the cryomodule testing (Courtesy of D. Noelle). One may see the waveguides hanging from the roof, the concrete shielding around, the movable support and the rails below.

3.3.1   The E-XFEL cold cryomodule RF measurements

The measurements at 2K started with the low power tests, for which the VNA was used to measure the FM spectrum (the details were given in Section 3.2.2). The measured TM_{010} resonant frequencies ensured that the π mode was shifted from $\approx 1.29775\,GHz$ at 300K to $\approx 1.2997\,GHz$ at 2K and the FF was not lost during the cool-down process. Recall that during the cavity test campaign the frequency was also recorded at 2K (see section 3.2.3). The control of the frequency of the π mode at 2K was required for the quality control of the production and the cryomodule assembly.

The measurement of the TM_{010} resonances was followed by the HOM spectra measurement (details were given in Section 3.2.4). After the HOM spectra measurement, it was checked that parasitic modes will be effectively dumped in the future and are unchanged after the cavities installation into the cryomodule.

Finally, the cavity's frequency was adjusted to the 1.3 GHz by activating the step motor, while the π mode frequency was tracked with the use of the VNA.

3.3.2   Test-stand for high power measurements at 2K

The test-stand for high power measurements (see Figure 3.19) consists of devices required to operate the E-XFEL cavities in the cryomodule under their normal working conditions. The control of the RF signals in the test-stand is performed by the LLRF system, which sets the RF frequency, phase and amplitude. The RF signals are amplified by the power amplifier and then amplification is continued by the klystron. The high power RF pulse is transferred from the klystron, through the waveguides and the input power coupler, to the cavity. The signals in the waveguide, from the pickup probe, and from the HOM couplers are monitored by the power meters and by the LLRF system. There are more components required to run the test-stand. They are listed below:

1. Cavity tuner driver - the hardware used to operate the cavity frequency tuners (step motors). The tuning is done by mechanical deformation of the whole 9-cell RF cavity.

2. Input power coupler driver - the hardware used to control step motors, which are moving the input couplers. The position of the input couplers requires a mechanical tuning.

3. Technical Interlock [60] - a system preventing from damaging the couplers and other equipment. It was set to measure the temperature of the warm and cold part of each coupler and light (sparks) in the waveguide. It was also monitoring the helium pressure and level in the test-stands, as well as the vacuum inside of the cryomodule.

4. Klystron - a special vacuum tube that uses the transit time of the electrons to generate and amplify high-frequency signals. It is supplied by the modulator - a device used to provide high voltage pulses to the klystron. The klystron and the modulator together provide high power RF pulses.

5. Waveguides with their subsystem - the pipes used to propagate the RF from the klystron to the cavity through the input power coupler.

6. Isolator - is a two port RF device that protects RF components from excessive signal reflection. The isolator is commonly replaced by the RF circulator and the RF load [71].
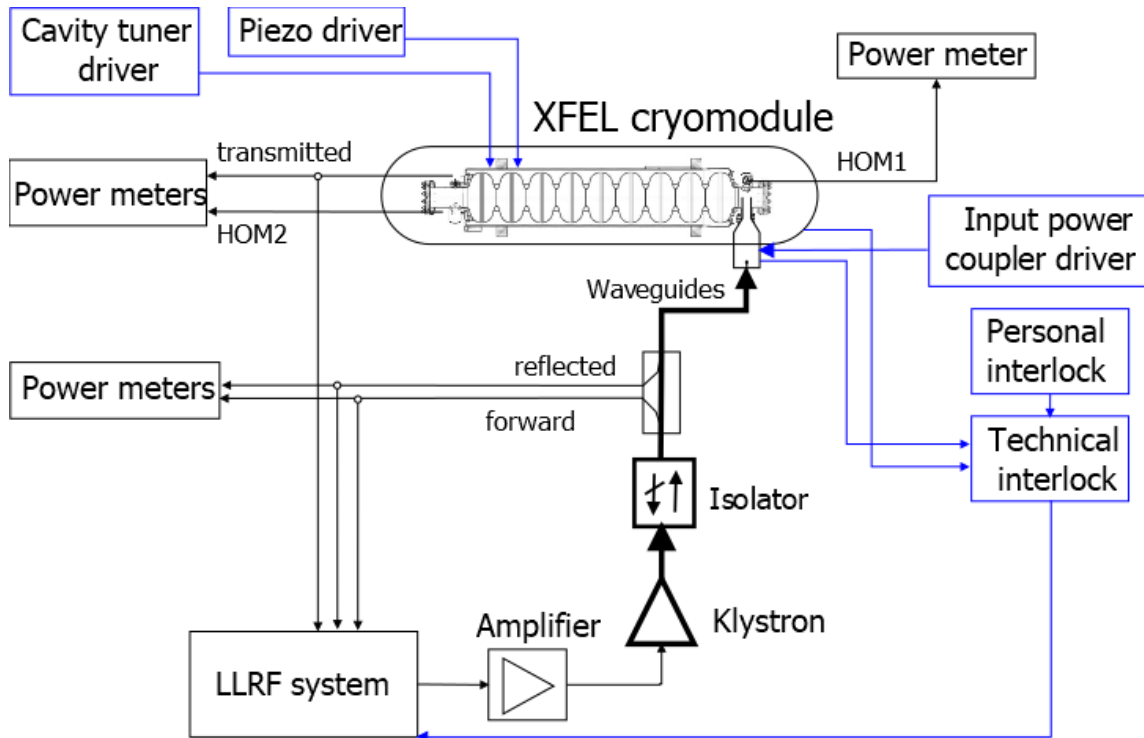
Figure 3.19: A simplified scheme of the high power test setup. The cryomodule is also simplified to the single cavity since all cavities in the cryomodule are performed in the same way.

7. Low Level Radio Frequency (LLRF) system - it is a system for controlling the RF signal (amplitude and phase control). It consists of μTCA crates with some additional external modules (the machine protection system, the timing system, the control system etc.). In this dissertation, LLRF denotes both the hardware and software.

8. Power meters - for the measurement of power: forward, reflected, transmitted, HOM1, HOM2.

9. Personal interlock - it is a safety system to prevent people from entering the test stand during the high power measurements. It consists of: gamma ray detectors for field emission detection, an oxygen sensor inside of the test-stand, an RF leakage detector, and a control system for locking the entry doors.

10. Piezo driver

3.3.3   RF signals during the high power cryomodule test

During the high power cryomodule test, the 1.3 GHz RF pulse of the *forward* power had a stepped shape and was different from pulses normally used in the accelerator (see Figure 2.6). In Figure 3.20 the RF pulses are shown as voltage waveforms. Because the testing of the RF cavities was done without beam the *forward* power was decreased (drop) during the Flat-Top time to mimic the RF-beam interaction. For the E-XFEL cavities the drop was set to the value within the range 6-8db in order to minimize the reflected power during the Flat-Top time and so that the stored energy in the cavity is constant. Moreover, the *forward* RF pulses were short ($\sim 1.4\,ms$) and powerful (the maximum value during the filling time was $\sim 250\,kW$).
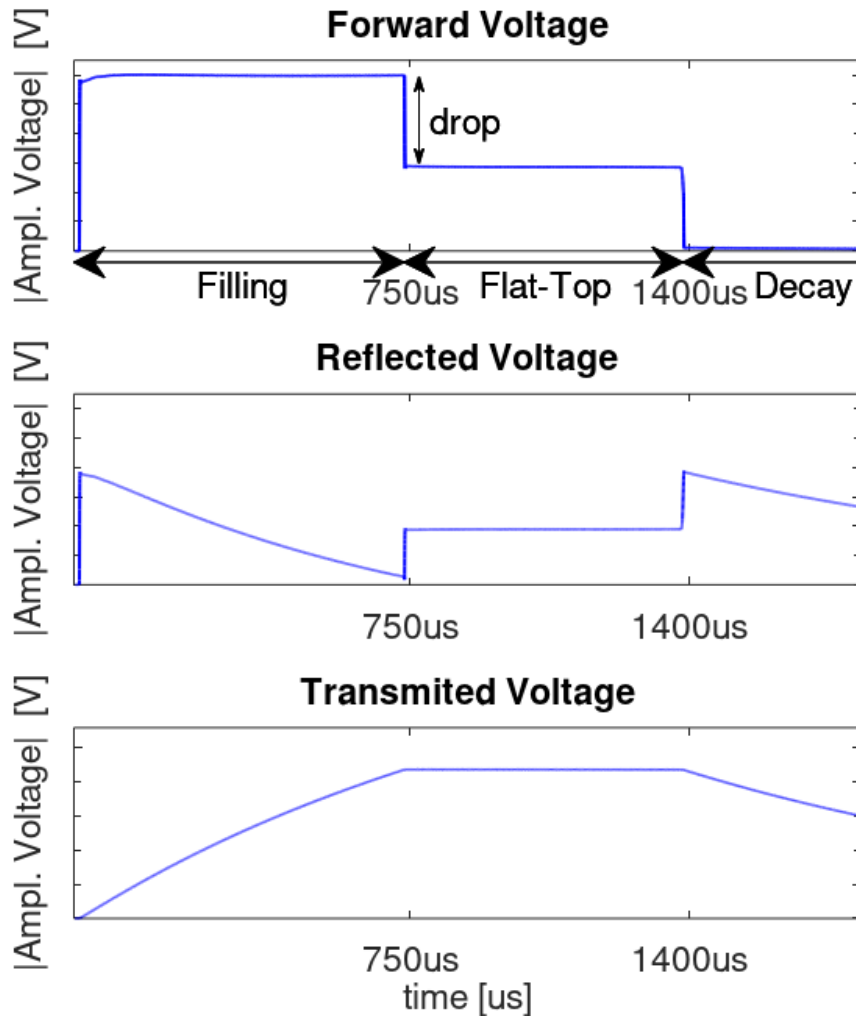

Figure 3.20: The amplitudes of voltages $V_{Ampl}(t)$ (see equation: (3.6)) recorded during the RF pulse.

The cavity behaviour during the high power cryomodule test was analysed in the same way as during the $Q_0 vs E_{acc}$ measurement, namely, with the use of the *transmitted* voltage. During the cryomodule test, the amplitude of the *transmitted* voltage was measured with use of the LLRF system [60-61]. The *transmitted, forward and reflected* signals (amplitudes of corresponding voltage) were also measured by power meters.

During the Flat-Top part of the RF signal, the *transmitted* voltage must be "in-phase" with the input (*forward*) voltage. It means that the cavity frequency must agree with the input signal and phase difference between the *transmitted* voltage and *forward* voltage must be constant (see Figure 3.21).
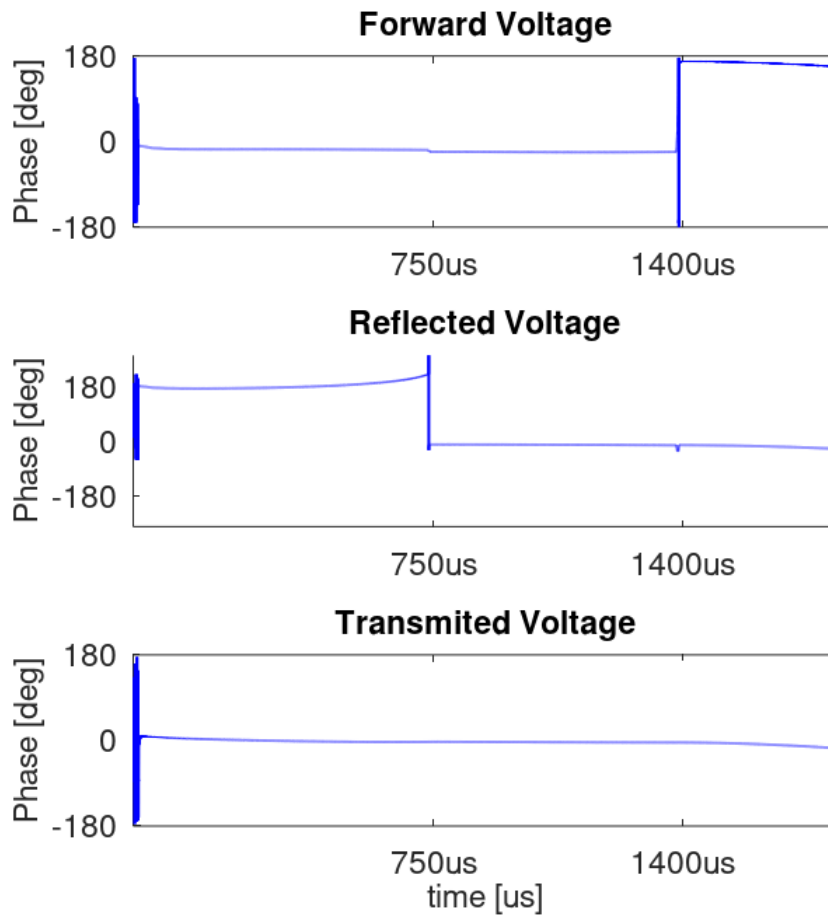

Figure 3.21: The phase difference between the voltage from RF generator in the LLRF system and phases $(\psi(t))$ of the voltages recorded during the RF pulse.

The procedure of adjusting the cavity's signal (*transmitted*) to be "in-phase" with the *forward* signal is called the cavity's fine-tuning. The cavity is coarse-tuned by activating the step motor and fine-tuned by adjusting the piezo actuator in order to deform the whole 9-cell structure to the 1.3 GHz at 2K. Based on DESY expertise, it is assumed that the fine-tuning of the SRF cavity at 2K does not affect the Field Flatness.

The cavity detuning (fine-tuning loss) is caused by the Lorentz force and microphonics (external vibrations). The EM resonating field produces the radiation pressure (P_L), which affects the cavity walls [61]. This pressure is caused by the Lorentz force and can be calculated with the use of the following formula:

$$P_L = \frac{\mu_0 |\vec{H}|^2 + \epsilon_0 |\vec{E}|^2}{4} \tag{3.15}$$

where $\vec{H}$ and $\vec{E}$ are the average magnetic and electric fields on the walls. μ_0 and ϵ_0 are permittivity and permeability in vacuum, respectively. These fields lead to the cavity walls deformation. As a result of the walls deformation and according to the perturbation theory, the cavity volume changes causing the change of the cavity resonant frequency. [64, 65]. The resonant frequency change (Δf_0) dependence on the accelerating gradient (E_{acc}) is defined as:

$$K_L = -\frac{\Delta f_0}{E_{acc}^2} \tag{3.16}$$

The K_L factor is called the Lorentz force parameter. For the E-XFEL cavity $K_L = 1 \frac{Hz}{(MV/m)^2}$ and, as a result, the frequency changes at the E-XFEL nominal gradient $\approx 700 Hz$.

The microphonics cause oscillations of the cavity resonant frequency. The known microphonics are caused by the helium bath pressure changes, vibrations of the vacuum pumps, or the mains frequency (50 Hz). Moreover, the E-XFEL cavity has its own mechanical modes (60 Hz, 152 Hz, 250 Hz), which might be excited [63].

In order to minimize the two above mentioned effects, a step motor is used for a wide range of the cavity dimension change ($\leq \sim 2$ mm). The piezo actuators are much quicker and work for the fine-tuning ($\leq \sim 3 \mu m$). The piezo works as an actuator, when a control voltage is applied to it from a driver (hardware). As a result the piezo deformation opposes the cavity deformation caused by the the Lorentz Force and microphonics. The second piezo is used at the same time as a sensor. More details about the piezo control is provided in Section 4.3.

3.3.4 Inspection of K_T and measurement of quality factors in the cryomodule

The objective of the first high power measurement at 2K was to inspect a parameter K_T for each cavity individually and to measure the following quality factors: Q_{load}, Q_{trans}, Q_{HOM1}, Q_{HOM2}. The K_T, characteristic parameter of each single cavity, has been measured and recorded during the single cavity test campaign. It allows to measure the accelerating gradient via the transmitted power instead of the forward one, what significantly simplifies the procedure.

The procedure of the inspection of K_T in the cryomodule started with the loaded quality factor measurement. Firstly, some *forward* power is applied to the cavity. Then, Q_{load} was obtained from the exponential *decay* time (see Figure 3.20) when the RF was off (see equation (2.27)). The loaded quality factor was adjusted to the desired one ($4.6 * 10^6$). By the adjustment of the position of the input power coupler, the Q_{ext} changed, and as a result Q_{load} at 2K also changed. The adjustment was performed by the step motor that was moving the coupler. The Q_{load} was adjusted each time during the high power measurements, when its value was changing ($> \pm 0.1 * 10^6$) due to the thermal expansion or contraction of the input power coupler.

Further, the accelerating gradient was measured from the *forward* power (P_{for}) with the use of the following equation:

$$E_{acc} = \frac{\beta_{ext}}{1 + \beta_{ext}} \frac{\sqrt{4P_{for} Q_{ext} R/Q}}{L(1 + \frac{\beta_{ext}}{1+\beta_{ext}}Q_{ext}(\frac{f}{f_0} - \frac{f_0}{f})^2)}(1 - e^{-\frac{\pi f_0 t_{fill}}{Q_{load}}}) \tag{3.17}$$

which depends on the constants: 9-cell cavity length (L), geometric shunt impedance (R/Q), the *filling* time (t_{fill}).

The equation (3.17) requires knowledge of the cavity resonant frequency (f_0). Thereby, the requirements for the measurement were given [70]:

- The cavity was perfectly tuned. The cavity resonant frequency $f_0 \approx f$, where f was the input (*forward*) frequency.

- The Lorentz force detuning and microphonics are negligible due to the small accelerating gradient (e.g. 5 MV/m).

- The value of the P_{for} is taken just before the end of the filling time.

- The LLRF worked in the open-loop control.

- $\beta_{ext} \sim 10^4$ - the power leaking out of the coupler was large as compared to the power being dissipated in the cavity walls (strong over-coupling) [21]. This also implied that in the superconducting state of the RF cavities $Q_{load} \approx Q_{ext}$ (see equation 2.25).

- The time of the RF pulse was set to the value corresponding to the case when the reflected power was 0 (zero) [51]. For practical cases - close to zero (see Figure 3.10).

- $Q_{trans} \approx 10 * Q_0$, which means that the pickup probe is weakly coupled to the cavity [21].

Under the above listed conditions, the formula was simplified to:

$$E_{acc} = \sqrt{4 \frac{P_{for} \, Q_{load} \, R/Q}{L^2} (1 - e^{-\frac{\pi f_0 t_{fill}}{Q_{load}}})} \qquad (3.18)$$

During the cryomodule test campaign, the calculation of the accelerating gradient started with the use of the *forward* power (P_{for}), for which the equation (3.18) was used. During the single cavity test campaign, the gradient was obtained for $\beta_{ext} \approx 1$ and long pulse. During the cryomodule test campaign, $\beta_{ext} >> 1$ and short pulse was used for the calculation of the accelerating gradient with the use of the *forward* power.

Next, the proportional factor (K_T) was obtained from the transmitted power (P_{trans}) and the accelerating gradient previously calculated:

$$K_T = \frac{E_{acc}}{\sqrt{P_{trans}}} \qquad (3.19)$$

During the cryomodule measurements, K_T was compared to the equivalent value obtained during the measurement ($Q_0 vs E_{acc}$) of the single cavity (before assembly into the cryomodule). The difference between K_T calculated during the cavity test campaign and the cryomodule test campaign was $\pm 0.1 * 10^7 \frac{MV/m}{\sqrt{W}}$.

The K_T parameter was inspected in order to measure the accelerating gradient from the transmitted power instead of the forward power. For all of the following measurements in the AMTF the equation (3.19) was used to calculate the E_{acc}. The equation (3.18) was not used for further measurements. Moreover, the value of K_T will be the reference value for the calculation of the gradient in the accelerator regime.

In addition to the inspection of K_T, the quality factors for the E-XFEL operating frequency of the HOM couplers and the pickup probe were measured.

$$Q_{trans} = \frac{(E_{acc} * L)^2}{P_{trans} * R/Q} \tag{3.20}$$

$$Q_{HOM1} = \frac{(E_{acc} * L)^2}{P_{HOM1} * R/Q} \tag{3.21}$$

$$Q_{HOM2} = \frac{(E_{acc} * L)^2}{P_{HOM2} * R/Q} \tag{3.22}$$

The acceptance criteria for quality factors were as follows:

- $Q_{trans} \approx 10^{11}$

- $Q_{HOM1} > 10^{12}$

- $Q_{HOM2} > 10^{12}$

Q_{trans} is measured to check whether power losses in the pickup coupler do not exceed the accepted limit.

Similarly, the HOM couplers, designed for an effective drainage of HOM frequencies, should - at the E-XFEL operating frequency - behave as rejection filters. Q_{HOM} acceptance criteria reflect the accepted RF power loss in HOM couplers at the E-XFEL operating frequency. During the single cavity test campaign the quality factors of HOMs were also monitored: during the HOM coupler tuning and $Q_0 vs E_{acc}$ measurement.

3.3.5 Flat-Top measurement

The name Flat-Top was derived from the shape of the amplitude of the *transmitted* voltage and from the part of the RF pulse (see Figure 3.20). The measurement was performed for each cavity in the cryomodule operating in the pulse mode from the klystron at 2K. Each cavity was tuned individually while other cavities were detuned. This ensured that any related effects (field emission, multipacting, quench) connected with the cavity currently measured.

During the Flat-Top measurement, the increasing steps of the pulsed *forward* signal were applied to the cavity until the it's maximum gradient was reached. The maximum gradient was determined by: the infrastructure limit was reached, the safety of humans was at risk or the cavity quenched. The AMTF infrastructure was limited by the waveguide's isolator (parts used to avoid reflection of the RF power to the klystrons). The isolators are limited by peak power and average power. The peak power is the maximum power during the RF pulse, while the average power is calculated for 1 second time slot. The isolator's

maximum average power was 2.2 kW [71]. For the E-XFEL parameters (10 Hz of repetition rate, pulse duration ~ 1.3 ms and power drop 6-8 dB), one may calculate the maximum possible equivalent power in the RF pulse, which is safe for the isolator. The optimal value during the RF pulse was ~ 250 kW. However, for a short period (2-5 minutes) power up to 270 kW were used. In order to simplify the testing procedure, the accelerating gradient was calculated from the *forward* power and the AMTF infrastructure limit was defined by the accelerating gradient and it was set to 31 MV/m.

As mentioned before, the maximum gradient was also limited by the human's safety. The accepted gamma radiation during the measurement inside of the test-stand was $10\,mGy/min$, which ensured that the safety limit outside the test-stand was not exceeded. The radiation was an effect of the electrons emitted from the cavity walls. The electrons emitted, due to e.g.: multipacting or field emission, were hitting the cavity walls and the surroundings.

Finally, if the cavity quenched before reaching the infrastructure limit and the safety limit, then the value of 0.5 MV/m less then the quench was recorded as the maximum E_{acc}.

During the Flat-Top measurement, the operating gradient was also determined. It is the future "work point" for the cavity in the E-XFEL accelerator and it was defined as the minimum value from:

- the gradient, when radiation starts exceeding $10^{-2}\,mGy/min$,

- the maximum gradient,

- the accelerating gradient, when temperature measured on the input power coupler exceeded the technical interlock limits during the measurement,

- the gradient, when the vacuum for input power coupler exceeded the technical interlock limits during the measurement.

The value of $10^{-2}\,mGy/min$ was set as safety limit in order to prevent damage of the electronic equipment located in the tunnel of the accelerator [72]. The technical interlock for the input power coupler were set to: 350K for the temperature sensor in the warm part of the coupler ($\sim 300K$), 120K for the temperature sensor in the 70K area inside of the cryomodule and 10^{-6} mbar for the vacuum in the coupler.

The maximum and operating gradients, recorded during the cryomodule test, are the values equivalent to those obtained for the single cavity test - during the $Q_0 vs E_{acc}$ measurement (the maximum and the usable gradient).

During the serial production test campaign, the maximum gradient from the single cavity measurement was compared to the maximum gradient of the cavity in the cryomodule. It was observed [74], that only two cryomodules had excessive gradients degradation, which was related to changes in the module assembly process. Moreover, as a result of the comparison of the maximum gradient between the cavity test campaign and the cryomodule test campaign a feedback to CEA was given. Thanks to the feedback, the assembly process changed. Finally, after 20 out of 100 cryomodules the assembly process was improved.

The usable gradient and operating gradient were also compared [72-74]. The usable gradient qualified single cavities for the assembly in the cryomodule. The operating gradient in the cryomodule characterized the cavity for the accelerator "work point". Usable and operating gradients were limited by different levels of X-rays. Moreover, the usable gradient was limited by Q_0. Whereas, the limit of the own quality factor was not defined for operating gradient. Based on the analysis of the results, the usable gradient was higher than the operating one.

In addition, the operating gradient, recorded during the cryomodule test, determined the power distribution in waveguides in the accelerator regime. The power distribution was tailored by one of DESY team based on the operating gradients and the waveguides were mounted to cryomodules after AMTF measurements. The adjustment of the power distribution was done because of the different power requirements for each cavity in the cryomodule and limited power budget. The klystron in the accelerator will provide power to 4 cryomodules [19, 76].

3.3.6   Heat Loads measurement

The objective of the Heat Loads measurement was to test the own quality factor at 2K. The Heat Loads result from RF power losses related to the own quality factor measurements, which are done at 2K. That measurements for cryomodules are similar to those for the single cavities, which were made when $Q_0 vs E_{acc}$ curve has been measured. However, for measurements of Heat Loads during the cryomodule test campaign one has measured averaged Q_0 value from eight cavities in the cryomodule.

It has also been decided to measure the own quality factor at the fixed gradients (at 23.6 MV/m) for each cavity in the cryomodule. For few cavities, for which that gradient could not be reached, that value was slightly reduced. It could eventually be also reduced for the neighbouring cavity because the AMTF waveguides supply a pair of cavities with the same power [76, 77].

During the measurement, the cavities in the cryomodule were measured at the fixed gradients for 2 hours. After the measurement, the effective emitted power from the cryomodule P_{cryo} was calculated from the helium massflow [78]. The heat load measurement of the single cavity in the cryomodule was not possible in the AMTF due to the low resolution of the flow meters. Afterwards, one calculates the instantaneous power P_{loss} during the RF pulse:

$$P_{loss} = \frac{P_{cryo}}{(t_{fill} + t_{FT}) * REP.RATE} \tag{3.23}$$

where REP. RATE is the repetition rate set to 10 Hz and t_{FT} and t_{fill} are the Flat-Top and the filling time respectively.

Finally, the averaged effective own quality factor of the cavities in the cryomodule is calculated [50]:

$$Q_0 = \frac{L^2 * \sum_{i=1}^{8}(E_{acc\_i})^2}{P_{loss} * R/Q} \tag{3.24}$$

where E_{acc_i} is the i-th cavity gradient.

The accepted Q_0 was $> 10^{10}$. This gave the $P_{cryo} < 6W$ of the Heat Loads for the 8 cavities supplied to the E-XFEL nominal gradient in the cryomodule. During the testing campaign, the average own quality was better than the design expectations, and only 4 cryomodules did not reach the specification [74].

3.3.7   Measurements of the LLRF functionality

The LLRF system (hardware and software) is used to control the RF signals that are provided to the cavity. A part of the software was developed and initially tested in the AMTF in order to validate its functionality for the future accelerator operation [79, 80]. Aims of the measurements are presented below:

1. *Cryomodule stable operation*

   During this measurement, the cavities in the cryomodule are maintained at the fixed gradients. The regulation through the LLRF of the *forward* voltages is done and changes of the cavity's *transmitted* voltages are measured.

2. *Cavity step motor characterization*

   The purpose of this test was to measure the cavity detuning (resonant frequency shift) as a function of the steps of the motor.

3. *Piezo capacitance and resistance*

   This measurement was performed during the cool down to 2K and warm up to the room temperature. Both piezos for each cavity in the cryomodule were measured. Their capacitance and resistance were recorded in order to find possible damages during the temperature changes [80].

4. *Input power coupler scan*

   The objective of the input power coupler scan was to measure the loaded quality factor as a function of the coupler position. The change of the Q_{load} is foreseen for the upgrade of E-XFEL, namely, for another type of cavity driving - CW instead of pulsed. The Q_{load} should be in the range $1.5 * 10^6 - 10^7$.

5. *Piezo DC scan*

   This measurement was performed in order to measure the cavity detuning as function of the piezo actuator DC voltage. It was done to check the maximum possible movement range.

6. *LFD coefficient*

   The measurement started for the cavities tuned at 3 MV/m. Then, the power was ramped up (without cavity tuning) to the higher gradients, until the cavity reached 18-20 MV/m. During each step the cavity detuning was measured as a function of the accelerating gradient.

7. *Lorentz Force Detuning compensation*

   During the Flat-Top measurement, the values of the piezo actuator parameters (DC Voltage, AC Voltage, Frequency, Advance time) were recorded for the maximum gradient. This operation is explained in dissertation in details later (see Section 4.3 High RF power cryomodule measurements).

8. *Identification of $7\pi/9$ and $8\pi/9$ modes*

   The amplitudes and frequencies of modes $7\pi/9$ and $8\pi/9$ were measured and recorded with and without digital notch filters. Such filters are applied to dump these unwanted modes, which are also excited in the cavities [79].

For the *Input power coupler scan*, the *Piezo DC scan*, the *Identification of $7\pi/9$ and $8\pi/9$ modes*, and the *Cavity step motor characterization* the cavities were tuned to 13 MV/m (approximately the half of the nominal E-XFEL gradient). The *Lorentz Force Detuning compensation* was performed during the Flat-Top measurement for the point recorded before the cavity quenched or in the power limitation point depending on the cavity performance. The *Cryomodule stable operation* was performed in parallel to the Heat Loads measurement (testing time optimization).

3.3.8 E-XFEL cryomodule test - final checks

After the cold E-XFEL cryomodule RF measurements, the cavities were detuned - the step motors used to tune the cavity were moved to their initial position. The π mode was tracked with the use of the VNA to ensure that its frequency went back to the value recorded before the cold test ($\pm 25\,kHz$). The procedure ensured us that the tension in the cavity was released before the warm-up, and that after warm-up the Field Flatness was not lost.

Finally, the cryomodule was warmed up to the room temperature and disassembled from the test-stand (see Figure 3.17). The cryomodule was then transported to the storage area.

3.4 Cavity and cryomodule measurements - summary

The RF measurements were divided into two groups called low and high power measurements. The low power measurements were performed with the use of the VNA in order to measure frequencies and the loaded quality factors of the cavity modes. The low power measurements were done for both single cavities and these installed in the cryomodules using the same measurement methodology:

- *Fundamental Mode spectrum measurement* - was done for the control of the cavity's field flatness during the cavity production and after installation of the cavities in the cryomodule as well as for the control of the desired frequency of the π mode. The validation of the Field Flatness was possible by comparing the measured resonant frequencies in TM_{010} and the frequencies recalled from the database. The frequencies in the database had been stored just after the Field Flatness tuning during single cavity tests. The Field Flatness change was represented by the Mean Spectrum Frequency Deviation, for which the acceptance limit was defined.

- *Higher Order Modes spectra measurement* - during this measurement, it was checked that the parasitic modes will be effectively dumped and that the HOMs extraction through the HOM couplers was assured. From the TE_{111}, TM_{110}, TM_{011} only these modes, whose frequencies are close to the synchronous condition with the relativistic beam, were validated. The quantity characterizing the HOM's expulsion was the loaded quality factor measured with the use of the VNA. The maximum loaded quality factor for each of the undesired mode was defined.

The high power measurements were performed in order to test the own quality factor and the accelerating gradient, for the cavities under the normal working conditions (pulsed operation, at the cryogenic temperatures). One $Q_0 vs E_{acc}$ measurement during the cavity test campaign corresponded to three measurements during the cryomodule test campaign, namely: *Inspection of K_T and measurement of quality factors in the cryomodule*, *the Flat-Top measurement* and *the Heat Loads measurement*:

- *Cavity test campaign*

    ○ *The $Q_0 vs E_{acc}$ measurement* - is the main high power measurement performed for each single cavity at 2K. The test was performed by applying the long RF pulse to the cavity. The power was gradually increased. The measurement was finished when the cavity quenched or the test's infrastructure limit was reached. At each power level, the Q_0 and E_{acc} were calculated. Finally, the $Q_0 vs E_{acc}$ curve was plotted. After the measurement, the cavity was accepted for the installation in the cryomodule, when the usable E_{acc} exceeded the defined threshold.

- *Cryomodule test campaign*

    ○ *Inspection of K_T and measurement of quality factors in the cryomodule* - during the measurement the stability of the proportional factor K_T between the single cavity and the cryomodule test campaign was measured. Maximal K_T deviance was defined. Moreover, during the measurement, the tuning of HOM couplers rejection filters was tested in order to validate that the operating mode frequency was not extracted from the cavity. The Q_{HOM} were calculated from the power extracted through the HOM couplers. The minimum Q_{HOM} was defined.

    ○ *Flat-Top measurement* - as a result of this measurement, the operating and maximum gradient E_{acc} of the cavity were established. The operating gradient is the working point for the cavities operation in the accelerator. The operating and design gradients were compared. As a result of the comparison, feedback on the cryomodule assembly process was obtained.

    ○ *Heat Loads measurement* - was performed in order to ensure that the heat load budget for the nominal E-XFEL gradient, assumed during the accelerator design, was achieved. The result of the Heat Loads measurement was the average own quality factor of all cavities in the cryomodule. The quality factor was compared with the design one.

During the high power measurements of the cryomodule, the validation of the cavity equipment was performed. Moreover, a part of the hardware and the software was tested, which was required for later accelerator operation:

- During the coupler conditioning, Flat-Top, Heat Loads and the measurements of the LLRF, the functionality of the input power coupler was checked. The mobility and its dependence on the Q_{ext} of the input power coupler was validated. Moreover, the input power coupler ability to transfer the high power RF waves within the microseconds to the cavity was proven.

- The step motor and piezo were also checked, so that the cavity under normal working conditions was tunable to the 1.3 GHz and the compensation of the Lorentz Force Detuning and microphonics was possible.

- The measurements of the LLRF functionality were the preparation for the LLRF algorithms implementation for the cavity control during the E-XFEL accelerator operation.

- During all high power measurements, the functionality of the hardware was proven: the input power coupler driver, the step motor driver, the piezo driver, the klystron (and modulator), the technical interlock, LLRF, as well as the software. All the components and software were validated before the accelerator is commissioned.

As a result of the low power, the high power and the measurements of the LLRF functionality, the set of the cavity parameters were stored in the reports. They are listed in Table 3.1. The values stored for the cavities in the cryomodules were measured and recorded separately for each cavity. The only exception was the averaged own quality factor measured for all cavities in the cryomodule during the Heat Loads measurement. The data marked with $\ddagger$ informs that during the single cavity and the cryomodule test campaign more gradients were recorded. Only the usable, the operating and both maximum gradients were stored to the final report. The similar applies to the own quality factor. The own quality factors were recorded for each step (gradient) during the single cavity test campaign during $Q_0 vs E_{acc}$ measurement. Only one Q_0 was recorded during the cryomodule test campaign, for the average gradient, from all cavities in the cryomodule, during the Heat Loads measurement. The data marked with $\dagger$ were not measured during the cavity test campaign, because the single cavity was not yet equipped with the final input power coupler, the step motor and the piezos. Dark current measurement was performed only during the cryomodule test campaign during the short RF pulse.

Finally, the typical values or ranges of the cavity parameters recorded during the cryomodule test campaign are listed in Table 3.2.

Cavity parameters	Single cavity test campaign	Cryomodule test campaign
$Reference\,FM\,spectrum$ $from\,database$	$9\,frequencies$	$see\,the\,single$ $cavity\,test\,campaign$
$FM\,spectrum\,@\,300K$	$9\,frequencies$	$9\,frequencies$
$FM\,spectrum\,@\,2K$	$9\,frequencies$	$9\,frequencies$
$Frequencies\,and$ $Q_{load}\,for\,HOMs$	$45\,frequencies$ $45\,Q_{load}$	$45\,frequencies$ $45\,Q_{load}$
$Propotional\,factor\,K_T$	$value$	$value\,(steady\,when$ $compared\,to\,single\,cavity\,test)$
$Gradient^{\ddagger}$	$maximum$ $(limited\,by\,the\,froward$ $power\,and\,limited\,by$ $the\,personal\,safety)$	$maximum$ $(measured\,up\,to\,31MV/m$ $and\,limited\,by$ $the\,personal\,safety)$
$Gradient^{\ddagger}$	$usable$ $(limited\,by\,Q_0\,and\,X_{ray})$	$operating$ $(limited\,by\,X_{ray})$
$Q_0\,for\,\pi\,mode^{\ddagger}$	$recorded\,for\,each\,step$ $during\,Q_0\,vs\,E_{acc}$ $measurement$	$averaged\,in\,the\,cryomodule$ $for\,operating\,gradient$
$Q_{ext}\,as\,a\,function\,of$ $input\,power\,coupler\,position$	$\dagger$	$minimum\,and\,maximum$ $value\,were\,recorded$
$Q_{ext}\,of\,the\,input\,power$ $coupler\,for\,\pi\,mode$	$\dagger$	$set\,to$ $the\,designed\,value$
$Q_{trans}\,for\,\pi\,mode$	$proportional\,to\,K_T$	$proportional\,to\,K_T$
$Q_{HOM1}\,and\,Q_{HOM2}$ $for\,\pi\,mode$	$value$	$value\,(steady\,when$ $compared\,to\,single\,cavity\,test)$
$Gamma\,radiation\,(X_{ray})$	$recorded\,for$ $maximum\,gradient$	$recorded\,for$ $maximum\,gradient$
$Dark\,current$	$\dagger$	$recorded\,when\,observed$
$Steps\,of\,the\,step\,motor$	$\dagger$	$recorded\,after\,rough\,tuning$
$Cavity\,detuning\,as\,a$ $function\,of\,the\,steps$	$\dagger$	$performed\,during$ $Cavity\,tuner$ $motor\,characterization$
$Cavity\,detuning\,as\,a$ $function\,of\,DC\,voltage$	$\dagger$	$performed\,during$ $Piezo\,DC\,scan$
$Advance\,time,\,DC\,Voltage,$ $AC\,Voltage,\,Frequency$	$\dagger$	$recorded\,during\,LFD\,for$ $the\,maximum\,gradient$

Table 3.1: The E-XFEL cavity parameters recorded for the cavity and the cryomodule test campaign.

Cavity parameters	Cryomodule test campaign
$FM\,spectrum$ @ $300K$	$1.2729 - 1.298\,GHz$; $\pi\,mode\,criterium:\ 1.29775\,GHz$
$FM\,spectrum$ @ $2K$	$1.2743 - 1.2998\,GHz$; $\pi\,mode\,criterium:\ 1.2997\,GHz$
$Frequencies$ and $Q_{load}\,for\,HOMs$	$1.6 - 1.9\,GHz\,(TE_{111}, TM_{110})$, $2.38 - 2.47\,GHz\,(TM_{011})\,and$ $10^3 - 10^6$
$Proportional\,factor\,K_T$	$1.38 * 10^7 \div 2.17 * 10^7 \frac{MV/m}{\sqrt{W}}$
$Maximum\,Gradient$	$31.0 MV/m$
$Operating\,Gradient$	$average\,27.7 MV/m$ $(design\,23.6 MV/m)\,[75]$
$Q_0\,for\,\pi\,mode$	$> 10^{10}$
$Q_{ext}\,as\,a\,function\,of$ $input\,power\,coupler\,position$	$1.5 * 10^6 - 10^7$
$Q_{ext}\,of\,the\,input\,power$ $coupler\,for\,\pi\,mode$	$4.6 * 10^6$
$Q_{trans}\,for\,\pi\,mode$	$\approx 10^{11}$
$Q_{HOM1}\,and\,Q_{HOM2}$ $for\,\pi\,mode$	$Q_{HOM1} > 10^{12}$ $Q_{HOM2} > 10^{12}$
$Gamma\,radiation\,(X_{ray})$ $for\,operating\,gradient$	$< 10^{-2}\,mGy/min$
$Cavity\,detuning\,as\,a$ $function\,of\,the\,steps$	$1\,Hz/Step$
$Cavity\,detuning\,as\,a$ $function\,of\,piezo's\,DC\,voltage$	$278 Hz/65V$
$Advance\,time,$ $Frequency,$ $AC\,Voltage\,Polarity$	$3 - 5ms,$ $260 - 280 Hz,$ $Minus$

Table 3.2: Typical values or ranges for the E-XFEL cavity parameters recorded during the cryomodule test campaign.

Chapter 4

The measurements of the serial production E-XFEL cryomodules

The work performed in AMTF consisted of two tasks: tests of the RF cavities and tests of the RF cryomodules. The aim of the cavities test campaign was to qualify them to the assembly in the cryomodule. The objective of the cryomodule test campaign was to qualify them for the installation in the E-XFEL accelerator tunnel. In this chapter the tests of cryomodules are described in details.

The cryomodule test procedure in AMTF covered: RF measurements at 300K, the installation of the cryomodule in the test-stand, the cool-down to the cryogenic temperature (namely to the operating temperature of 2K), RF measurements at 2K (the main part of these tests), the warm-up to the room temperature, deinstallation from the test-stand and preparation for the storage of the cryomodule. The RF measurements were performed for each of 8 cavities in the cryomodule and included the following measurements: the frequencies and loaded quality factors of the cavity modes, the own quality factor, and the accelerating gradient. Moreover, during the RF measurements, the functionality of equipment of each cavity in the cryomodule was validated under the normal working conditions.

The time foreseen for the cryomodule test was 21 days. The improvements of the cryomodule test procedure, which were developed by the IFJ PAN team, allowed to reduce the nominal testing time to 14 days [81, 82]. The standard cryomodule testing time included: time of the cryomodule installation to the test-stand, 48 hours of cool-down, 48 hours of warm-up, time of the RF measurements at 2K, time of the vacuum pumping and time of disassembly. The improvement of the testing time included: the automation of the measurements and the reduction of assembly and disassembly time. Not every betterment was possible due to the physical limitations of the test-stand's infrastructure or the cryomodule. The cool-down and the warm-up process was limited by the cryomodule material's properties and whole process had to be performed at strictly defined cool-down and warm-up speed. The vacuum operations were bounded by the test-stand's infrastructure restrictions (e.g. pumping speed).

During the preparatory phase (2010-2011), the team was trained with the use of pre-series cavities and cryomodules. The training resulted in: the final organization of test-

stands and a considerable development of the tests methodology, which is the main concern of this chapter. The excellent work during the preparatory phase has been validated by the successful serial-production test campaign performed in the years 2012 - 2016. The whole work described here was an effort of the large team from IFJ PAN, supported by DESY groups.

The author's main contribution was the development, optimization and implementation of the software, which became the principal working tool during tests of the serial-production cryomodules. The experience gained by the author's participation in the preliminary measurements and cryomodule tests during the preparatory phase was crucial for this work. Three packages are selected to present the functionality of the software:

- *FunMod* - package for steering of the Fundamental Mode spectrum measurement
- *HomMod* - package developed to perform the Higher Order Mode spectra measurement
- *TuneCAV* - package developed to tune the cavity with the use of the piezo and the step motor

Both low power measurements: Fundamental Mode spectrum and HOM Spectra were performed in the same way during cavity test campaign and cryomodule test campaign. Thus, the packages *FunMod* and *HomMod* were used during both campaigns.

The automation of the measurements procedures allowed to shorten the time and to improve the precision and reproducibility of measurements, which was also important for further data analysis.

In the following sections the considerable improvements of the measurement methodology supported by the novel software are described. This software is not only a safe guide line through numerous steps of the measurement procedure but also automatize some of its steps, which are tedious and time consuming, when performed manually.

4.1   FM spectrum measurement

During the preparatory phase for the serial-production tests (2010-2011), low RF power measurements were performed manually in order to gain experience with the RF cavities measurements and to familiarize the team with the hardware (VNA). Because a large number of cavities in cryomodules was measured during the serial-production test campaign in years 2012-2016, it was crucial to automate these RF measurements. The cryomodule low power tests consisted of the Fundamental Mode (FM) and Higher Order Mode (HOM) spectra measurements. The basic purpose of the Fundamental Mode test was to measure the frequencies of the modes in TM_{010} at 300K and at 2K. The purpose of the Higher Order Modes test was to measure the loaded quality factors of HOMs at 2K (for details see Section: *3.3 The E-XFEL cryomodule test campaign*).

In order to introduce the subject of the improvement of the Fundamental Mode spectrum measurement, the procedure, which existed before the preparatory phase and which was developed by DESY experts for the FLASH cavities [47, 83, 84], is described in details in the following section.

4.1.1 The measurement procedure before the preparatory phase

The measurement procedure was composed of three steps:

I. *Rough determination of all 9 resonant frequencies in passband 1.27-1.3 GHz of the TM_{010} mode with the use of the VNA.*
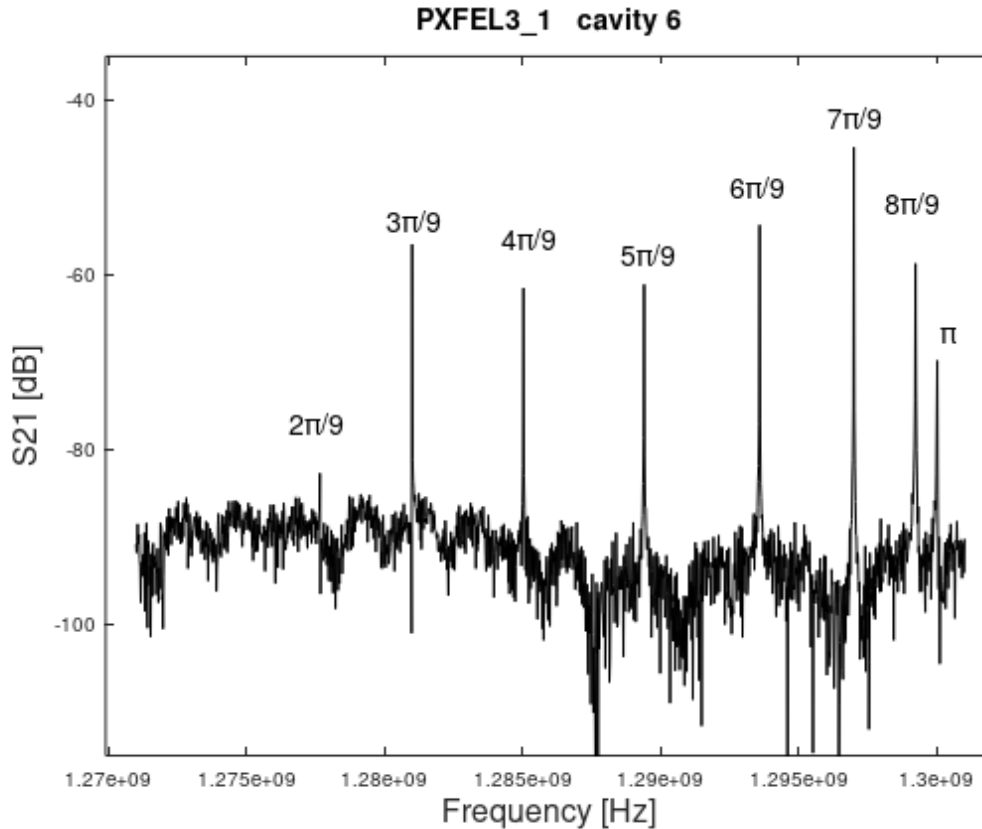

Figure 4.1: FM view in the band 1.27-1.3 GHz at 2K for the cavity 6 in the cryomodule PXFEL3_1. Mode $\pi/9$ is not visible.

An operator sets markers on the selected peaks on the distribution displayed on the VNA. The resonant frequencies (modes π, $8\pi/9$, ... , $\pi/9$) correspond to the 9 maxima (peaks), which can be found in the plot on the display of the VNA. The absence of any of the peaks does not mean that the mode does not exist. The mode might rather not be visible due to the limited VNA resolution, or bad cable connection, or weak power of the signal from the cavity, which was below the noise level of the VNA. In such a case the operator sets the marker in the rough location of the mode based on the knowledge or reference values. The search of the invisible mode was laborious and required additional measurement time, which depended on the operator's experience.

The examples of such plots are shown in Figure 3.6 at 300K and in Figure 4.1 at 2K for 30 MHz span (1.27-1.3 GHz). The span of 30 MHz was chosen so that, regardless of the conditions, the frequencies of 9 modes were within the plot. The number of points (1601) was equal for 300K and 2K.

II. *Measurement of each resonant frequency with the high precision.*

Each of the previously marked peaks were re-measured with the small span: 50 kHz at 2K and 100 kHz at 300K. The number of points used for this measurement was 201 at 300K and 2K. The frequency measurement with such the high precision (presented in Figure 4.2) was required in order to compare the results with those obtained with the same precision collected during: the single cavity measurement, before and after the assembly into the cryomodule and also with the reference data recalled from the database.

The absence of the peak in this step of the measurement procedure required tedious action: either return to the first step (rough determination) or/and extension of the small span to be able to find the resonance.
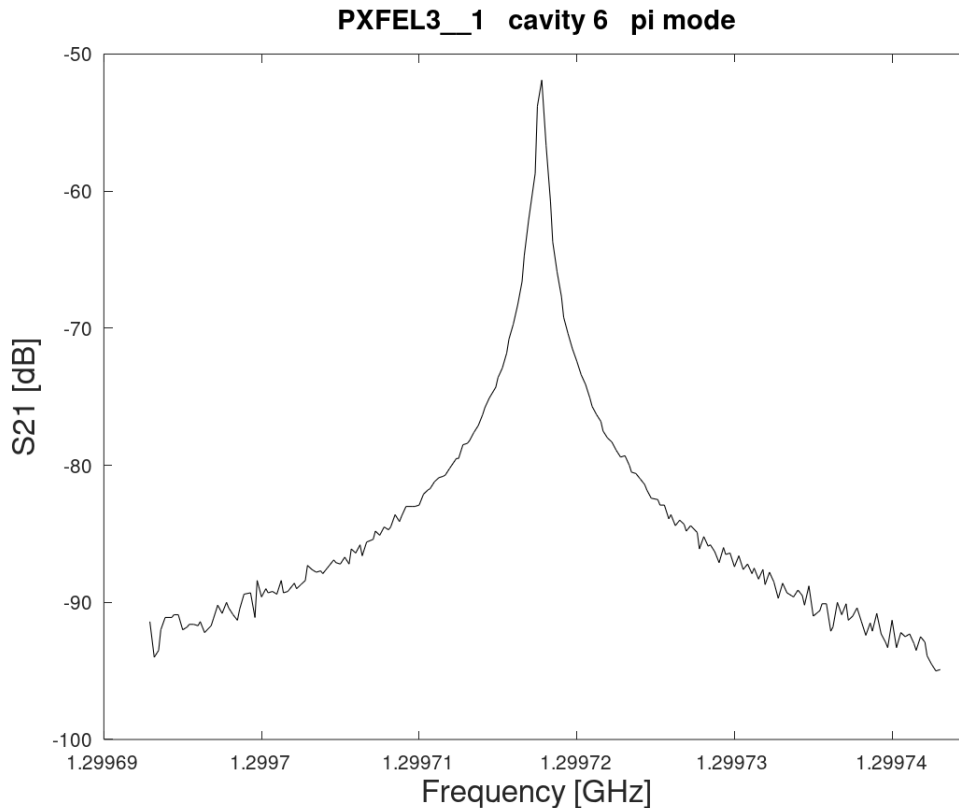
Figure 4.2: Measurement of the π-mode for cavity 6 in cryomodule PXFEL3_1 with the high precision (50 kHz span).

III. *Check the Field Flatness.*

The Field Flatness and its stability is controlled by the MSFD parameter as explained in the chapter 3. MSFD was calculated for just measured frequencies and the reference frequencies recalled from the database. If the acceptance criteria were not met, then the measurement was repeated.

4.1.2 Preparatory phase to the FM measurement

During the preparatory phase for the measurements of the serial-production cryomodules (2010-2011), several improvements of the FM measurement procedure (listed in the previous section) were investigated. In general, it was assumed that the improvement should lead to the development of a software with an automatic or semi-automatic control of the measurement, which should speed up tests and make it possible to measure the FM at any temperature between 2K and 300K. Discussions during preparatory phase resulted in the decision, that it is sufficient to test cryomodules only at two temperatures: 300K and 2K. Yet, even that did not guarantee that recorded spectra of previous measurements (from the cavities test campaign) will provide useful, valuable reference values which an operator could use in the peak marking process. Neither the stability of the cavity FM spectra, after transports and installation into cryomodules nor the corresponding stability of the Field Flatness was known at that time. Hence, the author proposed to approximate the measured resonant frequencies of the TM_{010} in step I of the procedure with the use of the cavity model.

4.1.3 Cavity LC Model for frequency estimation (Procedure: step I).

In order to approximate the resonant frequencies of TM010 during the first (I) step of the FM procedure (described in Section 4.1.1), the use of the LC cavity model was proposed. This model is described in details in Appendix A. It allows to predict seven resonant frequencies out of nine of the TM010 if any two are known (e.g. previously measured).

Author's idea was to use the frequencies of the modes with the highest mode numbers (starting from $m = 8$ and $p = 9$) to calculate the $7\pi/9$ mode. To calculate the $7\pi/9$ mode, the coupling $k_{8,9}$ related to the 8 and 9 modes is used. Next, in order to estimate the $6\pi/9$ mode's frequency: the coupling $k_{7,8}$ and frequency of mode $7\pi/9$ are used. The same steps are repeated until $\pi/9$ mode is estimated.

The cell to cell coupling $k_{m+1,m+2}$ related to the $m+1$ and $m+2$ modes is calculated as follows:

$$k_{m+1,m+2} = \frac{1}{2} \frac{f_{m+2}{}^2 - f_{m+1}{}^2}{f_{m+1}{}^2(1 - cos\frac{(m+2)\pi}{N}) - f_{m+2}{}^2(1 - cos\frac{(m+1)\pi}{N})} \tag{4.1}$$

where N is the number of cells : 9.

With the use of the equation (4.1) it is possible to predict all searched frequencies:

$$f_m = f_{m+1}\sqrt{\frac{1 + 2k_{m+1,m+2}(1 - cos(\frac{m\pi}{N}))}{1 + 2k_{m+1,m+2}(1 - cos(\frac{(m+1)\pi}{N}))}} \tag{4.2}$$

where m is the estimated mode number. $m \in< 1, 7 >$.

In the LC model, it is assumed that, all cells are identical. In the case of the real cavity not all cells are identical due to the allowed tolerances. This model was validated with the cavities in two pre-series cryomodules: PXFEL2_1 and PXFEL3_1. The cavities were measured for each cryomodule at 300K and at 2K. The validation of the model is discussed in the next section.

4.1.4   Observation - predicted and measured frequencies (Procedure: step I).

From the results of the pre-series modules, two observations crucial for the improvement of the measurement were made. The first observation was done on the difference between the measured resonant frequencies of the pre-series modules and their approximation during the peaks detection. The deviations between the approximated and measured values were analysed in order to estimate the worst prediction.

It was observed that the measurement difference was larger than 50 kHz (span at 2K) for 44% of the predicted values in the pre-series modules. In Figure 4.3 the difference between the measured and predicted frequencies of a single RF cavity is shown. These results show that the approximation method and a small span would not be wide enough for the correct determination of frequencies.
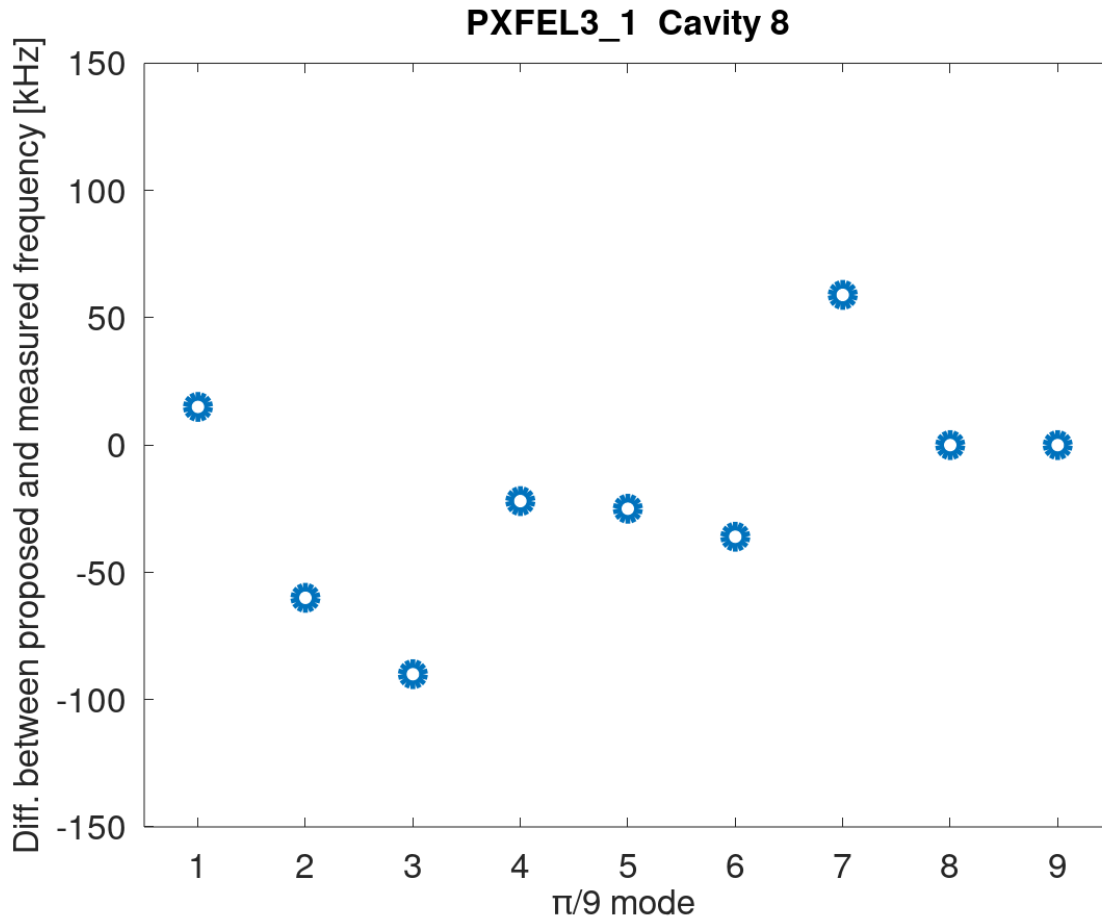
Figure 4.3: The difference between measured and approximated frequencies for the given mode for cavity 8 in cryomodule PXFEL3_1. Modes $8\pi/9$ and π were not predicted (at 2K).

For a large (more than 50 kHz) difference in a frequency determination, the searched resonant frequency was out of the measurement range. The solution proposed, on the basis of the observation, was to increase the span of the measurement. An additional sweep was added to the procedure with the 600 kHz span. The span was chosen from the biggest prediction (262 kHz) difference. 801 points measured in this 600 kHz span provided sufficient resolution, for narrowest peak - $\pi/9$ mode, which is approx. 10 kHz).

4.1.5 Observation - measurement of each resonant frequency with high precision (Procedure: step II).

The second observation was made in step II of the procedure described in Section 4.1.1, namely during the measurement with the high precision. In Figure 4.2 the test example for $6\pi/9$ mode measured with the high precision for cavity 8 in $PXFEL3\_1$ is presented, where

the resonant frequency was measured incorrectly at 2K. At this step of the measurement the peak is visible, but it was observed in a few cases that the maximum of the peak is shifted and then the peak is located at the beginning or at the end of the measurement range. This observation was interpreted as the measurement error.

In Figure 4.4 an example of this error is shown. The maximum of this plot was at the right end of the span (still on the rising edge), but the searched maximum of that peak was outside of the measured span. In such cases, repeating of the measurement with the high precision was required. The frequency of the previously found maximum was set as a center frequency. The test was repeated until the maximum of the resonance was within the measured span (few kHz from the edges).

PXFEL3_1   Cavity 8 6pi/9 mode
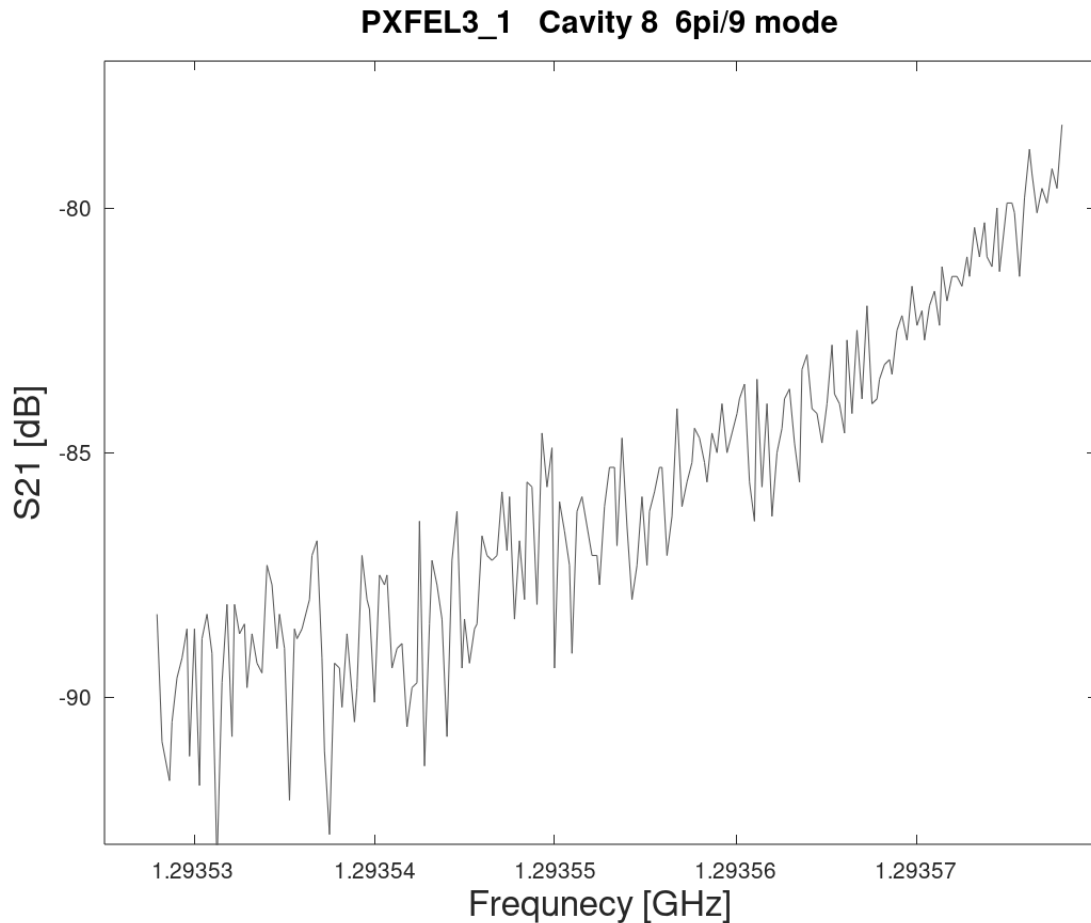
Figure 4.4: Test example for $6\pi/9$ mode measured with the high precision for cavity 8 in PXFEL3_1, where the resonant frequency was measured incorrectly (at 2K).

4.1.6 Practice - Field Flatness check (Procedure: step III)

In step III of the procedure the MSFD parameter was calculated in order to estimate the Field Flatness. When the acceptance criteria were not met, then the relative spectrum was displayed. In Figure 4.5 the Front Panel of the *FunMod* package for MSFD calculations with the relative spectrum is presented. The relative spectrum (red) and its linear approximation (dashed blue) for a single E-XFEL cavity is shown. The acceptance criterion are marked with use of the solid green and solid blue. In the Figure 4.5 one may see the example of control of the measured resonant frequencies. The fifth resonance of the relative spectrum caused exceeding of the acceptance criteria (solid orange). The re-measurement of the 5th mode was required. It was the only one deviating from the linear regression line thus the cause of this issue was wrongly measured resonance. After the re-measurement of the fifth resonance, the correct frequency was found and the acceptance criterion were not exceeded.
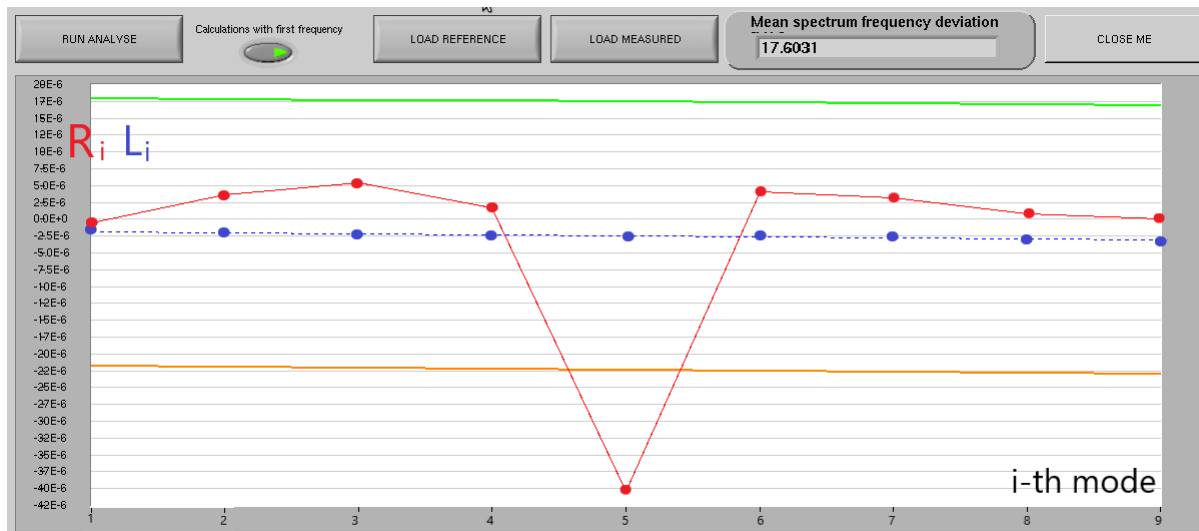
Figure 4.5: The LabVIEW Front Panel for the MSFD calculation. R_i is a relative spectrum. L_i are used to draw a linear regression line. For details see Section 3.2.2. Green and orange lines are drawn to show which mode is responsible for exceeding of the MSFD.

4.1.7   Summary of upgrades in the FM measurement procedure

Based on the two observations listed above, the FM measurement procedure (described in Section 4.1.1) was modified in the following way:

I. Rough determination of all 9 resonant frequencies in 1.27-1.3 GHz (30 MHz) of the TM_{010} mode. Choose which peaks will be predicted by the software and which will be set by the operator (except modes $8\pi/9$ and π). Measure automatically each predicted resonant frequency with the 600 kHz span.

II. Measure automatically each resonant frequency with the high precision (with 50 kHz span at 2K and 100 a at 300K). Repeat search of frequency of maximum in the loop until the maximum is determined within the measured span.

III. Check the Field Flatness and when acceptance criteria are not met then perform the re-measurement of a given mode.

The equivalent LC circuit of the RF cavity was used in order to approximate the resonant frequencies of TM_{010} in step I of the procedure. The cavity LC model enabled to perform the automatic measurement except of the two frequencies ($8\pi/9$ and π modes). This procedure led to the implementation of the software *FunMod* developed in LabVIEW, which controlled the VNA.
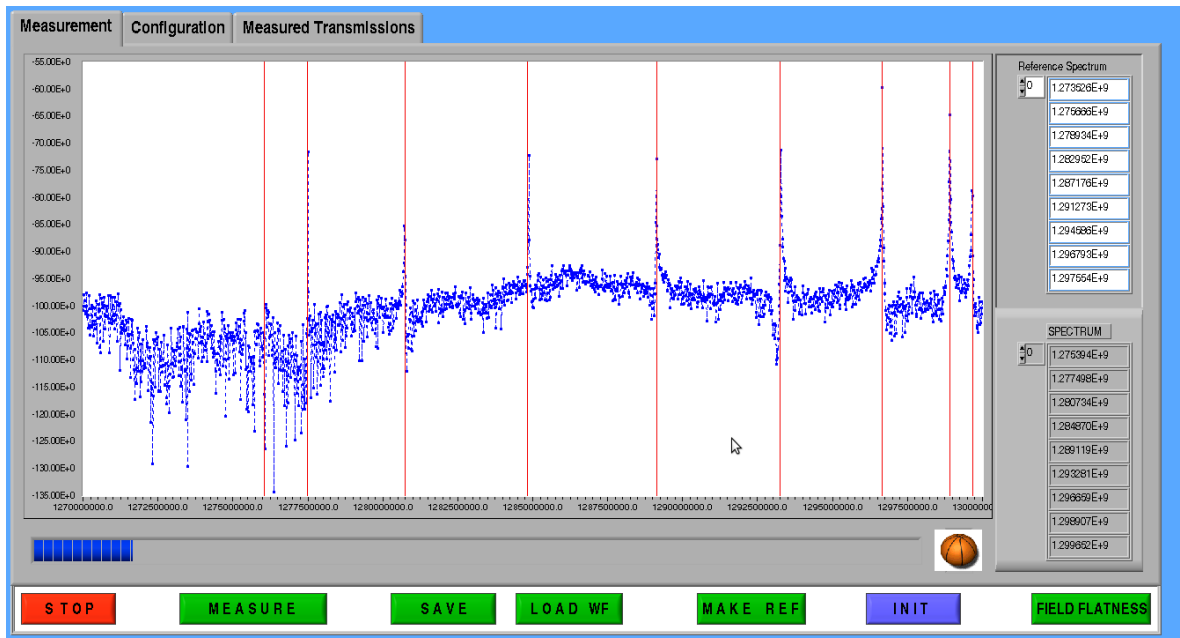
Figure 4.6: The LabVIEW Front Panel of *FunMod* package.

In Figure 4.6 the main Front Panel of the *FunMod* package is presented during the measurement at 2K. The frequencies of the modes are marked with the red line.
The $\pi/9$ mode is marked as the first one from the left side on the plot.

The *FunMod* software had the following functionalities: loading and saving data in DESY database formats, saving full sweep data from the VNA in raw data files and defining reference test parameters for warm and cold conditions. Additionally this software was also used during HOM couplers rejection filter tuning - another important task to be done during single cavity testing for its high quality operation [36, 40].

The *FunMod* package determined the testing time for each step of the procedure which was independent of the operator and which was crucial in order to plan the work in the serial-production regime. The first (I) step of the procedure consumed most of the time of the measurement, it took about 3 min. The second (II) step was performed very fast ($\sim$ 3 sec for each resonance). The third one (III) required only to download the reference file from the database. One may notice that the most time consuming step (I) might be then excluded from the procedure because the model enabled to perform the automatically measurement. However it was recommended to record the whole 1.27-1.3 GHz band from the VNA in order to control the measurement. This procedure is shown in details in the block diagram in Figure 4.7.

In case of step I, the peaks approximation was used mainly for the two resonant frequencies at 2K ($\pi/9$ and $2\pi/9$) and there was no additional time required for the manual resonance search. At 2K, the peaks approximation was very useful. Typically, the operator was not able to see all the resonances because of their width (the smallest were about 10 kHz) and a relatively small test system resolution (1601 points for 30MHz span). In step II, the improvement was based on the recurrent process in order to avoid unwanted measurement errors, namely when the maximum was found at the ends of the measured span. The III-rd step was not changed.

To summarize, *FunMod* package ensured that no human error occurred during the measurement and provided the control of the measured resonant frequencies with the use of LC model. The human errors are typically expected during the measurements of serial-production components, since the same measurements are repeated thousands times.

START

Reset and initialize VNA

300K ← Condition → 2K

Set warm params   Set cold params

Operator determines roughly 9 resonant frequencies for 30 MHz span .

Operator chooses which modes are going to be approximated (except $8\pi/9$ and π mode).

i=9; j=FALSE;

Move the span's center frequency
+25 kHz @ 2K or +50 kHz @ 300K

Measure $i\pi/9$ mode with the high precision.
Span: 50 kHz @ 2K or 100 kHz @ 300K

Move the span's center frequency
-25 kHz @ 2K or -50 kHz @ 300K

No ← Rising slope → Yes

No ← Maximum within the measured span → Yes

i=i-1

No ← i > 7 → Yes

Yes ← Peak i approximated → No

Calculate approximated mode $i\pi/9$ with the use of
the $(i+1)\pi/9$ and $(i+2)\pi/9$ modes. Use LC model for calculation

Measure mode $i\pi/9$ with the center frequency approximated (600 kHz span).

Move the span's center frequency
+25 kHz @ 2K or +50 kHz @ 300K

Move the span's center frequency
-25 kHz @ 2K or -50 kHz @ 300K

Measure $i\pi/9$ mode with the high precision.
Span: 50 kHz @ 2K or 100 kHz @ 300K

No ← Rising slope → Yes

No ← Maximum within the measured span → Yes

i=i-1

Yes ← i=0 OR j=TRUE → No

Operator points the file with the reference frequencies from the database

Calculate the MSFD for the reference and measured data.

Yes ← MSFD < 10kHz OR j=TRUE → No

STOP

Operator sets the i-th mode to be re-measured.
J=TRUE;

Figure 4.7: Algorithm of the *FunMod* package.

4.1.8   The discussion of the test results

The FM measurement was the main test for the quality assurance of the cavities installed in the cryomodules. During the cryomodule testing campaign, the FM spectrum measurement was performed for all the cavities installed in the cryomodules minimum two times: at 300K and after reaching of the stable temperature by the cryomodule at 2K. The basic information collected from the frequencies of the FM was the Mean Spectrum Frequency Deviation, which provides information about the Field Flatness (FF) deviation. The amplitudes of the FF notifies about the efficiency of the multicell E-XFEL cavity acceleration. The constant dependence of frequencies in the FM is an essential information about cell's shape stability during: the transport, the assembly, the installation to the test-stand and the cool-down/warm-up processes.

As mentioned in the previous paragraphs, the LC equivalent circuit methodology implemented into *FunMod* package for the FM measurement was essential when peaks were not identified correctly or were not visible during the rough resonances identification (step I of the procedure). During the preparation and testing campaign, it was noticed that peak $\pi/9$ mode at 2K was the crucial one for the method, because this resonance had the smallest amplitude and the narrowest peak in TM_{010}. In Figure 4.8, the distribution of the difference between the measured and approximated values with the use of the LC model versus number of cavities was presented. The red line shows the normal distribution. The predicted $\pi/9$ mode was calculated with the use of $3\pi/9$ and $2\pi/9$ mode. The difference between the calculated and measured values was validated in order to obtain the worst precise   prediction. The worst difference for $\pi/9$ mode at 2K was 272 kHz, which is a proof of the validity of the adopted method, where 600 kHz span was used.

The methodology ensured that no human error occurred and provided the data control of the measured resonant frequencies, because the resonances calculated from the model were in agreement with the measured resonances. The prediction of resonances is reliable for multicell cavities without knowing the statistics of similar cavities before to measurement, and is universal for any temperature.
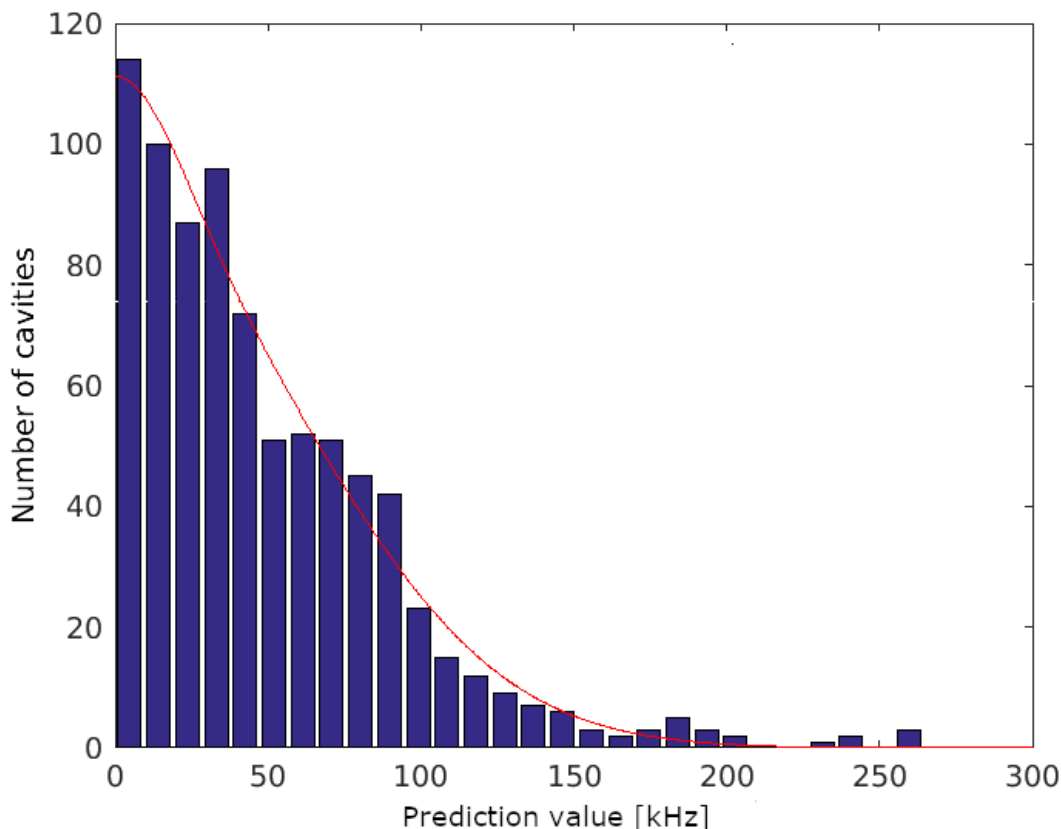
Figure 4.8: Histogram of the $\pi/9$ mode prediction value.

4.2   HOM spectra measurement

As mentioned before, for the FM test, the measurement's procedure improvement was based on the idea of using the LC model of the RF cavity in order to determine the resonant frequencies of the cavities. The same method was investigated to be used for the HOM spectra measurements. The HOM spectra analysis of the RF cavity model to assess the resonant frequencies [85] showed that this method is not appropriate for HOMs approximation. The obtained results have shown that the resonant frequencies, especially for the dipole modes, do not correspond to the values obtained with the LC model.

Thus, another method to enhance the measurement was implemented. Based on the experience and observations made during the HOM spectra measurement, the sequence of actions to obtain the loaded quality factors and the frequencies of HOM resonances formed an algorithm implemented in the *HomMod* package.

The general block diagram of the *HomMod* software is presented in Figure 4.12. The software is organized in the following way:

I. *Rough determination of resonant frequencies in a passband of a measured mode with the use of the VNA.*
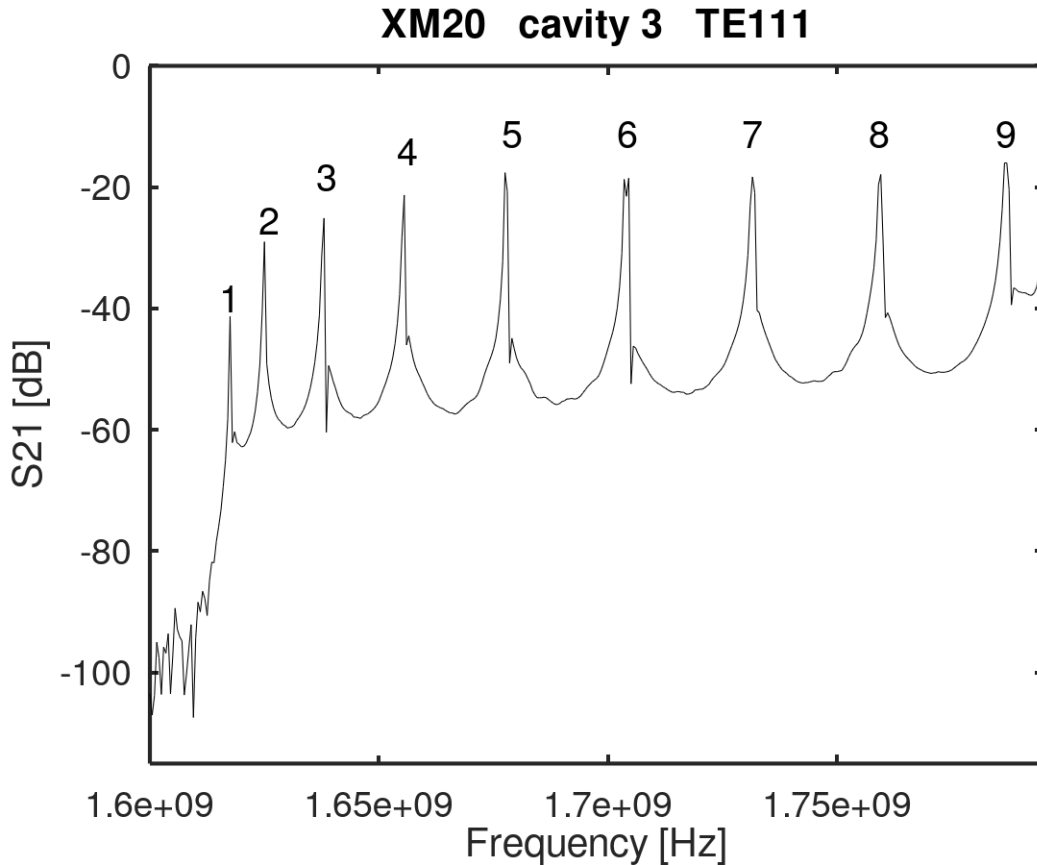
Figure 4.9: TE_{111} view in the passband 1.6-1.8 GHz measured for cavity 3 in cryomodule XM20.

The operator set markers on the selected peaks on the distribution displayed on the VNA. The distributions were displayed for 3 measured modes TE_{111}, TM_{110}, TM_{011} in passbands 1.6-1.8 GHz, 1.78-1.9 GHz and 2.36-2.5 GHz respectively. Within the passband of the monopole mode (TM_{011}) 9 resonant frequencies were marked. For the dipole modes (TM_{110} or TE_{111}) each peak representing a single HOM was marked (9 markers in total). The frequencies of each component of the dipole modes were very close to each other (the difference was less than 1 MHz) and their individual selection was almost impossible. In Figure 4.9, an example of the dipole mode TE_{111} is presented, where only for the 6th pair of components two resonances are clearly visible with the use of the large span: 200 MHz. In the next step of the *HomMod* software, the marked peaks are used to measure each resonance of the dipole modes.

II. *Automatic high precision measurement of the quality factors and the frequencies.*

For each of the previously determined markers the frequencies and the loaded quality factors were measured automatically. For the monopole mode (TM_{011}) the quality factor was measured with use of the equation (2.28) for 3dB drop in the frequency domain. For dipole modes (TM_{110}, TE_{111}) firstly the selection of both components within 2 MHz span was done. Then, the quality factor and the frequency for each component of a dipole mode was measured. For dipole modes (TM_{110}, TE_{111}) obtaining of the 3dB drop from the resonance was often impossible. In Figure 4.10, an example of such measurement is presented. For the "left" resonance, the 3dB drop was only measurable on the left side of this resonance. The proposed solutions for the measurement were: to use the only one side (left or right) of the resonance with 3 dB drop for the calculation or use both sides of the resonance but with 1 dB drop. Finally, the 1dB method was used, because this method was faster and the accuracy was good enough for the measurement purpose. In rare cases, when 1dB drop was not measurable, then only the frequency of the resonance was recorded. Sometimes 2 maxima were not visible - they were fully overlapped. The detailed algorithm of automatic finding of a single quality factor is presented in Figure 4.13.
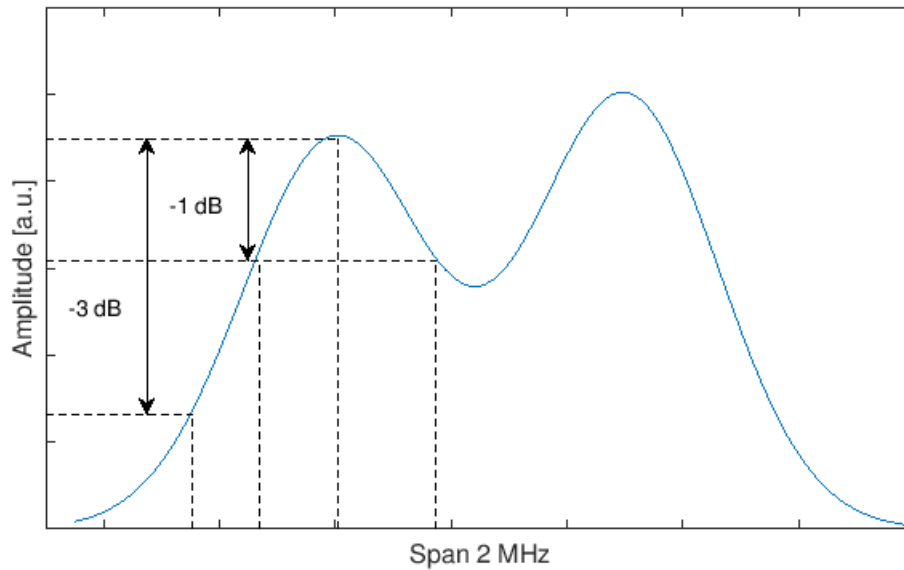
Figure 4.10: The amplitude of the driven resonator for two components of a dipole mode.

III. *Verification of the measurement and the re-measurement by the operator.*

The RF operator verified, which of the previously automatically measured resonances with the high precision should have been re-measured. The verification was required for the dipole modes. The decision was taken by the operator taking into account the plots analysis stored in previous step (II).

Span 2 MHz
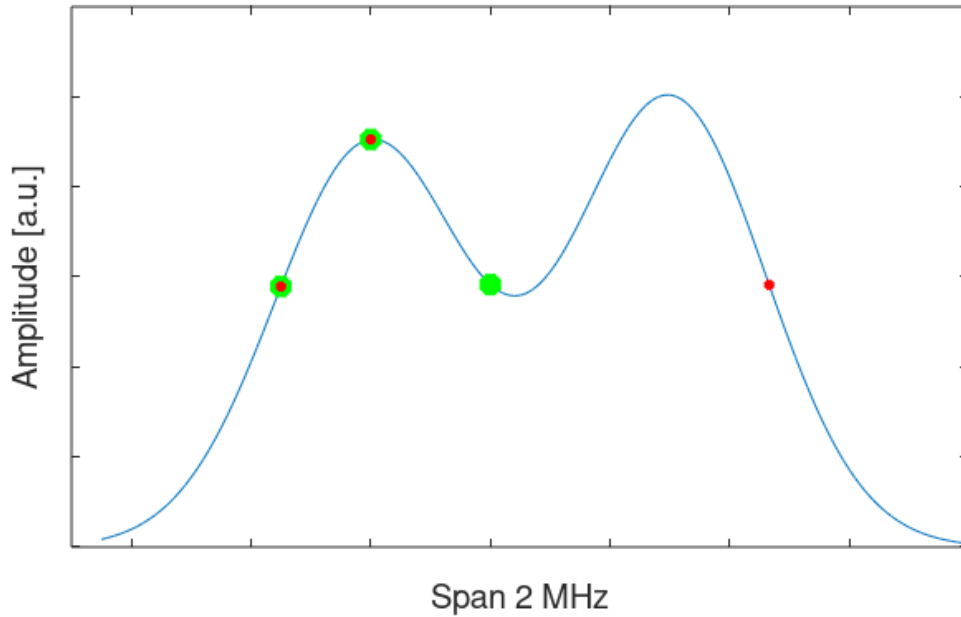
Figure 4.11: The example of the markers analysis.

In each plot, special markers were placed in order to show how the Q_{load} was calculated in the VNA. In Figure 4.11 two examples of such markers are depicted. For the green dots no re-measurement was needed. For the red dots the re-measurement was required. Next, the operator repeated the measurements of selected peaks. The *HomMod* package was updated for this part of the test procedure and covered the most frequently used VNA parameters (span, scale etc.) in order to speed up the time needed for the measurement.

IV. *Verification of the measurement results.*

The fulfilment of the acceptance criteria was presented in the *HomMod* package (for details about the acceptance criteria recall Section 3.2.4). When the threshold of the loaded quality factor was exceeded, then the non-conformity report was performed and the DESY experts were notified.

START

i = 1

Set nominal parameters in VNA for a given mode (span, frequencies)

Measured passband is a monopole mode

YES

NO

Operator sets markers on 9 maxima

Operator sets 9 markers
(one for every two components representing
a single HOM resonance)

j = 1

Find maximum in 2 MHz span for j-th marker

Measure Qload and frequency for a maximum
(Execution of subroutine shown in Figure 4.13

Measured passband is a dipole mode

YES

NO

Measure Qload and frequency for 2nd peak
in 2 MHz span for j-th marker
(Execution of subroutine shown in Figure 4.13)

j = j + 1

j≤9

NO

YES

Operator decides which Qloads and
frequencies should be re-measured.
Operator performs re-measurement.

i = i +1

i≤3

NO

YES

STOP

Figure 4.12: Block diagram of the HOM spectra measurement.
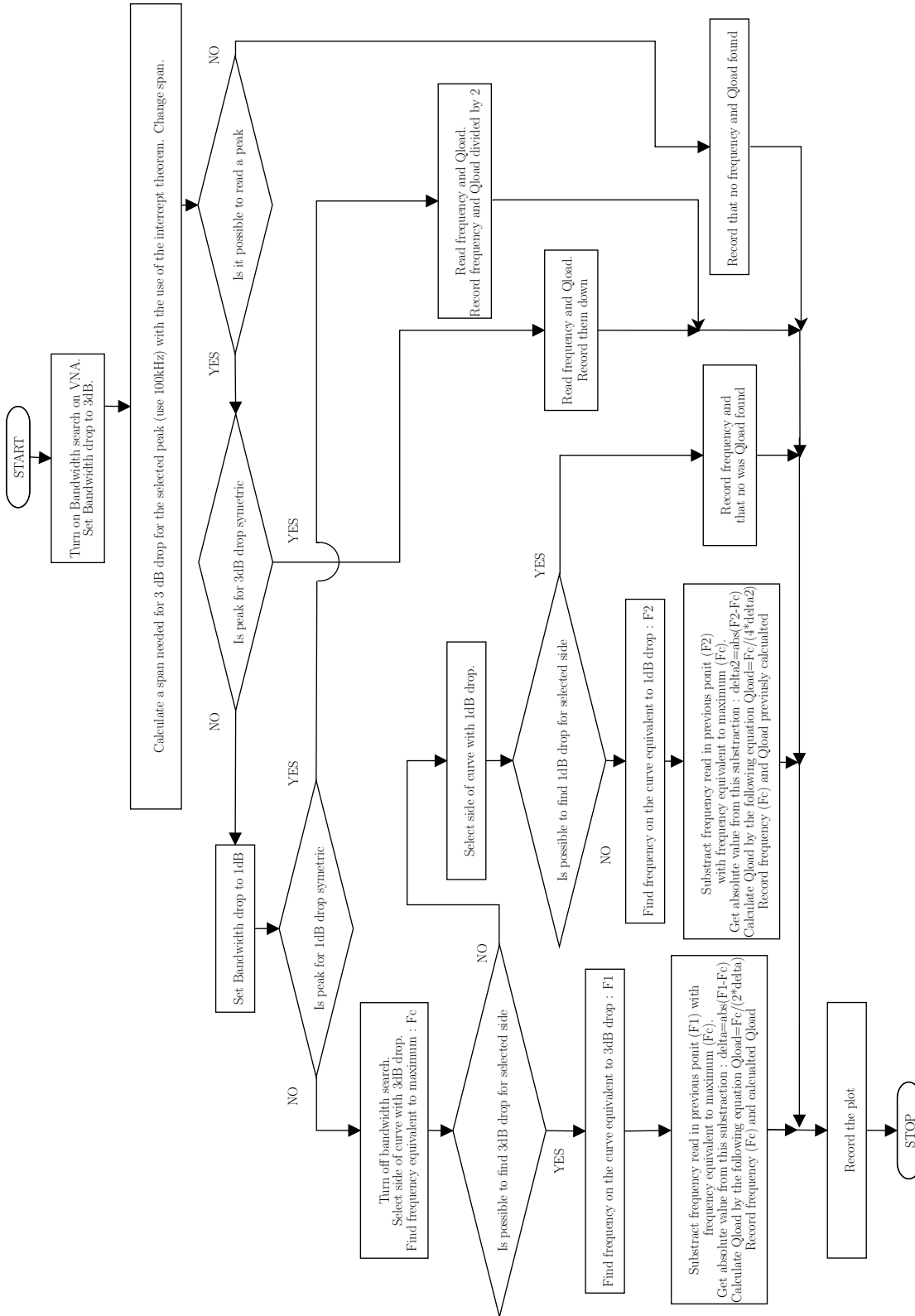
Figure 4.13: Block diagram of a quality factor measurement for HOM.

4.2.1   Methodology validation

The observations from the preparatory phase indicated that the standard test (see equation (2.28)) of the loaded quality factor [86] in the frequency domain for 3dB drop was not always measurable to determine the loaded quality factor of the dipole modes. Two components representing a single HOM resonance were often overlapped. Thus, the concept of using 1dB drop instead of 3dB for Q_{load} measurement was used and it is depicted in Figure 4.14.
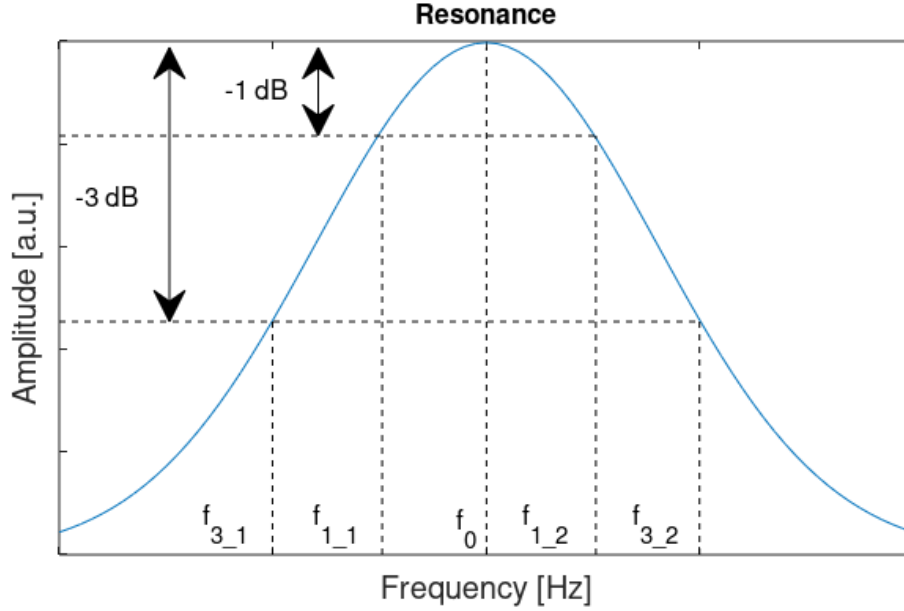
Figure 4.14: Amplitude of the driven resonator (eg. superconducting cavity).

For the 3dB drop the power ratio is 0.501, for the 1dB drop it is 0.794. Using this idea the plot (see: Figure 4.14) of the resonance was treated as a triangle, and the intercept theorem was used:

$$\frac{f_{1\_2} - f_{1\_1}}{f_{3\_2} - f_{3\_1}} = \frac{-1dB}{-3dB} \approx \frac{1 - 0.794}{1 - 0.501} \approx \frac{1}{2} \tag{4.3}$$

Using the 1dB drop the approximation of the loaded quality factor was used as follows:

$$Q_{load} = \frac{1}{2} \frac{f_0}{f_{1\_2} - f_{1\_1}} \tag{4.4}$$

This approximation was experimentally proved, practically convenient, and precise enough for the purpose of this test.

4.2.2 *HomMod* - software implementation

The concept of usage of 1dB drop instead of 3dB for Q_{load} measurement was implemented into the software *HomMod*. The software (Front Panel is presented in Figure 4.15) for the HOM spectra measurement enables to measure first two dipole modes (TE_{111} and TM_{110}) and the second monopole (TM_{011}) by setting the markers within the areas, where the quality factors should be measured. It has some additional services: loading and saving data in the database format, saving full sweep data from the VNA in raw data file, checking the acceptance criteria during the measurement, drawing of plots with loaded quality factors vs frequency and defining test parameters.
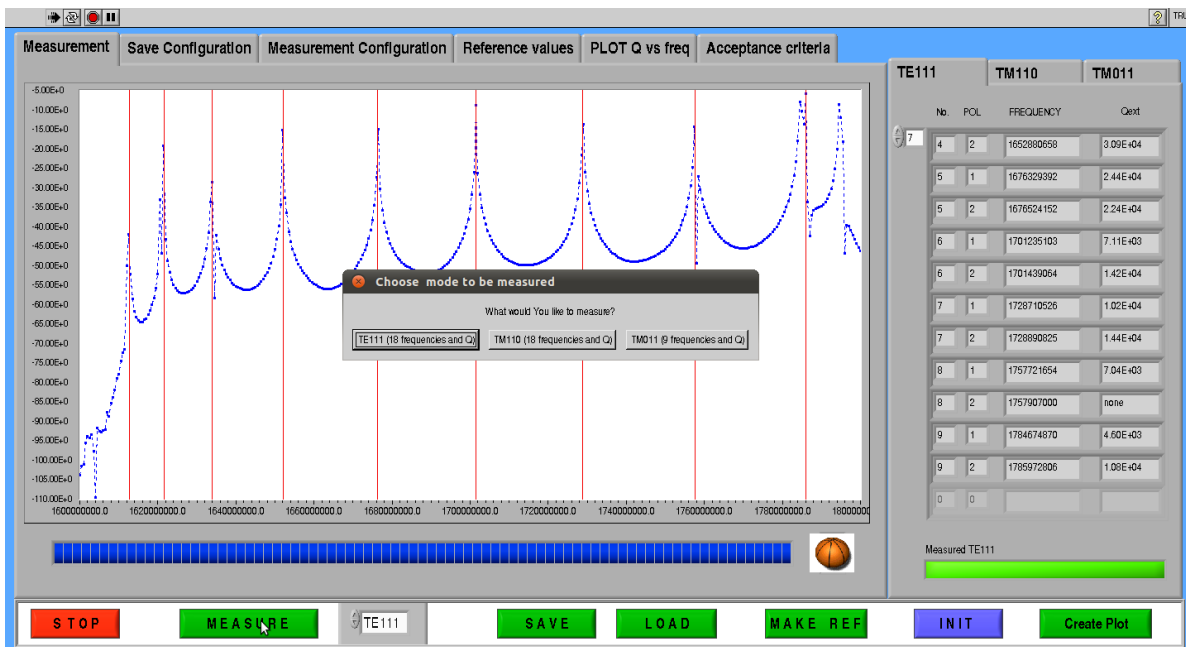
Figure 4.15: The main Front Panel of *HomMod* package.

The most common functionalities used during this measurement are listed in the additional panel of the software (see Figure 4.16). It is possible to measure the frequencies only or together with the loaded quality factors. The most common spans are also implemented. On the right side of this panel, colour boxes inform whether HOMs were measured by the software or by the operator.

Figure 4.16: The part of *HomMod* package for manual measurement.

4.2.3   HOM spectra analysis

The measurement of the HOM spectra was performed redundantly. The requirement of the maximum loaded quality factor was not specified for all resonances in the passbands because the power induced by the beam in most of the modes will be negligible. For the resonances, which were not included in the acceptance criteria, the measurement of the frequencies was carried out in order to ensure that the resonances defined in acceptance criteria are n-th in passbands.

The measurement of the 9-th resonance of the passband TM_{011} was identified as the crucial one. The first two dipole modes were well dumped (their quality factors fulfilled the acceptance criteria). In order to dump the monopole mode, the cavities needed an additional change of their shape in order to suppress the 9-th mode of the TM_{011} [48, 55]. The change of cells' shape had been done during the Field Flatness tuning. Also, the high quality of the cavity welding was a factor which improved the suppression of the 9-th mode [53]. All corrective actions were performed for single cavities before the assembly in cryomodules.

In Figure 4.17 quality factors for all measurements were presented with the acceptance criteria marked by a red line. Tests were performed during the cavity test campaign in the vertical cryostat (before installation in the cryomodule) and during the cryomodule test campaign. As for the cryomodule tests, HOM spectra was not measured for all cavities in the cryomodules. The tests were suspended from the 36th cryomodule tested. No change was observed for the quality factors measured during single cavities test campaign and during the cryomodule test campaign. The measurement was performed only for the single cavities tests in the vertical cryostats. The HOM spectra measurement was repeated during the cryomodule test campaign only for cavities, which did not fulfilled the acceptance criteria during the cavity test campaign. By skipping the HOM spectra measurement an additional reduction of the testing time was obtained.
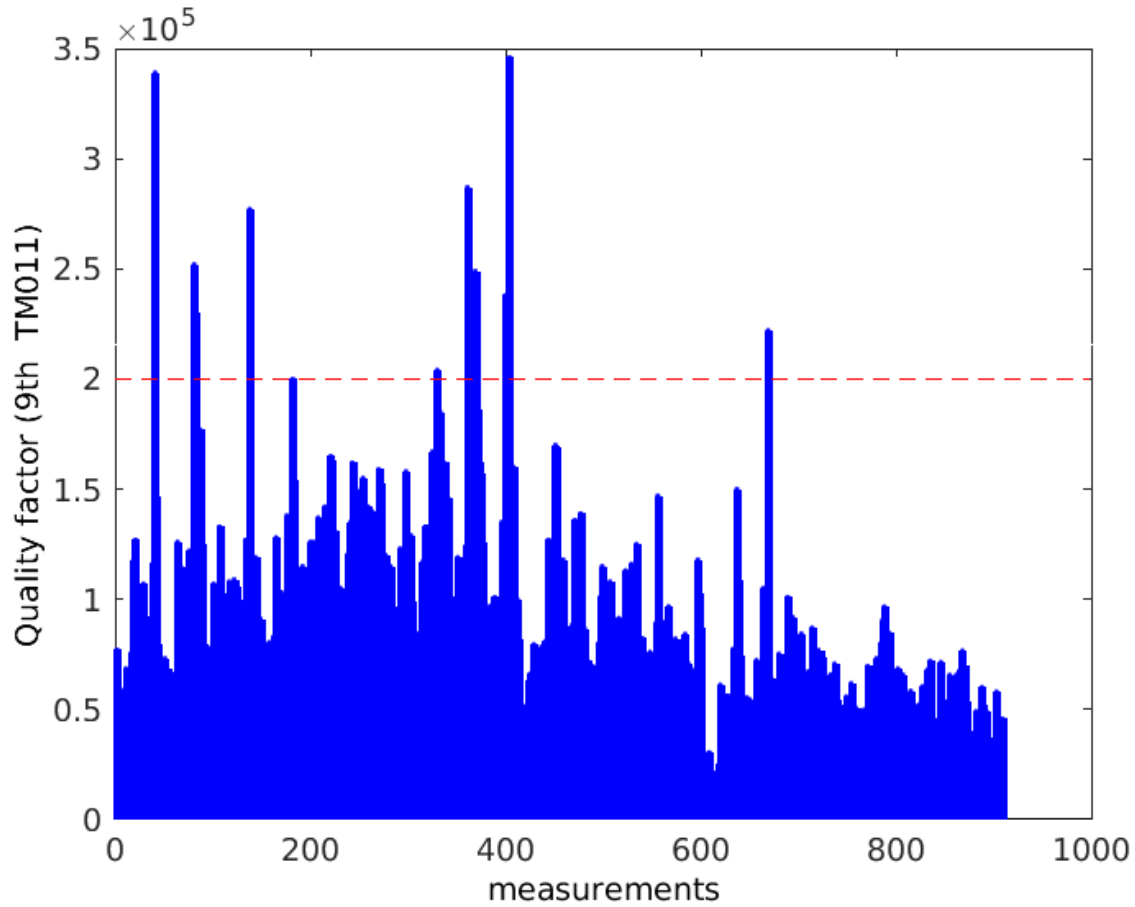
Figure 4.17: Loaded quality factor of the 9-th mode in the TM_{011} during all E-XFEL cavities measurements.

The developed *HomMod* software improved the measurement's procedure of the HOM spectra in the serial production regime. The automation of the measurement was the natural consequence of previously described improvements. The operator was not able to measure 90 values for each cavity (the frequencies and the quality factors) as fast as software did it. Furthermore, the human error was also eliminated. The operator had the full control of the values of the acceptance criteria. Moreover, the approximation of the quality factor in the frequency domain, while 1dB drop was used instead of 3dB, was successfully used for the E-XFEL measurements. This idea was also used to measure the quality factors of HOMs for other cavities, for example, for those tested at CERN [87, 88].

4.3   High RF power cryomodule measurements

The high power measurements, namely Flat-Top (FT) and Heat Loads, were performed in order to test the own quality factor and the accelerating gradient. The purpose of the FT measurement was to determine the operating and the maximum gradient of the cavity in the cryomodule (details are described in section *3.3.5*). The operating gradient is the working point for the cavities operation in the accelerator. The objective of the HL measurement was to determine the thermal loads during the normal cryomodule operation (details are described in section *3.3.6*). The result of the Heat Loads measurement was the average own quality factor of all cavities in the cryomodule.

4.3.1   Lorentz Force Detuning

The high power measurements measurements of the cavities in the cryomodules require perfect fine-tuning to ensure the correctness of the measured parameters of the cavity. During the preparatory phase for the cryomodule test campaign (2010-2011), the cavities were tuned based on the analysis of the phase difference between the voltage from RF generator and the phase of the *transmitted* signal (see Figure 3.21). In this method of the cavity's fine-tuning the operator activated only the step motor in order to keep the phase difference constant during the Flat-Top (FT) time of the pulse. Above 20 MV/m of the measured gradient, the limit for the cavity tuning with the step motor was reached due to the Lorentz Force Detuning (LFD), which requires much faster mechanical reactions. As a consequence, the author's idea was to tune the serial-production cryomodules by automatically adjusting each cavity's piezo[*] and step motor.

Every step motor's fine-tuning lasted few seconds, while adjustment of the cavity length with the piezo is possible for every pulse ($10Hz$). The piezos have two functions. In the first function the piezo adjusts the cavity statically in the same way like the step motor does - to counteract the changes of *forward* power and to counteract the helium level change. In the second function, the piezo adjusts the cavity length dynamically before (and/or during) the RF pulse to counteract the microphonics and the mechanical frequency oscillation of the cavity induced by the Lorentz Force. The second functionality is not realizable by the step motor.

---

[*]Piezoelectric sensors and piezoelectric actuators are shortly named piezos.

The piezo signal (see Figure 4.18) used for the cavity fine-tuning was a full period of a sinusoidal signal on the top of a bias voltage and was described by:

- DC voltage - a bias signal that is adjusting the cavity length in the same way like the step motor,

- AC voltage - amplitude of the sinusoidal signal,

- Advance - time before the beginning of the RF pulse, when the sinusoidal distortion is applied to the piezo, and consequently to the cavity, in order to induce mechanical frequency oscillation in the cavity that counteracts the detuning change before the RF pulse appears,

- Actuator Frequency - a frequency (< 1 kHz) of the sinusoidal signal.

The signal shape applied to the piezo actuator does not have to be sinusoidal. For E-XFEL, the sinusoidal shape was chosen because of the experience with the sinusoidal shape technique applied to the FLASH accelerator [91, 93, 94]. The rectangular or the trapezoidal shapes are also used in other projects [89, 90].
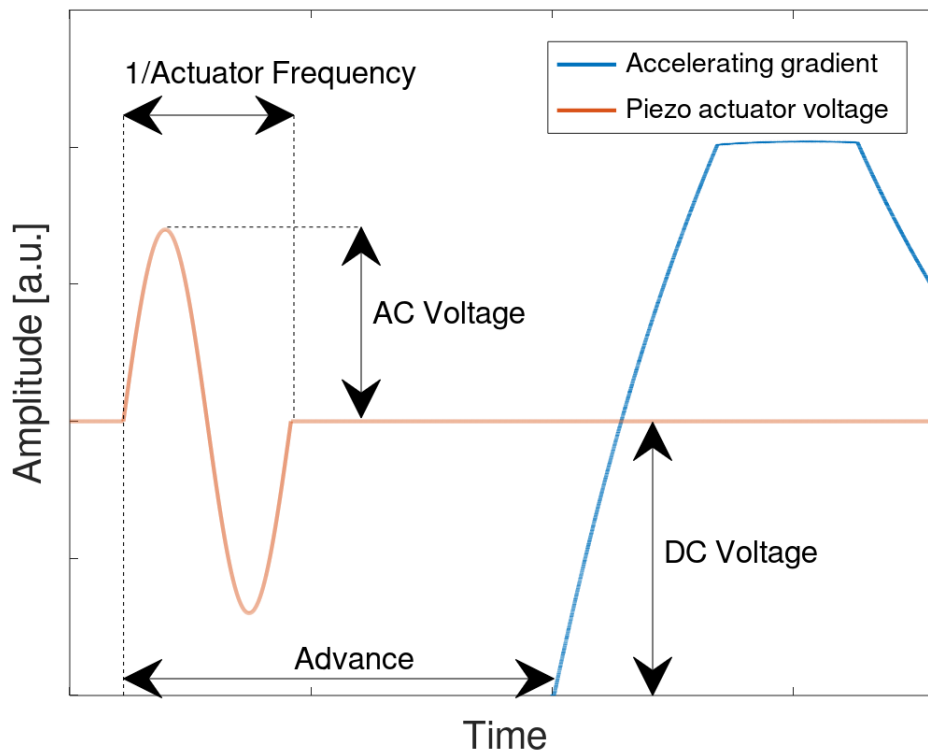
Figure 4.18: Piezo actuator parameters in relation to the RF pulse (cavity gradient).

The author's idea was to adjust the cavity length with the use of both the piezo and the step motor for 8 cavities in the cryomodule with the use of the *TuneCAV* package. The piezo was used for the fine tuning ($\leq\sim 3\mu m$) in the two previously mentioned functions: statically and dynamically. The step motor was used for the rough tuning ($>\sim 3\mu m$) and for the relaxation of piezo's DC voltage (decreasing to zero) in order not to exceed the piezo voltage "budget". The voltage "budget" was the piezo driver limit for the sum of AC and DC voltage.

The piezo parameters were obtained and modified with the use of the Distributed Object Oriented Control System (DOOCS) [95]. DOOCS is a software and a hardware, which provides an access to control parameters of all the devices in the AMTF via network. Thus, in *TuneCAV* package, DOOCS is used to control steps of the step motor and 4 piezo parameters.

4.3.2 Cavity RLC Model

In the *TuneCAV* package, the calculation of the difference between the cavity's resonant frequency and the *forward* signal frequency during the RF pulse was based on the model of RF system. The model is presented in Figure 4.19. The model is used to describe the transient behaviour of the cavity during the RF pulse and the energy transfer between the klystron, the cavity and the beam. In order to describe the transient behaviour of the cavity during the measurement, the beam is excluded from the model. The differential equation of a harmonic oscillator, which is describing the circuit of the RF system with the cavity, was used, for example, by Schichler [61], Przygoda [91] or Brandt [96]:

$$\frac{\partial^2 V_c}{\partial t^2} + \frac{1}{R_L C}\frac{\partial V_c}{\partial t} + \frac{1}{LC}V_c = \frac{1}{C}\frac{\partial I_c}{\partial t} \tag{4.5}$$
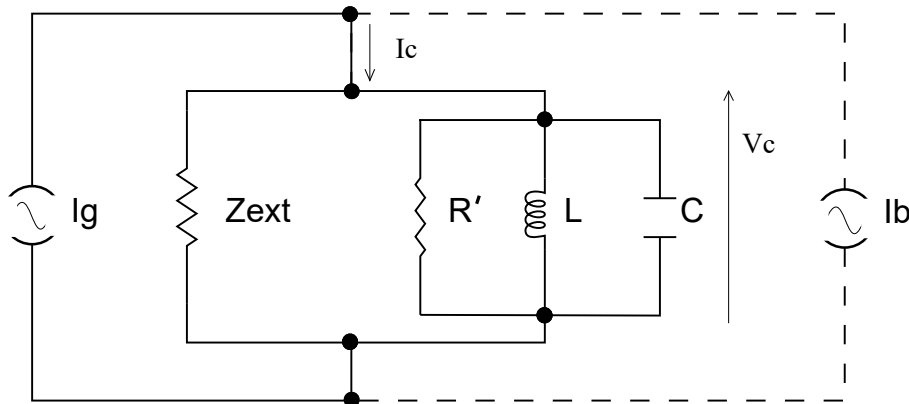
Figure 4.19: The RF system model.

Where:

- C,L,R$'$ - capacitance, inductance and resistance of RF cavity,

- Z$_\text{ext}$ - external load impedance - represents losses from the generator (klystron) to the cavity - mainly of the input power coupler [61],

- R$_\text{L}$ - loaded shunt impedance (parallel connection of the two parameters R$'$ and Z_{ext}). The power stored in the LC part of the cavity is dissipated in the cavity walls (R'), but the major part is dissipated outside of the cavity (Z_{ext}) [61]. Thus the external losses are transferred to the cavity,

- V$_\text{c}$ - cavity (*transmitted*) voltage,

- I$_\text{c}$ - cavity current,

- I$_\text{g}$ - generator (klystron) current,

- I$_\text{b}$ - beam current.

The parameters of the cavity [61, 96] are expressed by the parameters of the model and they are listed in Table 4.1. The parameters of the cavity are applied to equation (4.5):

$$\frac{\partial^2 V_c}{\partial t^2} + \frac{1}{\tau}\frac{\partial V_c}{\partial t} + \omega_0{}^2 V_c = \frac{R_L}{\tau}\frac{\partial I_c}{\partial t} \tag{4.6}$$

Parameter	Equivalent	
ω_0	$\dfrac{1}{\sqrt{LC}}$	resonant frequency of an undamped cavity
Q_0	$R'\sqrt{\dfrac{C}{L}}$	unloaded quality factor
R	$2R'$	shunt impedance
R/Q	$2\sqrt{\dfrac{L}{C}}$	geometric shunt impedance
Q_{load}	$R_L\sqrt{\dfrac{C}{L}}$	loaded quality factor
τ	$R_L C$	decay time

Table 4.1: RF cavity parameters listed in section 2.5 and their equivalents [61].

The cavity (*transmitted*) signals are sinusoidal: $e^{j\omega t}$, where j is the imaginary unit and ω is a generator (*forward*) angular frequency. The V_0 and I_0 are slowly varying in time amplitudes of cavity voltage and current. The example of the amplitude of the *transmitted* voltage during the high power measurements was already presented in the Figure 3.20.

$$V_c = V_0 e^{j\omega t}, \quad \frac{\partial V_c}{\partial t} = (\frac{\partial V_0}{\partial t} + j\omega V_0)\, e^{j\omega t}, \quad \frac{\partial^2 V_c}{\partial t^2} = (\frac{\partial^2 V_0}{\partial t^2} + 2j\omega\frac{\partial V_0}{\partial t} - \omega^2 V_0)\, e^{j\omega t} \quad (4.7)$$

$$I_c = I_0 e^{j\omega t}, \quad \frac{\partial I_c}{\partial t} = (\frac{\partial I_0}{\partial t} + j\omega I_0)\, e^{j\omega t} \quad (4.8)$$

From equations (4.6), (4.7) and (4.8) one sees that:

$$\frac{\partial^2 V_0}{\partial t^2} + \frac{\partial V_0}{\partial t}(2j\omega + \frac{1}{\tau}) + V_0(j\omega - \omega^2 + \omega_0{}^2) = \frac{R_L}{\tau}(\frac{\partial I_0}{\partial t} + j\omega I_0) \quad (4.9)$$

Dividing equation (4.9) by $2j\omega$ one may observe that:

- $\frac{\omega_0{}^2 - \omega^2}{2\omega} \approx \omega_0 - \omega = \Delta\omega$: **cavity detuning** - a frequency difference between the frequency from the generator and the resonant frequency of the cavity,

- $\frac{1}{2\tau\omega} \approx 0$,

- $\frac{\partial^2 V_0}{\partial t^2}$ is much smaller than other terms in the equation (4.9),

- $\frac{\partial I_0}{\partial t}$ is negligible.

Taking into account these assumptions the equation (4.9) is reduced to the following form:

$$\frac{\partial V_0}{\partial t} + (\frac{1}{2\tau} - j\Delta\omega)V_0 = \frac{1}{\tau}R_L I_0 \quad (4.10)$$

One might notice that the complex signals representation is also proper [61, 96] and that the $R_L I_c$ may be represented by the V_{for} - *forward* voltage:

$$\frac{\partial V_c}{\partial t} + (\frac{1}{2\tau} - j\Delta\omega)V_c = \frac{1}{\tau}V_{for} \quad (4.11)$$

The detuning is finally calculated as a real part from the following equation with the use of the complex *forward* and *transmitted* voltages [92]:

$$\Delta\omega = \text{Re}(\frac{\frac{\partial V_c}{\partial t} - \frac{V_{for}}{\tau} + \frac{V_c}{2\tau}}{jV_c}) \quad (4.12)$$

The detuning ($\Delta\omega$) defines the difference between the actual frequency of the cavity and the source frequency. It is calculated for the whole duration of the RF pulse, for the *forward* and *transmitted* voltages. The τ - decay time is calculated from the amplitude of the *transmitted* voltage from the previous pulse (see Figure 2.7).

The detuning ($\Delta\omega$) within the RF pulse, before the fine tuning takes place, is presented in Figure 4.20. For the *TuneCAV* control package, three parameters were defined as the representation of the detuning within the Flat-Top time: Static Detuning (SD), Dynamic Detuning (DD) and Lorentz Force Detuning (LFD):

$$SD = \frac{\Delta\omega_{FTstart} + \Delta\omega_{FTstop}}{2} \tag{4.13}$$

$$DD = \Delta\omega_{FTstop} - \Delta\omega_{FTstart} \tag{4.14}$$

$$LFD = abs(SD) + abs(DD) \tag{4.15}$$
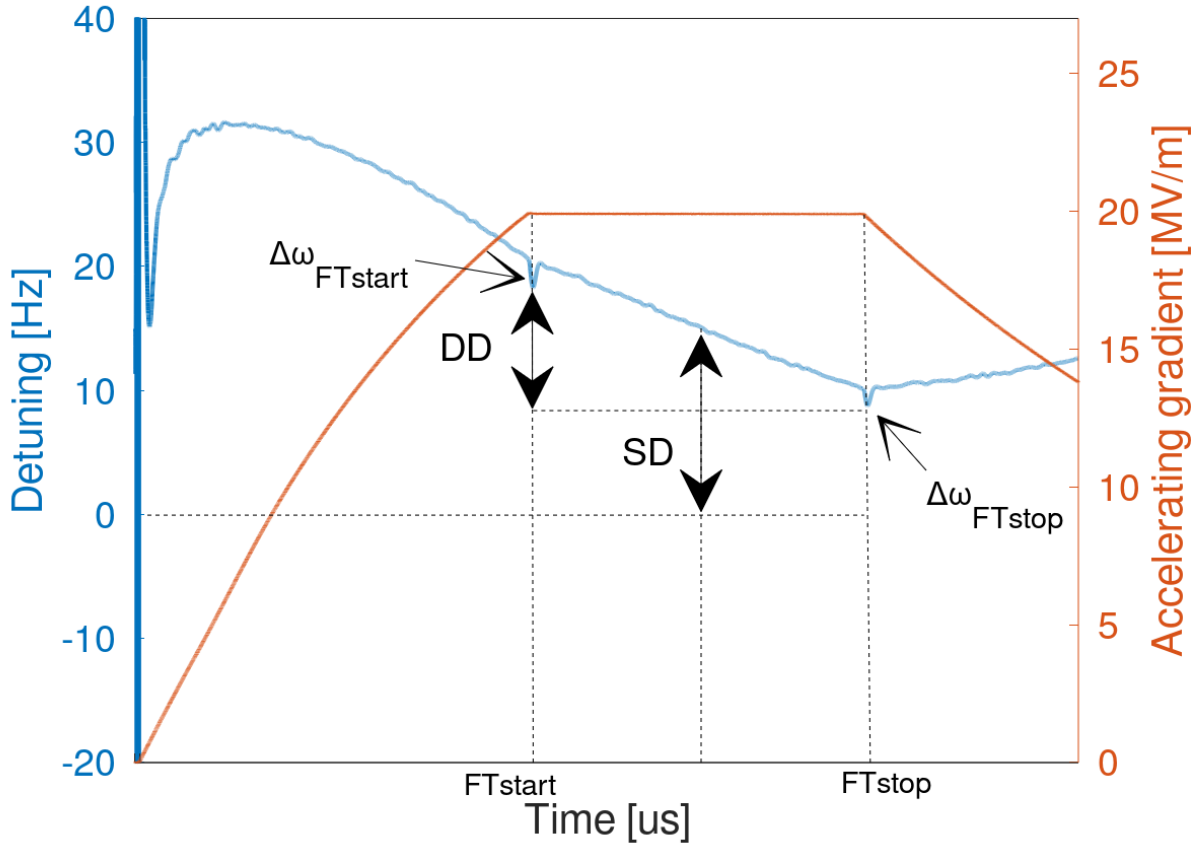
Figure 4.20: Cavity detuning during the RF pulse.

The Static Detuning (SD) is the cavity detuning value in the middle of the Flat-Top (FT) duration and is calculated by author as an average value of the detuning at the end and at the start of the FT. The Dynamic Detuning (DD) is calculated as the difference between values at the end and at the start of the FT. The values used to calculate SD and DD are taken some μs closer (with respect to the middle of the FT) to avoid non-linearities in these points. Finally, the Lorentz Force Detuning is defined as the sum of absolute values of the SD and the DD. LFD is a parameter describing the quality of the tuning.

4.3.3   Cavity tuning algorithm

The control package *TuneCAV*, was composed of two stages: initialization and control. During the initialization stage, two piezo default parameters: *frequency* and *advance time*, were set for each cavity and stayed unchanged during the cavity tuning. The initialization stage was done for "middle" gradients ($\sim 15 - 20\,MV/m$), when the Lorentz Force is noticeably influencing the cavity behaviour, but is still compensated only by the step motor. As mentioned before, above 20 MV/m of the measured gradient, the limit for tuning of the E-XFEL cavity with the step motor will be reached.

During the control stage three controllers were used in order to minimize SD and DD. Here a noticeable improvement was made in comparison to the FLASH methodology. Two controllers were used to adjust the length of the cavity in order to minimize the SD. The first controller was used to steer the step motor ($|SD| >= 1\,kHz$). The second one was used to adjust the extension or contraction of the cavity with the use of the piezo actuator's *DC voltage* for smaller SD ($|SD| < 1\,kHz$). The third controller was counteracting the mechanical resonance of the cavity excited by the RF pulse. It adjusted the *AC voltage* in order to compensate the cavity length change caused by the upcoming RF pulse (see: Figure 4.18). Each of the above mentioned stages are discussed in details in the following sections.

Initialization (mechanical frequency)

During the initialization phase the mechanical frequency response (< 1 kHz) to the RF pulse was measured. The response was measured from the voltage oscillations of the piezo sensor, which was connected to the cavity. The mechanical frequency was calculated (with the use of the Fast Fourier-Transformation (FFT)) from the piezo sensor signal for each cavity in the cryomodule. The amplitude of the *AC* and *DC voltages* on the actuators were reduced to 0 (ZERO) to avoid the situation, in which the frequency induced by the piezo actuator could have been measured on the piezo sensor.
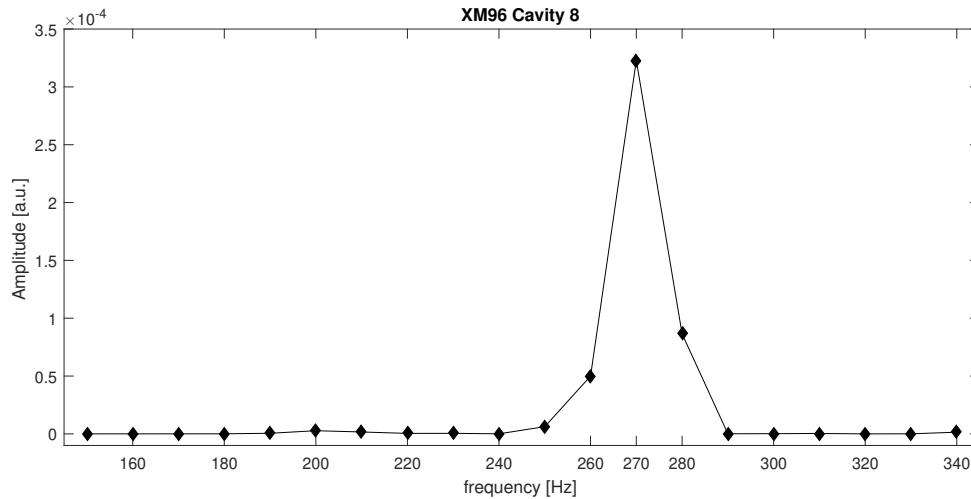
Figure 4.21: Mechanical resonance - frequency identification using piezo.

In Figure 4.21 the typical result of the FFT calculation is presented. The plotted range was shortened to the default frequency band. Only single mechanical resonance, out of 3 expected, was excited significantly. This mechanical resonance frequency was in the range of 200-300 Hz.

The block diagram of the mechanical frequency search is presented in Figure 4.22.
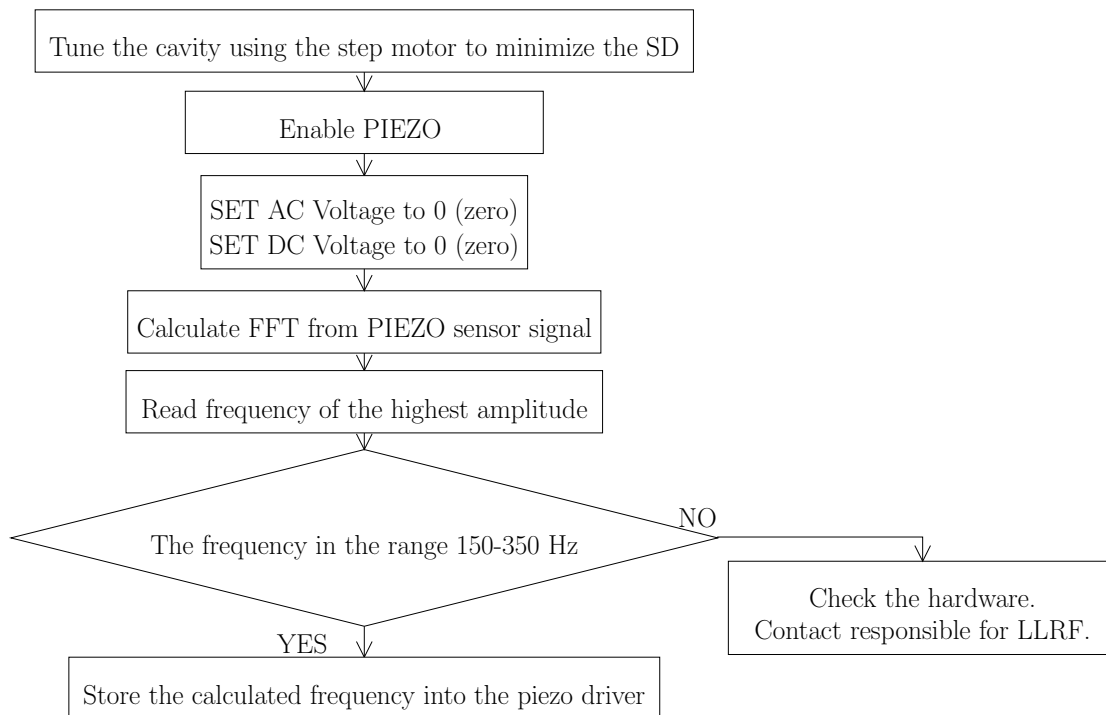
Figure 4.22: Block diagram of the cavity mechanical frequency response search.

Initialization (advance time)

Using the previously found cavity mechanical frequency, the optimum *advance* time was searched. The *advance time* was a time when the piezo actuator should apply the sinusoidal signal in order to minimize the cavity mechanical oscillation (detuning) caused by the pulsed RF signal (see Figure 4.18). In this case, sinusoidal voltage (-5V of *AC voltage*) was applied to piezo actuator in order to suppress the cavity mechanical frequency. The cavity reaction as Dynamic Detuning to the piezo signal was measured. The procedure was repeated for a different *advance* time. Each step was recorded and formed a DD vs *advance time* distribution. The minimum value (see Figure 4.23) of this scan was used as the *advance time* (in case of the piezo reversed polarity - maximum).
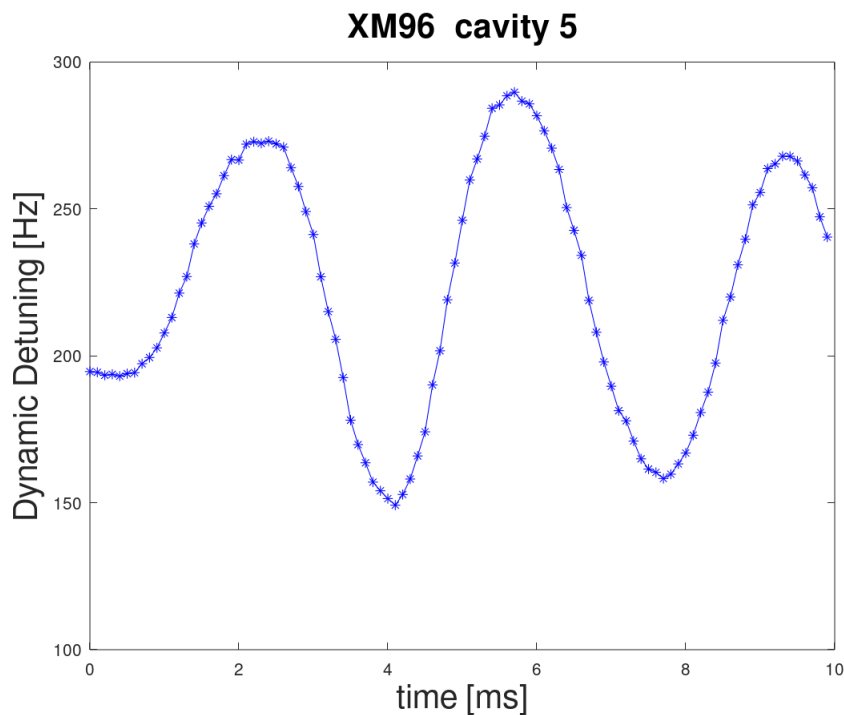
Figure 4.23: Advance time identification using piezo

During the scan 2 or 3 minima were observed on the plot. The minima and maxima were the result of stimulating the piezo which was connected mechanically with the RF cavity. The time of minima depended not on the gradient but on the frequency of the sinusoidal signal applied to the piezo actuator. For similar minima, the initialization procedure had to be done again at higher gradients to clarify the best *advance time* - to enhance the effect from Lorentz force. Consequently, the *advance time* ranged $3 - 5ms$, which corresponded to 200-333 Hz of the cavity mechanical resonance. The optimum value of the advance time was not shorter than that period.

-5V (minus five) of *AC voltage* was quite small in comparison to the maximum value used during the AMTF measurements ($\pm$ 65 V), but large enough to assure, that the

changes of the DD during the advance time scan were observable. In case of the highest voltage, the crossing of 0 (zero) took place on the DD plot and, in consequence, the wrong advance time was identified. In order to choose the right value of the *AC voltage* several values between -65V ÷ +65V had been checked and finally -5V was used. The *advance time* corresponds to the period of the *frequency* and together with the polarity of the *AC voltage* they correspond to the appropriate phase of the sinusoidal distortion.

During the optimization of the software some other observations were made. For a part of cavities, during the measurements, the gamma (X-rays) radiation was observed as a result of e.g. field emission. Wrong advance time was found when gamma radiation was rapidly changing during the DD advance time scan, because changes of the field emission considerably influence the cavity detuning, gradient and sometimes induce the cavity quench. For the cavities without measurable field emission, it was recommended to perform this step with the highest possible gradient.

To sum it up, during the initialization stage and for a given cavity frequency, the optimum advance time was found in order to counteract the upcoming RF pulse and to suppress the single cavity mechanical resonance during the cavity operation. The block diagram of the advance time identification algorithm is presented in Figure 4.24.
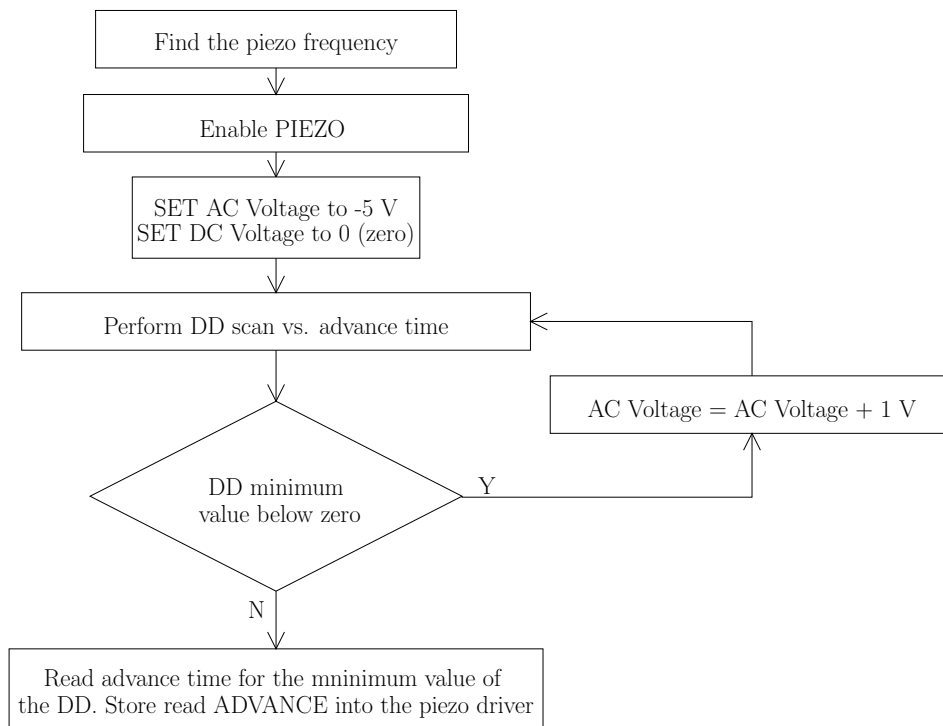
Figure 4.24: Block diagram of the *advance time* identification algorithm

Piezo and step motor controllers

As mentioned before *TuneCAV* package had 3 controllers. The first one was minimizing the DD (see equation (4.14)) by adjusting the AC voltage. The second and third controllers were reducing the SD (see equation (4.13)) and they were working separately. When the second controller was setting the signal, the third one was not active and vice versa (depending on the detuning value $\Delta\omega$). The second controller was adjusting the DC voltage and the third was changing the steps of the step motor. The Set Points (SP) for all were zero.

Below, the block diagrams of 3 control systems were presented as well as 3 formulas. According to these equations, the piezo signals or the steps of the step motor were changed:

a) Piezo Dynamic Detuning controller
   AC voltage = AC voltage + GainDD · DD
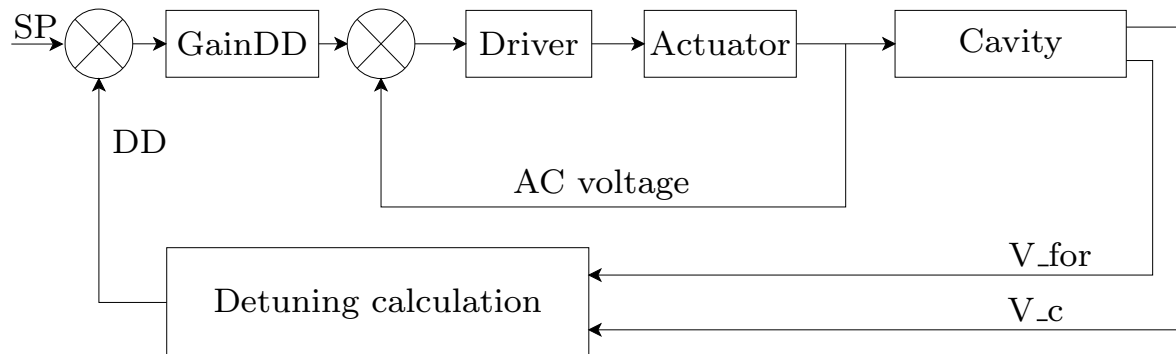
Figure 4.25: Piezo control system for minimizing the DD.

b) Piezo Static Detuning controller
   DC voltage = DC voltage + GainSD · SD
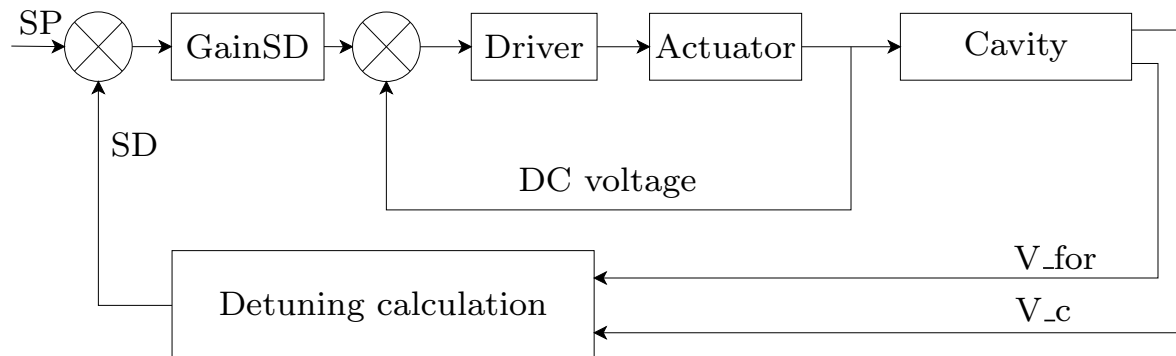
Figure 4.26: Piezo control system for minimizing the SD.

c) Step motor Static Detuning controller
   STEPS = STEPS + GainStepMotor · SD
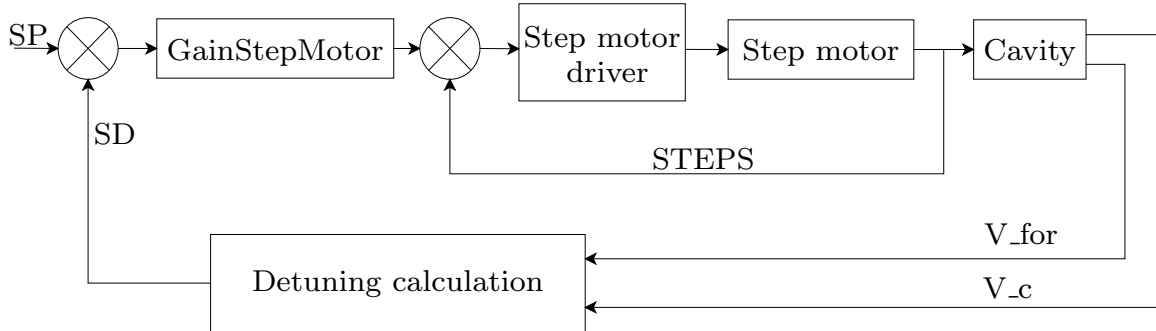
Figure 4.27: Step motor control system for minimizing the SD.

The methodology included an approach of integration of the automatic control using both types of the controllers (piezo and step motor) for cavities testing. The measurements were also done in parallel for all cavities in the cryomodule. It is worth to notice that the control of the SD was set either by the slow tuner or by the piezo DC voltage controller. For normal operation, the step motor was used for the cases, in which the detuning was too large ($> 1kHz$) and using the full piezo "budget" was not sufficient due to the fact that it was limited by the driver: 65 V for the sum of *AC* and *DC voltage*. Moreover, the algorithm also included piezo relaxation. When any of the software limits for piezo "budget" was exceeded, then some additional steps were performed by the step motor ("over-tuning"). It gave piezo the possibility to reduce the *DC voltage* to zero.

4.3.4 *TuneCAV* - software implementation

The tuning algorithm described in previous sections was implemented into the *TuneCAV* package to control steps of the step motor and 4 piezo parameters. In the Figure 4.28 the LabVIEW Front Panel of *TuneCAV* package during the Heat Loads measurement is presented. All four parameters (*DC voltage, AC voltage, frequency, advance time*) are listed for each piezo. It is possible to see each parameter of the Lorentz Force Detuning (LFD) and control the tuning separately for each cavity. When pressed "Init" button, the procedure of finding the optimum advance time and frequency is performed as well. Besides there are plots in the right side of the panel, which could have been saved
(see: Figures 4.28, 4.29, 4.30):

- Detuning plots in the RF pulse
- LFD since start of the software
- SD and DD separately since start of the software
- Signals from piezo actuator and sensor
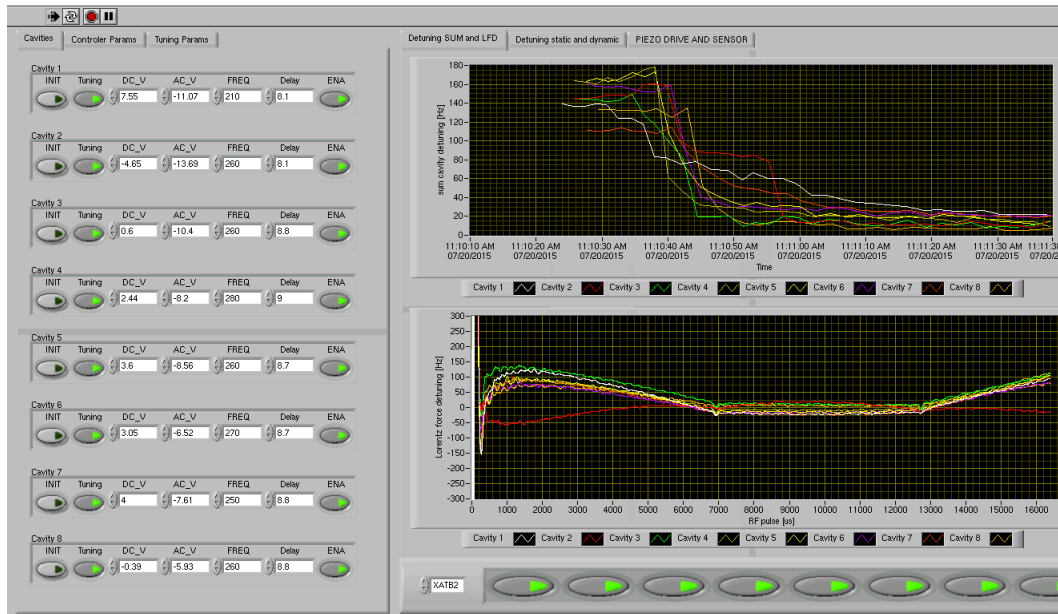
Figure 4.28: The LabVIEW Front Panel for *TuneCAV* package. Tabs: "Cavities" and "Detuning SUM and LFD".
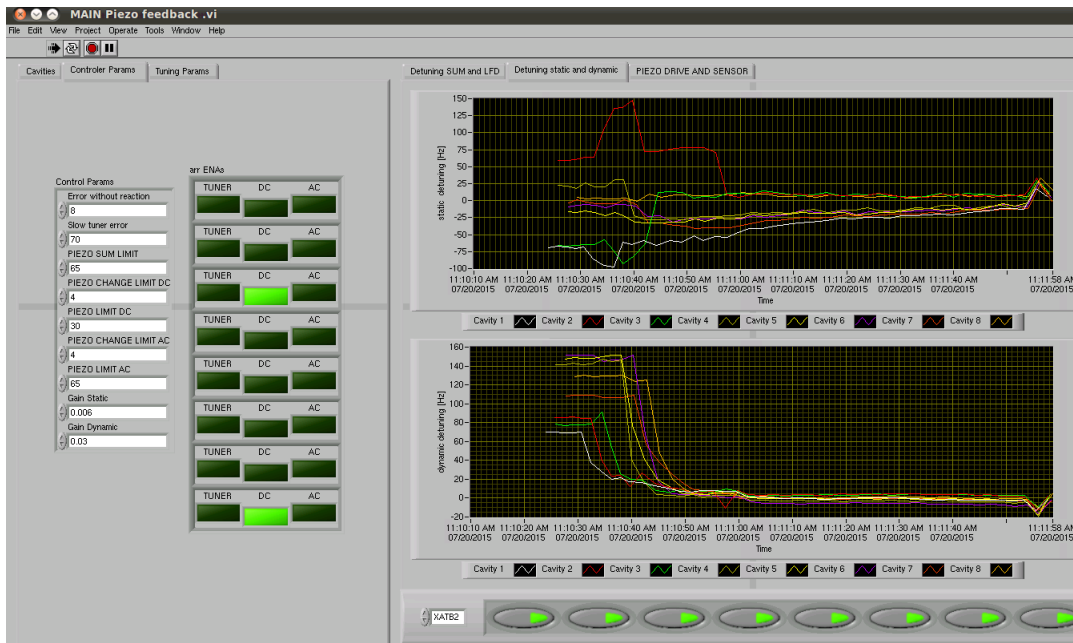
Figure 4.29: The LabVIEW Front Panel for *TuneCAV* package. Tabs: "Controller Params" and "Detuning static and dynamic".

As mentioned before, because piezos and step motors have some physical limitations, the software limiters are included in the package. For the expert users, these parameters are configurable from the main panel (see the Figure 4.29):

- Error without reaction - DD or SD value, below which the controllers do not react

- Slow tuner error - value of the SD, when the step motor is used instead of the piezo

- PIEZO SUM Limit - maximum used value of the piezo voltage. When exceeded the piezo DC voltage is relaxed by the step motor.

- PIEZO Change LIMIT DC - maximum voltage change of the DC part

- PIEZO LIMIT DC - maximum value of the piezo DC voltage. When exceeded the piezo *DC voltage* is relaxed by the step motor.

- PIEZO Change LIMIT AC - maximum voltage change of the *AC voltage*

- PIEZO LIMIT AC - maximum value of the piezo *AC voltage*

- Gain Static - proportional gain of the controller for the PIEZO *DC voltage*

- Gain Dynamic - proportional gain of the controller for the PIEZO *AC voltage*

Furthermore during each iteration of the controller it is visible, which one changes the parameter of the piezo or the step motor (see lights in the left side in the Figure 4.29). Moreover values of SD, DD, LFD are presented (see Figure 4.30).
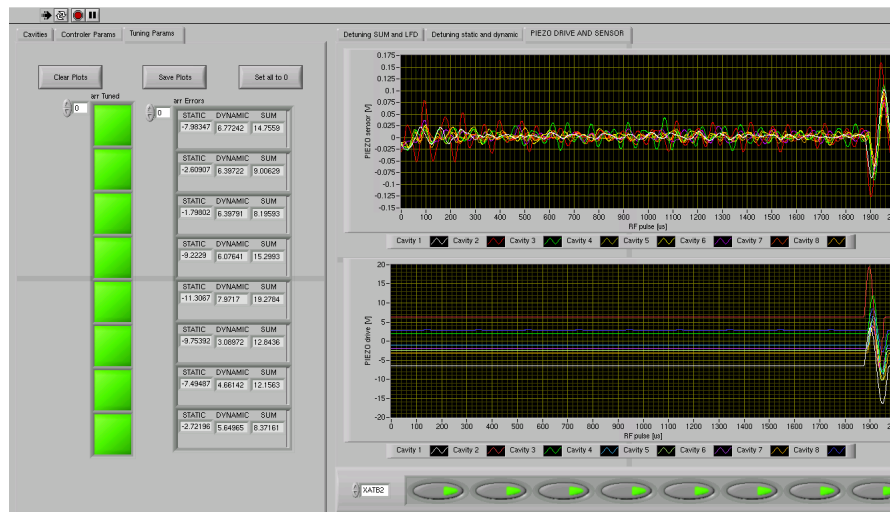
Figure 4.30: The LabVIEW Front Panel for *TuneCAV*. Tabs: "Tuning params" and "Piezo drive and sensor".

The methodology of the package is presented in Figure 4.31, where the block diagram of the developed *TuneCAV* software is shown. The methodology was also investigated based on the measurements and is presented in the following sections.
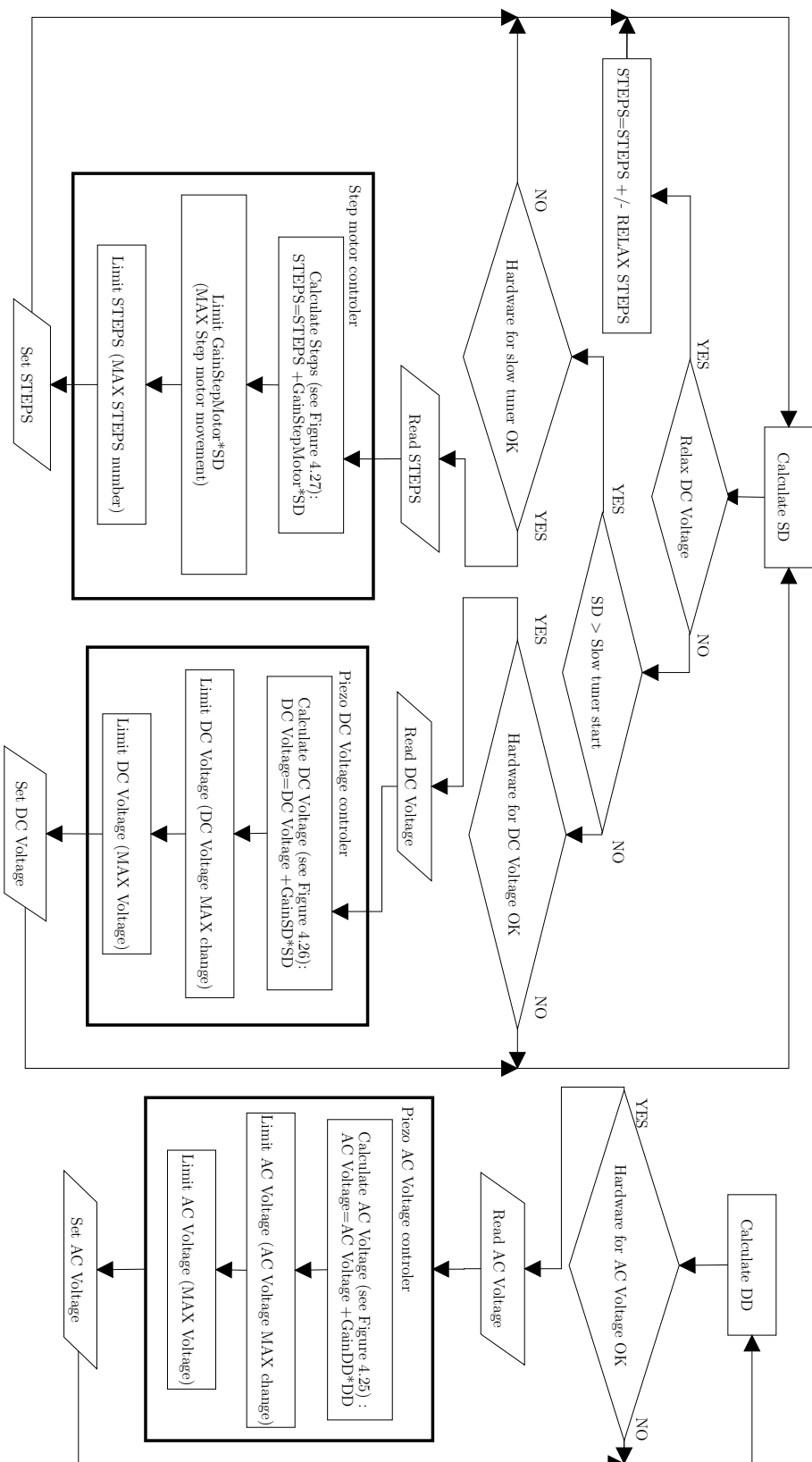
Figure 4.31: Block diagram for piezo and step motor controllers, which is describes the *TuneCAV* package.

4.3.5   High power RF measurements - results analysis

TuneCAV package used to tune the cavities in the cryomodules improved the quality of the following measurements: the Flat-Top, the Lorentz Force Detuning compensation and the Heat Loads. This software was prepared in two versions. In the first one [72, 97, 98], the application included only the tuning part with 3 controllers. The final version included the initialization part. *TuneCAV* package was applied after tests of first 15 cryomodules.

Lorentz Force Detuning compensation for the maximum gradient

The measurements made during the cryomodule test campaign confirmed that *using the automated measurements with the cavity RLC model significantly improves the cavity detuning.* In Figures 4.32 and 4.33, one may find the absolute values of the Static Detuning and Dynamic Detuning stored in the testing time order. These values were measured and recorded for the maximum gradient during the Flat-Top measurement. The types of tuning were coloured differently. First, the tuning was performed manually (blue), then using the first (green) and final version (red) of *TuneCAV* package.
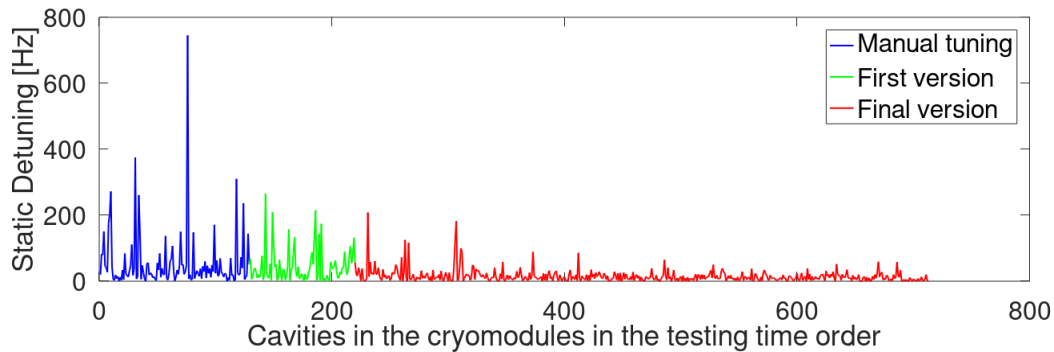
Figure 4.32: Absolute values of the SD for each E-XFEL cavity in the testing time order saved during the Flat-Top measurement.
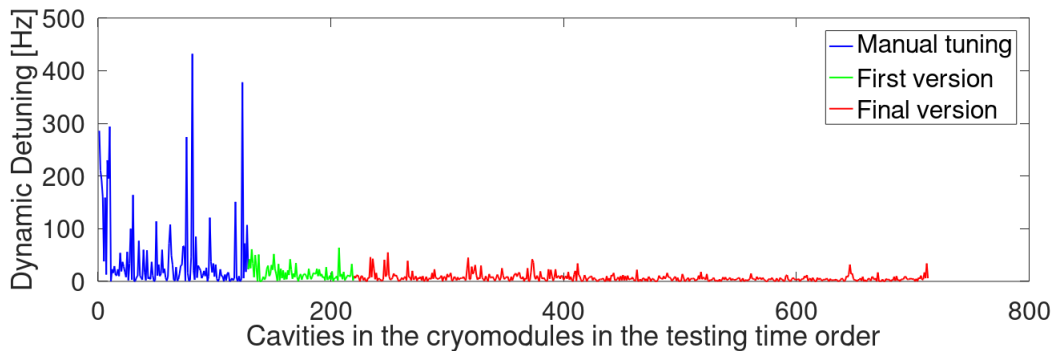
Figure 4.33: Absolute values of the DD for each E-XFEL cavity in the testing time order saved during the Flat-Top measurement.
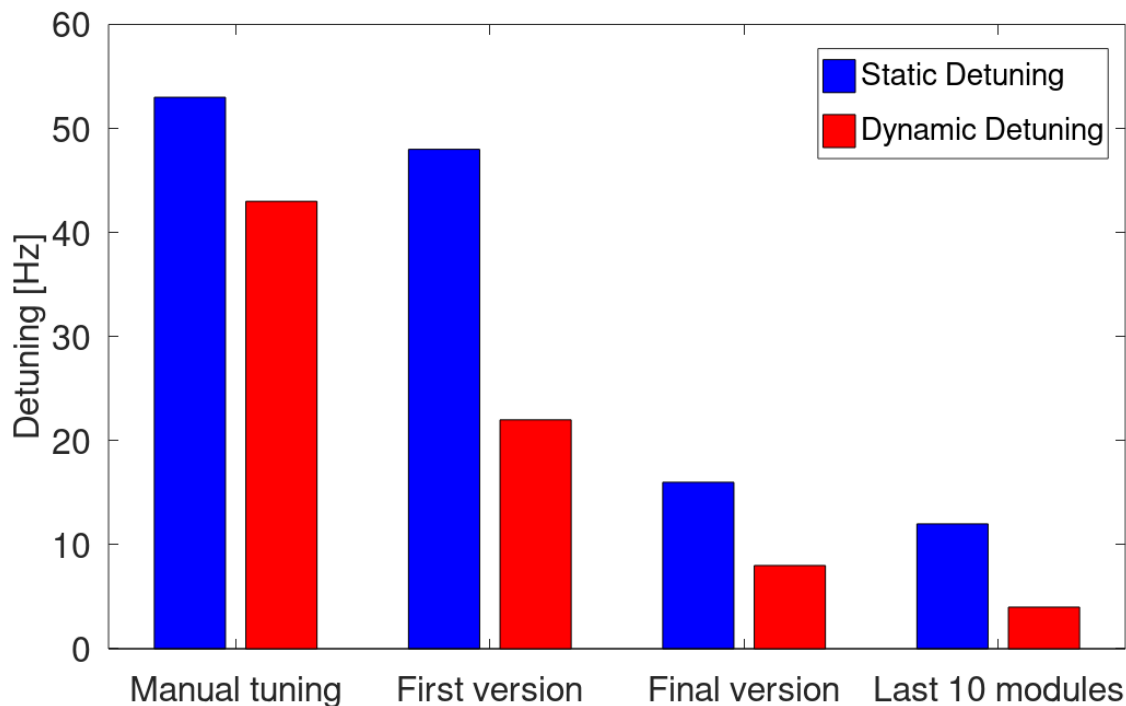
Figure 4.34: Average value of the absolute values of the SD and DD saved for the various *TuneCAV* software status.

The average value (see: Figure 4.34) of absolute values of SD, while using the final *TuneCAV* package version, was decreased more than 3 times in comparison to the manual tuning. The DD was decreased 6 times. It meant that the cavities were better tuned with the final version of *TuneCAV* software. The average values of the cavities in the last 10 modules were also compared. They were also improved because, during the last tests, the parameters of the controllers in the *TuneCAV* package were optimized.

After analysing the results of the Lorentz Force Detuning compensation, it was noticed that *TuneCAV* package could be further improved. Firstly, it was presented [91] that 10 Hz threshold for LFD was attainable for FLASH cavities. However, the average results given in Figure (see: Figure 4.34) exceeded this threshold. It stems from the fact that *TuneCAV* package was implemented as a high level software in LabVIEW. Thus, for 10 Hz repetition rate, the parameters of the piezo and the step motor were changed every second.

Secondly, the author found also another explanation of exceeding of 10 Hz threshold for the LFD. It was found in the detuning plot during the RF pulse. In Figure 4.35, an representative example is presented of a detuning plot for the cavity at the high gradient. The detuning plots for a single measurement for cavity 3 in the module XM100 are presented at 29 MV/m in two different ranges and scales. Analysing the blue plot, no relevant information about the reason for exceeding the 10Hz of LFD was visible. Such range was
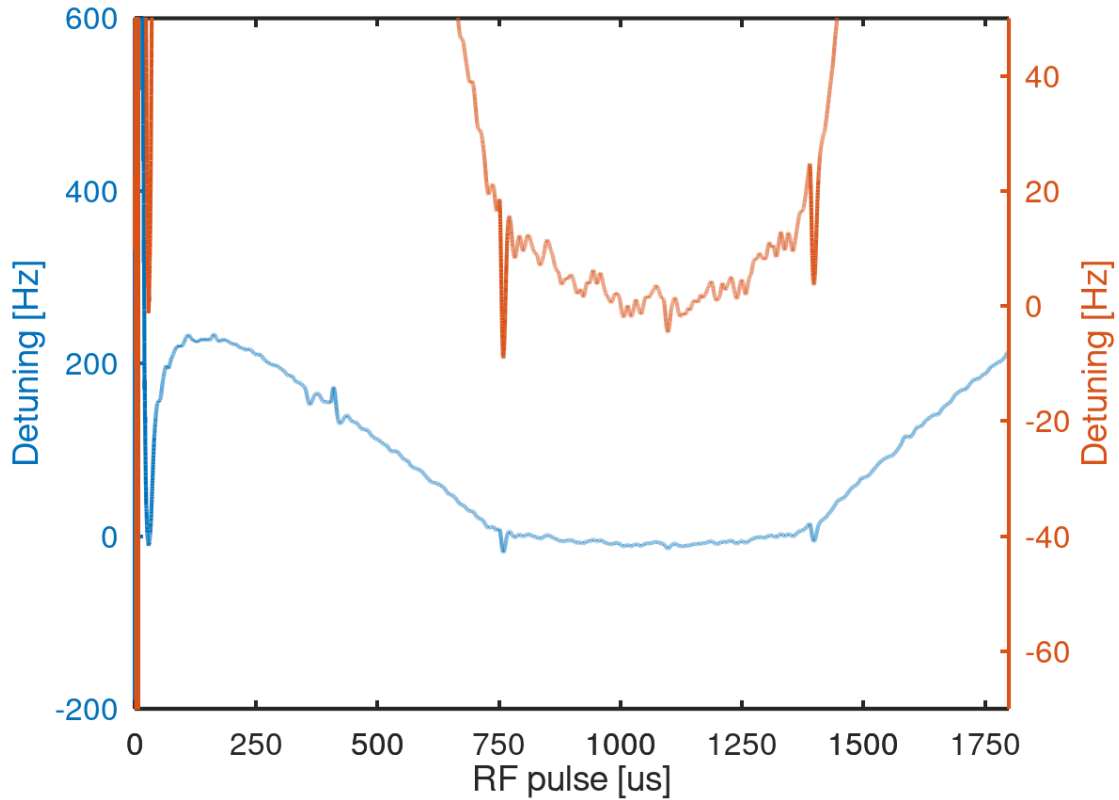
Figure 4.35: Detuning plot of a single measurement in two scales for cavity 3 in the module XM100 saved for the high gradient (29 MV/m).

typically used to depict the detuning of the cavity. Later, when the area at the FT time was enlarged (see red curve), a characteristic bend was noticed, which might be explained as an effect of microphonics. The microphonics were not actively dumped in the tuning algorithm. Furthermore, the increased SD was the effect of the difference between the two systems calculating detuning parameters. The first one was a server for data acquisition, which was independent of *TuneCAV* package presented in this dissertation. The acquisition server recorded SD in the middle of the FT duration [97], while the package presented here uses average of the detuning from the beginning and end of the FT (see equation 4.13). If only one application (acquisition server or *TuneCAV*) had been used to calculate the SD, 10 Hz would have been achieved.

Flat-Top measurement

The tuning improvement with the use of *TuneCAV* package and during the Flat-Top measurements can be described in terms of power. When the frequency of cavity's *transmitted* voltage is better tuned to the input (*forward*) voltage then less *forward* power is required to achieve the maximum gradient. The author wanted to show this improvement using the results of the measurement of the XM24 cryomodule. This cryomodule was the only one that was measured two times during the cryomodule test campaign. During the first test, the cavities were tuned manually by the operator. The second test was performed with the use of the *TuneCAV* package in the final version. The reason for the two measurements of this cryomodule was a leak in the beam vacuum, which caused that the cryomodule was re-assembled and re-tested.

In Table 4.2, the results of these measurements are presented. The outcomes of the tests were the values of the maximum cavity gradient and the related *forward* power. The first measurement of cavity 1 was finished at 2 mGy/min, while the second at 10 mGy/min. The maximum accelerating gradient for cavity 4 in the 2nd test with use of the tuning software was 19.98 MV/m. To be able to compare the 1st and 2nd test the gradient equal to the value of the first one was used. The cryomodule results were, however, very good: the average gradient was above the E-XFEL specification.

$Cavity$	$Parameter$	$I-st\ meas.$	$II-nd\ meas.$
$C1$	$Power\ \ [kW]$	172.3	206.2
	$Gradient\ \ [MV/m]$	27.0	29.2
$C2$	$Power\ \ [kW]$	237.8	219.7
	$Gradient\ \ [MV/m]$	31.0	31.0
$C3$	$Power[kW]$	230.7	227.3
	$Gradient[MV/m]$	31.0	31.0
$C4$	$Power[kW]$	93	90
	$Gradient[MV/m]$	19.7	19.7
$C5$	$Power[kW]$	236.0	227.6
	$Gradient[MV/m]$	31.0	31.0
$C6$	$Power[kW]$	244	244.4
	$Gradient[MV/m]$	31.0	31.0
$C7$	$Power[kW]$	252.8	249.3
	$Gradient[MV/m]$	31.0	31.0
$C8$	$Power[kW]$	257.0	223.0
	$Gradient[MV/m]$	31.0	31.0

Table 4.2: Comparison of the values of the gradients and *forward* power used to set those amplitudes for the cryomodule XM24.

The values of the gradients before and after the re-assembly agreed. The equal gradients depended on assembly, treatment and the repeatability of the measurement. For cavity 4, the degradation to the same accelerating gradient for both measurements was visible. For

other cavities (except for cavity 1), the power limit was reached. The average accelerating gradient of this cryomodule exceeded the E-XFEL's nominal (23.6 MV/m). The maximum gradients did not depend on the effectiveness of the tuning.

The quality of the tuning with the use of *TuneCAV* package is shown in terms of power. The power gain with the use of *TuneCAV* package, when compared to manual tuning, is presented in Figure 4.36. Cavity one was not taken into account (different gradients). For the analysed 7 cavities, during the second measurement less power was needed to reach the maximum gradients, except for the cavity 6. It was believed that for cavity 6 the difference was only the test error [99]. After summing all the power gains and one loss, *the profit of the software usage for the cryomodule XM24 in comparison with the manual cavities tuning was 70 kW.*
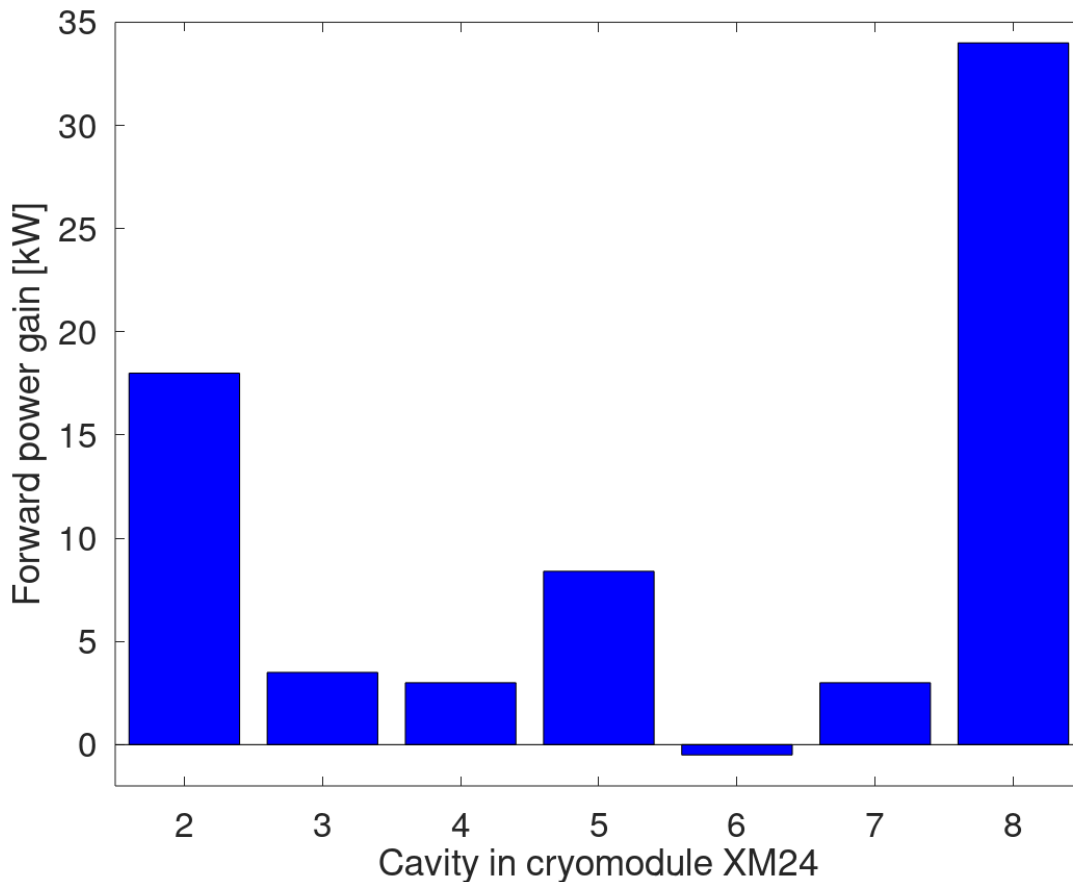
Figure 4.36: Forward power gain by the *TuneCAV* software usage for the cryomodule XM24.

Heat Loads measurement

The results received during the cryomodule test campaign confirmed that the usage of the *TuneCAV* package improved the Heat Loads (HL) measurement. Author chose the results of cryomodule XM100. The calculated thermal loads for this cryomodule resulted in 2.21×10^{10} of the own quality factor, what fulfilled the design threshold. The result of the thermal loads was obtained for the average gradient 21.66 MV/m.

Proper tuning of the cavity with the *TuneCAV* package resulted in stable HL measurement. The tuning results are shown in SD, DD and LFD in Figures 4.37, 4.38, 4.39. The results are separated into 3 phases. During the phase P1 the cavities were roughly tuned, with the use of *TuneCAV* package. During the second phase (P2), the *TuneCAV* package was not used to control the step motor and the piezos, because the preparation for another measurement - *Cryomodule stable operation* took place (see Section 3.3.7). This measurement was performed in parallel to the HL measurement during the following phase. During phase P3, calculations of the thermal loads and average own quality factor during the cryomodule stable operation lasted about 2 hours. The cavities were operating at the fixed gradients (set during phase P1) and the fine tuning was maintained with the use of *TuneCAV* package.
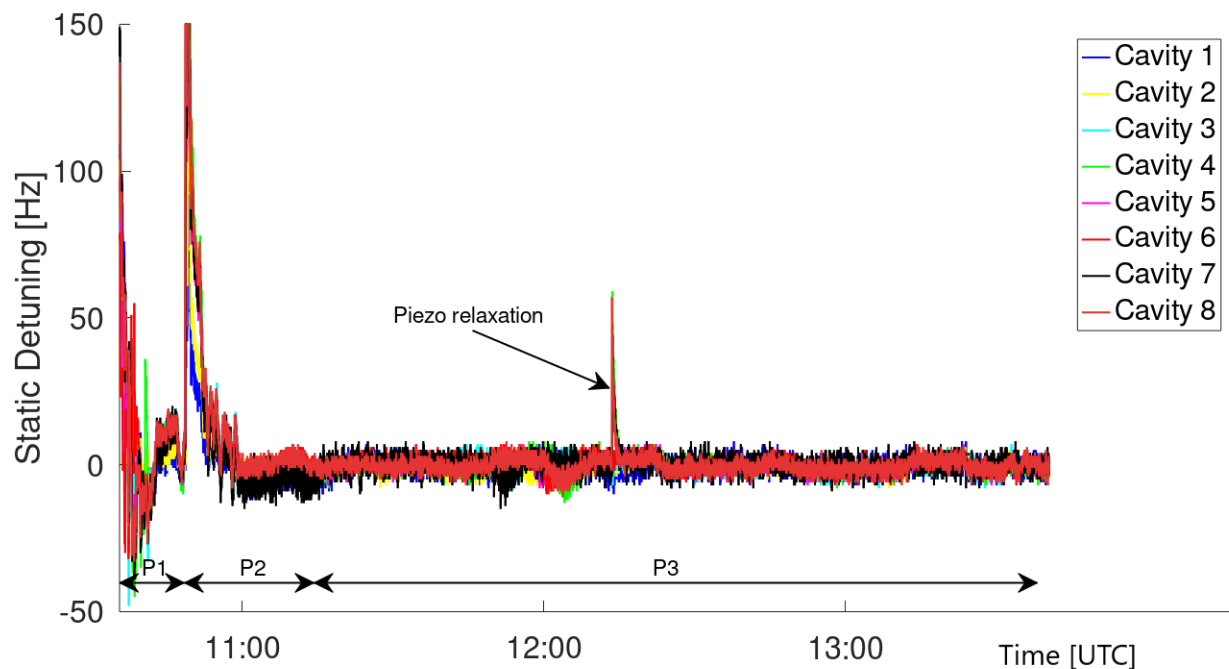
Figure 4.37: Static detuning during the Heat Loads measurement of the cryomodule XM100.
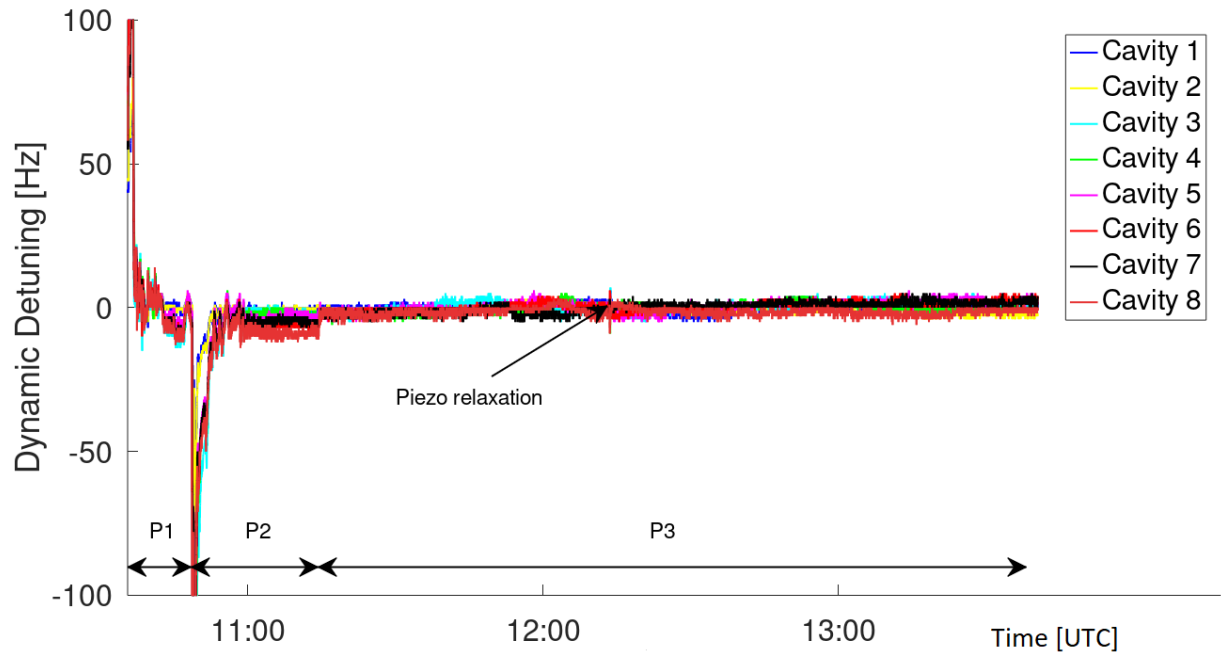
Figure 4.38: Dynamic detuning during the Heat Loads measurement of the cryomodule XM100.
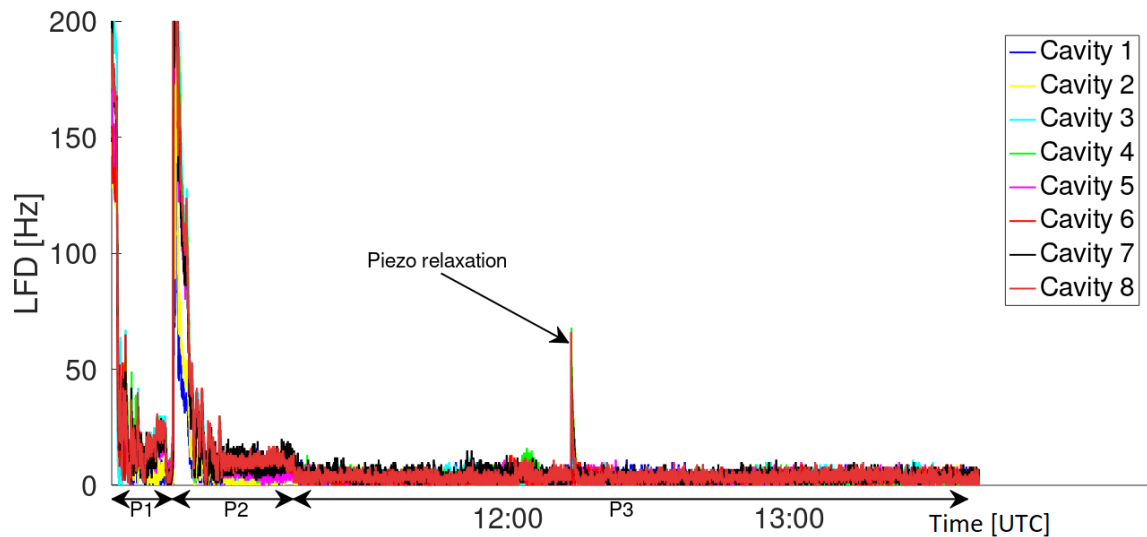
Figure 4.39: LFD during the Heat Loads measurement of the cryomodule XM100.

One may see in Figures 4.37, 4.38, 4.39 the stable results in phase P3 except the time of the piezo relaxation. The evaporating helium during the HL measurement was overcome by the change of DC voltage of the piezo until the "budget" of piezo was exceeded. Accordingly the piezo relaxation was switched on. During the HL measurement the relaxation was done only once due to the limited time and helium level. The relaxation of the piezo did not affect the final result of the thermal loads.

$Cavity$	1	2	3	4	5	6	7	8
$Abs(SD)\ [Hz]$	2.36	2.09	2.31	2.46	1.96	2.20	2.69	2.13
$Abs(DD)\ [Hz]$	1.20	1.43	1.82	1.58	2.00	2.10	2.18	2.62
$LFD\ [Hz]$	3.56	3.53	4.12	4.03	3.96	4.30	4.87	4.74
$Acc.Gradient\ [MV/m]$	16.99	17.16	23.3	24.2	22.97	22.58	22.69	23.41

Table 4.3: Average values of the parameters obtained during the Heat Loads measurement of XM100.

The average values (of absolute values) of the SD, DD and LFD during the Heat Loads measurement of XM100 are listed in Table 4.3. The average value of the LFD is 4.14 Hz, which is below the 10Hz threshold mentioned in the previous FT analysis.

4.3.6   High power RF measurements - summary

To summarize, the control package *TuneCAV* was used to tune 8 cavities in the cryomodule at one time during the high power measurements by adjusting both: the piezo and the step motor. The *TuneCAV* was composed of two stages. During the initialization stage the *frequency* of the mechanical oscillation induced by the RF pulse was calculated. For that frequency the optimum *advance time* was set. The *advance* was the time before the beginning of the RF pulse, when the sinusoidal distortion is applied to the piezo, and consequently to the cavity, in order to induce mechanical frequency oscillation in the cavity that counteracts the detuning change before the RF pulse appears. These two parameters, namely *frequency* and *advance time*, stayed unchanged during the second stage of *TuneCAV* package - during the cavity tuning.

The control of the cavity tuning was realized based on the parameter called the cavity detuning ($\Delta\omega$). $\Delta\omega$ was calculated during the RF pulse and characterizes the difference between the cavity resonant frequency and the 1.3 GHz. During the RF pulse 2 points from $\Delta\omega$ were used for the control purpose: from the start and at the end of the Flat-Top time. As a result the Static Detuning (SD) and Dynamic Detuning (DD) were calculated to characterize the detuning during the RF pulse. SD was used to describe the quality of the static tuning - to counteract the changes of *forward* power and helium level change. The DD was used to describe the quality of the tuning with the use of the sinusoidal distortion. The calculation of the SD and DD was implemented into the *TuneCAV* software.

Two controllers were used in the *TuneCAV* software to regulate the length of the cavity in order to minimize the Static Detuning. The first controller was used to regulate the step motor ($|SD| >= 1\,kHz$) for the rough tuning ($> \sim 3\mu m$). The second one was used to control the extension or contraction of the cavity, but for the fine tuning ($\leq \sim 3\mu m$) and with the use of the piezo actuator's *DC voltage* ($|SD| < 1\,kHz$). The third controller was counteracting the mechanical resonance of the cavity excited by the RF pulse with the use of the Dynamic Detuning. It adjusted the *AC voltage* in order to oppose the change of the cavity length during the RF pulse. Moreover, in the *TuneCAV* software the relaxation of piezo's DC voltage was implemented in order not to exceed the piezo voltage "budget". The voltage "budget" was the piezo driver limit for the sum of AC and DC voltage.

The control of the cavity detuning ($\Delta\omega$) with the use of *TuneCAV* software was required to perfectly simulate the working conditions of the cryomodule in the accelerator. The purpose of the software during the Flat-Top measurement, was to tune the cavity, while *forward* power was changing during the cavity processing or finding of the operating and the maximum gradients. The recorded Static Detuning and Dynamic Detuning for the maximum gradient are the indication for the cavities optimum tuning in the E-XFEL accelerator. The recorded *frequency* was the reference for the accelerator operation. The *advance time* corresponds to the period of the *frequency* and together with the polarity of the *AC voltage* they correspond to the appropriate phase of the sinusoidal distortion in order to damp the mechanical excitation.

Moreover, the *TuneCAV* was also used during the Heat Loads measurement for a single value of the *forward* power (that corresponds to the operating gradient) to check the cavity under normal working conditions for two hours. In this case the operating conditions were simulated not only for a single cavity but for the whole cryomodule at once. The recorded *frequency*, sign of the *AC voltage* and the *advance time* were also unchanged. Finally, the relaxation of the *DC voltage* was also executed during every Heat Loads measurement, which confirms the correctness of the chosen methodology in the *TuneCAV* software.

Chapter 5

Conclusions

This thesis presents the measurement process including the quality assurance and the control methods. During this process, namely cryomodule test campaign, the serial-production RF cavities assembled in the cryomodules were measured. The objectives of the cryomodule test campaign were: the measurement of cryomodule parameters required for its commissioning and operation in the accelerator, the validation of the values of the design parameters and the verification of the cavity parameters before and after installation in the cryomodules.

The work, presented in this thesis, was performed in the frame of Polish in-kind contribution to the E-XFEL project in the years 2010-2016. During the first two years (2010-2011), the author participated in tests of 3 pre-series cryomodules and in the development of the software in order to improve the testing methodology. The developed software was successfully implemented and used during the serial-production test campaign (2012-2016). The author contributed to these tests of 100 serial-production cryomodules and together with the IFJ PAN team completed the tests of all cryomodules on time, according to the E-XFEL project schedule.

The cryomodule test campaign consisted of two parts, low and high power RF measurements, which are summarized below:

- Low power RF measurements;

  During the low power RF measurements the frequencies and the loaded quality factors of modes excited in the cavities were tested. These measurements were performed with the use of the Vector Network Analyzer (VNA) and were composed of two following tasks:

    ○ The Fundamental Mode (FM) spectrum measurement;

  The Fundamental Mode (FM) spectrum measurement was used for the quality assurance of the Field Flatness (FF) and for the control of the frequency of π mode. It was shown that the deformation of each individual cell of the 9-cell cavity changes: the Field Flatness for the π mode and all 9 frequencies within the Fundamental Mode.

The relation between the change of the frequencies within the FM and the Field Flatness was observed. The change of the frequencies within the FM was described by the Mean Spectrum Frequency Deviation (MSFD). The limit of the accepted values of the MSFD was equivalent to the accepted degradation of the Field Flatness. Thereby, the measurement of the FM frequencies was used to determine the FF for cases when it was not possible to access the interior of the cavity to perform the field profile measurement with the use of the bead pulled through the cavity. During the cryomodule test campaign the interior of the cavity was not accessible. Thus, the validation of the FF was possible by comparing the measured resonant frequencies of the FM to the reference values stored just after the FF tuning.

  ○ The HOMs spectra measurement;

The HOMs spectra measurement provided an information about the HOMs extraction through the HOM couplers. Two groups of dipole modes (TE_{111} and TM_{110}) and the group of monopole mode (TM_{011}) were measured. Only part of measured modes were validated, whose phase synchronous condition with the beam was met. The HOM's suppression was validated with the use of the loaded quality factor. Q_{load} was measured: through the HOM couplers and in the frequency domain from the width of the resonance curve.

- High power RF measurements;

  High power measurements performed during the cryomodule test campaign are equivalent to the one $Q_0 vs E_{acc}$ measurement performed during the cavity test campaign (before assembly in the cryomodule). Moreover, during the high power cryomodule measurement, the cavity equipment (input power coupler, step motors, piezos, HOM couplers) was validated under the nominal working conditions: at 2K, with the cavities powered from the klystron and with the high power RF pulse.

  ○ K_T and quality factors in the cryomodule;

The K_T is a parameter used to calculate the accelerating gradient E_{acc} from the *transmitted* power. The determination of K_T was performed in order to check its stability between the cavity test campaign and the cryomodule test campaign. In addition to the inspection of K_T, the quality factors for the E-XFEL operating frequency of the HOM couplers and the pickup probe were measured. The inspection was performed with the use of the high power setup for each cavity in the cryomodule. The measurements of K_T and quality factors were carried out with the similar accelerating gradient, to that one, at which K_T was calculated during $Q_0 vs E_{acc}$ test.

  ○ The Flat-Top measurement;

The Flat-Top measurement provided an information about the maximum and the operating gradient of each of the cavity in the cryomodule individually. The maximum gradient from the cavity test campaign was used as a reference value for the maximum gradient during the cryomodule test campaign. The maximum gradient

was measured during the cryomodule test campaign in order to validate the confines of the RF cavity technology production. The difference between the single cavity test and cryomodule test was the result of the assembly process. The control of this difference allows to manage the quality of the cryomodule production.

The operating gradient, which was measured during the cryomodule test campaign, defined the accelerator's work point. The operating gradient was compared to the equivalent usable gradient, which was measured during the cavity test campaign. The control of the difference between the usable and the operating gradient allows to manage the quality of the production as well.

- ○ The Heat Loads measurement;

The Heat Loads measurement was performed in order to ensure that the heat load budget for the design E-XFEL gradient was not exceeded. The Q_0 measured during the Heat Loads measurement was the average value over all operating cavities in the cryomodule. The purpose of this procedure was to estimate the cooling power demands of the cryogenic infrastructure in the accelerator for different working gradients of the cavities in the cryomodule.

The cryomodule measurement's methodology has been optimized with the use of the automated software. Three packages were selected to demonstrate the functionality of the developed software. The first package *FunMod* is used to measure the Fundamental Mode spectrum. In *FunMod* package the lumped LC circuit model of the accelerating RF cavity was implemented and it was used to predict its resonant frequencies. This package had a significant impact on the measurements efficiency of the $\pi/9$ mode (of TM_{010}) at 2K, determined the testing time and provided the control of the resonant frequencies. The use of the model can be applied to all multicell RF cavities measurements and at different temperatures.

The second package, *HomMod*, was used for the HOM spectra measurement. During the manual measurement of the HOM spectra, the author noticed the reproducibility of the sequence of actions. This sequence of actions was implemented into *HomMod* package. The 1dB drop used instead of 3dB was a significant improvement and it was successfully used for the E-XFEL measurements.

The third package, *TuneCAV*, was used for the control of the tuning of the cavity with the use of the piezo and the step motor. The *TuneCAV* package was implemented in order to tune the cavities during the Flat-Top and Heat Loads measurements. The purpose of the package during the Flat-Top measurement, was to tune the cavity, while *forward* power was frequently changed during cavity processing or finding of the operating and the maximum gradients. The Static Detuning and Dynamic Detuning were measured and recorded as the guiding values for the tuning of the E-XFEL accelerator. In particular the recorded *frequencies* and *advance time* together with the polarity of the AC Voltage were the reference for the accelerator operation.

The *TuneCAV* package usage improved also the Heat Loads measurement. During the Heat Loads measurement the operating conditions were simulated for all cavities in cryomodules at one time. The cavities were tuned to their operating gradients and the stability of the tuning was controlled for each tested cryomodule for several hours. The relaxation of the *DC Voltage* was also executed during every Heat Loads measurement.

In conclusion, the main contribution of this work to the cryomodule test campaign, consists of the serial production measurement methodology improvements of the SRF cavities installed in the cryomodules by the automation of the RF measurements. A vital gains of this work were: keeping the repeatability of the measurements, minimizing of human's errors and keeping the project's deadline. The results of such an improved measurement methodology does not need to be limited to the E-XFEL. *The optimal designed testing methodology and automated software is useful for projects with linear accelerators, which are designed to have hundreds of RF cavities - e.g. for the quality control of European Spallation Source or Proton Improvement Plan-II cryomodules.* The measurement methodology adaptation requires further studies due to the different project needs (pulse time, quality factors and power supply scheme) and different design of the RF cavity equipment (fixed input power coupler).

Appendix A

Cavity LC Model
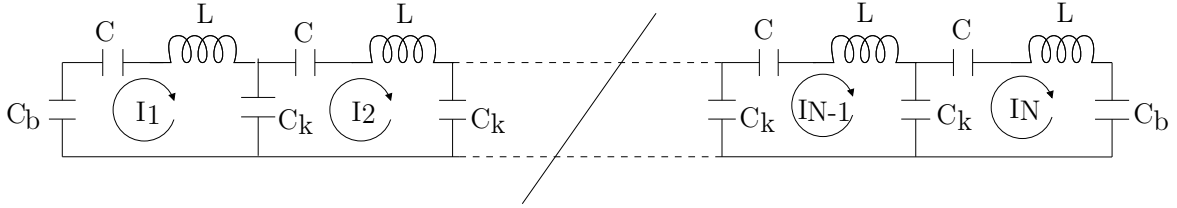
Figure A.1: The LC equivalent circuit of cavity with beam tube [91].

In this section, the equivalent LC circuit (demonstrated by Sekutowicz [17] and Padamsee [21]) of the RF cavity and beam tubes, in order to approximate resonant frequencies of TM_{010} (FM)) mode during the FM spectrum measurement is presented [105]. The figure A.1 shows a scheme of a lumped circuit of the E-XFEL multicell cavity with the beam tubes.

In the Figure A.1, the elements are described as follow:

- C_k - capacitance represents cell to cell coupling,

- C - capacitance of each symmetric cell,

- L - inductance of each symmetric cell,

- C_b - capacitance of beam tubes.

From Kirchhoff equations, where j is a loop (cell) number, one calculates:

$$(\frac{1}{i\omega C_b} + i\omega L)I_1 + (\frac{1}{i\omega C})I_1 + (\frac{1}{i\omega C_k})(I_1 - I_2) = 0 \tag{A.1}$$

$$(\frac{1}{i\omega C_k})(I_j - I_{j-1}) + (i\omega L + \frac{1}{i\omega C})I_j + (\frac{1}{i\omega C_k})(I_j - I_{j+1}) = 0 \tag{A.2}$$

$$j \in \langle 2, N-1 \rangle$$

$$(\frac{1}{i\omega C_k})(I_N + I_{N-1}) + (i\omega L + \frac{1}{i\omega C})I_N + (\frac{1}{i\omega C_b})I_N = 0 \tag{A.3}$$

The equations (A.1-A.3) (multiplied by $i\omega C$) are expressed as a matrix, where currents I_j are replaced by voltages in each cell in the cavity v_j:

$$
\begin{bmatrix}
1+k+\gamma & -k & 0 & \cdots & & 0 \\
-k & 1+2k & -k & & & \vdots \\
0 & & \ddots & & & 0 \\
\cdots & & -k & 1+2k & & -k \\
0 & & \cdots & & -k & 1+k+\gamma
\end{bmatrix} \boldsymbol{v} = \Omega \boldsymbol{v}
\tag{A.4}
$$

where the consecutive quantities are defined:

$$
\omega_0 = \frac{1}{\sqrt{LC}} \qquad k = \frac{C}{C_k}
$$
$$
\gamma = \frac{C}{C_b} \qquad \Omega^{(m)} = \frac{\omega_m^2}{\omega_0^2}
\tag{A.5}
$$

They have the following meaning:

- k is cell to cell coupling constant,

- γ is end cell to beam tube coupling constant,

- ω_0 is a cell resonance angular frequency,

- $\Omega^{(m)}$ is an eigenvalue of the $m\pi/9$ mode for the matrix (A.4).

- N is the number of cells in the cavity, which is equal to the number of resonance modes of the TM_{010} in the cavity. For E-XFEL N=9

Moreover it is known [21] that π mode is flat when:

$$
\boldsymbol{v}^{(N)} = \frac{1}{\sqrt{N}} \begin{pmatrix} 1 \\ -1 \\ 1 \\ \vdots \end{pmatrix}
\tag{A.6}
$$

Thus, using (A.6) in the matrix equation (A.4) one could get that γ=2k, so the matrix becomes:

$$
\begin{bmatrix}
1+3k & -k & 0 & \cdots & & 0 \\
-k & 1+2k & -k & & & \vdots \\
0 & & \ddots & & & 0 \\
\cdots & & -k & 1+2k & & -k \\
0 & & \cdots & & -k & 1+3k
\end{bmatrix} \boldsymbol{v} = \Omega \boldsymbol{v}
\tag{A.7}
$$

In this tri-diagonal matrix all entries on subdiagonal are equal and those on super diagonal are also equal except of two end elements. For such matrices the eigenvalues and the associated eigenvectors are known explicitly [106, 107]. The known eigenvalues are:

$$\Omega^{(m)} = (\frac{f_m}{f_0})^2 = 1 + 2k(1 - cos(\frac{m\pi}{N})) \tag{A.8}$$

And corresponding eigenvectors to m eigenvalue are:

$$v_j^{(m)} = sin[m\pi(\frac{2j-1}{2N})] \tag{A.9}$$

Where: j is a cell (loop) number, m is mode number and N is the maximum number of cell. The maximum number of m and j are the same (N). The equation (A.8) defines the resonant frequencies dependency of the $m\pi/9$ mode. $v_j^{(m)}$ represents the voltage in the j cell of the m resonance frequency ($m\pi/9$ mode) of the TM_{010}.

The same eigenvectors and eigenvalues have been found also by others [21], but they have been calculated by other method. The eigenvectors are as:

$$v_j^{(m)} = B^{(m)} sin[m\pi(\frac{2j-1}{2N})] \tag{A.10}$$

where $B^{(m)}$ is a normalizing coefficient $B^{(m)} = \sqrt{(2 - \delta_{mN})/N}$ and δ_{mN} are a Kroneker delta. Other parameters have the same meaning as in the equation A.9. The eigenvalues are found by taking j equation of the matrix (A.7):

$$(1 + 2k)v_j - k(v_{j-1} + v_{j+1}) = \Omega v_j \tag{A.11}$$

The following relation is noticeable $v_{j-1} + v_{j+1} = 2v_{j-1}cos(m\pi/N)$ and it is used in the equation (A.9). The eigenvalue of mode m is the same as (A.8) .

Finally, from the equation (A.8) one can calculate f_m (resonant frequency of the $m\pi/9$ mode in TM_{010}):

$$f_m = f_0\sqrt{1 + 2k(1 - cos(\frac{m\pi}{N}))} \tag{A.12}$$

Bibliography

[1] XFEL GMBH, *xfel.eu*, [web page], [online: June 2017],
url: `http://xfel.eu`

[2] A. Massimo et al., *The European X-Ray Free-Electron Laser The Technical Design Report (TDR)*, 2007

[3] W. Decking et al. (**K. Kasprzak**), *A MHz-repetition-rate hard X-ray free-electron laser driven by a superconducting linear accelerator*, Nature Photonics volume 14, pages 391–397(2020), DOI: `https://doi.org/10.1038/s41566-020-0607-z`

[4] Wayforlight.eu, [figure], *Peak brilliance*, [Online January 2017] ,
url:`http://www.wayforlight.eu/eng/synchrotrons/petra-iii.aspx#`

[5] J.M.J.Madey. H.A. Schwettman, W.M.Fairbank, *A Free Electron Laser*, 1973

[6] P. Bryant, *Introduction to Accelerators. Cern Accelerator School*, 2012, Granada, Spain,
url:`http://cas.web.cern.ch/cas/Granada-2012/Lectures/GranadaLectures/Bryant.pdf`

[7] B. Ziaja, *X-ray free electron lasers - status and applications.*, 2016

[8] *TESLA TDR. The Tesla Technical Design Report*, 2001, [online: January 2017],
url: `http://tesla.desy.de/new_pages/TDR_CD/start.html`

[9] S. Henderson, J. Holmes, Y. Zhang, *Fundamentals of Accelerator Physics and Technology with Simulations and Measurements Lab*, Oak Ridge National Lab, 2010
url:`http://uspas.fnal.gov/materials/09VU/VU-Fund.shtml`

[10] CERN Accelerator School: RF for Accelerators, 2010, Ebeltoft, Denmark,
url:`http://cds.cern.ch/record/1231364/files/CERN-2011-007.pdf`

[11] CERN Accelerator School, Introduction to Accelerator Physics Prague, Czech Republic, 2014, url:`http://cas.web.cern.ch/cas/CzechRepublic2014/Prague-after.html`

[12] S.Y. Lee, *Accelerator Physics*, 2004.

[13] G. Burt , *Lecture 1 Introduction to RF for Accelerators*

[14] R. Steerenberg, *Introduction to Accelerators*, Introduction to Accelerator Physics, 2-16 October 2016, Budapest, Hungary

[15] S. Belomestnykh, *Superconducting RF for storage rings, ERLs, and linac-based FELs*, USPAS 2009

[16] Interactions.org, [figure], *TESLA cavity*, [Online January 2017] , url:`http://www.interactions.org/cms/?pid=2100&image_no=DE0083`

[17] J. Sekutowicz, *Multi-cell superconducting structures for high energy e collideres and free electron laser linacs*, 2007

[18] F. Gerigk, *RF for Accelerators. Cavity Types*, Cern Accelerator School, 2010, url:`http://cas.web.cern.ch/cas/Denmark-2010/Lectures/Gerigk.pdf`

[19] V. Katalev S. Choroba, *Waveguide Distribution Systems for the European XFEL.*, TUPCH116 Proceedings of EPAC 2006, Edinburgh, Scotland, url:`https://accelconf.web.cern.ch/accelconf/e06/PAPERS/TUPCH116.PDF`

[20] J. Sekutowicz, *High duty factor operation of sc linacs driving X-ray FELs*, 2016, url:`spas2016.ifj.edu.pl`

[21] H. Padamsee, J. Knobloch, T. Hays, *RF Superconductivity for Accelerators*, 2008.

[22] Superconductors.org, [website], [online: January 2017], url:`http://superconductors.org`

[23] A. Romanenko, *Dependence of the residual surface resistance of superconducting radio frequency cavities on the cooling dynamics around Tc*, Journal of Applied Physics 115, 184903 (2014); https://doi.org/10.1063/1.4875655

[24] K. Wille, *The Physics of Particle Accelerator, An introduction*, 2005.

[25] CERN Accelerator School, General Accelerator Physics, 2011, Chios, Greece, Intermediate, url:`http://cas.web.cern.ch/cas/Greece-2011/Greece-after.html`

[26] E. Jensen, *RF Cavities*, Cern Accelerator School, 2010, url:`https://cas.web.cern.ch/cas/Bulgaria-2010/Talks-web/Jensen-web.pdf`

[27] R. Wanzenberg, *Monopole, Dipole and Quadrupole Passbands of the TESLA 9-cell Cavity*, 2001, TESLA 2001-33

[28] J. Sekutowicz, *Superconducting elliptical cavities*, Specialised Course on RF for Accelerators; CERN Yellow Report CERN-2011-007, pp. 369-393

[29] S. Molloy et al, *High precision superconducting cavity diagnostics with higher order mode measurements*, PHYSICAL REVIEW SPECIAL TOPICS - ACCELERATORS AND BEAMS 9, 112802 (2006), DOI: 10.1103/PhysRevSTAB.9.112802

[30] Standard IEEE, *521-2002 - IEEE Standard Letter Designations for Radar-Frequency Bands*, 2009.

[31] Group W. Decking and T. Limberg for the DESY XFEL Project, *TECHNICAL NOTE European XFEL Post-TDR Description*, Hamburg, 2013

[32] MicroTCA, [online: March 2019], `https://techlab.desy.de/`

[33] AMICI, *eu-amici.eu*, [web page], [online: January 2019], url: `http://eu-amici.eu`

[34] J. Swierblewski, *Large Scale Testing of SRF Cavities and Modules*, Geneva, LINAC2014, 2014, TUIOC01, url:`http://accelconf.web.cern.ch/AccelConf/LINAC2014/papers/tuioc01.pdf`

[35] D. Reschke at al, *Performance in the vertical test of the 832 nine-cell 1.3 GHz cavities for the European X-ray Free Electron Laser*, DOI: 10.1103/PhysRevAccelBeams.20.042004

[36] K. Krzysik, B. Dzieza, W. Gaj, D. Karolczyk, **K.Kasprzak**, L. Kolwicz-Chodak, A. Kotarba, A. Krawczyk, W. Maciocha, A. Marendziak, K. Myalski, Sz. Myalski, T. Ostrowicz, B. Prochal, M. Sienkiewicz, M. Skiba, J. Swierblewski, M. Wiencek, J. Zbroja, A. Zwozniak, *Tests of the 1.3 GHz Superconducting Cavities for the European X-Ray Free Electron Laser*, Proceedings of SRF2013, Paris, France, MOP037, url:`http://accelconf.web.cern.ch/AccelConf/SRF2013/papers/mop037.pdf`

[37] F. Dziuba, *Entwicklung von normal- und supraleitenden CH-Strukturen für den 17 MeV EUROTRANS-Injektor-Linac*

[38] Y. Bozhko, [figure], *AMTF aufbau - 3D drawing*.

[39] S.-W. Lee, *Bead-Pulling Measurement Multi-cell Cavity Field Flatness* USPAS 2008; `http://uspas.fnal.gov/materials/08UMD/SRF/Bead-Pulling.pdf`

[40] A. Sulimov, *"Warm" RF measurements for XFEL.* , Hamburg, 2011.

[41] G. Kreps, *Tuning of the TESLA Superconducting Cavities and the Meeasurement of Higher Order Mode Damping*, Protvino, Russia, 1996, XV Conf. Particle Accelarating

[42] R. Carcagno, *Automatic Tuning Machines for SRF Cavities*, 2010, [online: January 2012], url:`http://www.fnal.gov/directorate/program_planning/all_experimenters_meetings/special_reports`

[43] J. Sekutowicz, et. al, *A DIFFERENT TUNING METHOD FOR ACCELERATING CAVITIES.*, Proceedings of the Fourth Workshop on RF Superconductivity, KEK, Tsukuba, Japan

[44] Keith W. Whites, *S parameters and the scattering matrix.*, 19.01.2018 url:`http://whites.sdsmt.edu/classes/ee481/notes/481Lecture15.pdf`

[45] Agilent Technologies, *User's Guide Agilent E5061A/E5062A*, 2009

[46] A. Sulimov, *Specification of RF measurements during module assembly*, [E-mail] 2012, Revision A.

[47] A. Sulimov, *Private Communication.* 2010-2016, alexey.sulimov@desy.de.

[48] A. Sulimov, *RF Measurements for Quality Assurance During SC Cavity Mass Production*, Proceedings of SRF2015, Whistler, BC, Canada WEBA02, url:`http://accelconf.web.cern.ch/AccelConf/SRF2015/papers/weba02.pdf`

[49] T. Powers, *Theory and Practice of Cavity RF Test Systems*, [online: October 2012], url:`http:/uspas.fnal.gov/materials/11ODU/RF_Test.pdf`

[50] D. Reschke, *Measurement Techniques*, Erice, CAS on Superconductivity for Accelerators, 2013

[51] J. Sekutowicz, *Superconducting elliptical cavities*, url:`https://arxiv.org/ftp/arxiv/papers/1201/1201.2598.pdf`

[52] J.P. Holzbauer, et. al, *Systematic Uncertainties in RF-Based Measurement of Superconducting Cavity Quality Factors*, 2016, arXiv:1602.02689 [physics.acc-ph]

[53] W. Singer et al., *Production of superconducting 1.3-GHz cavities for the European X-ray Free Electron Laser*, PHYSICAL REVIEW ACCELERATORS AND BEAMS 19, 092001 (2016)

[54] J. Sekutowicz, *HOM Damping and Power Extraction From Superconducting Cavities*, WE2005, Proceedings of LINAC 2006, Knoxville, Tennessee USA

[55] A. Sulimov, J.Iversen, D.Kostin, W.-D. Moeller, D.Reschke, J. Sekutowicz, J.-H. Thie, D.Karolczyk, **K.Kasprzak**, S.Myalski, M.Wiencek, A. Zwozniak, *Efficiency of high order modes extraction in the European XFEL LINAC*, Geneva, LINAC2014, 2014. THPP022, url:`http://accelconf.web.cern.ch/AccelConf/linac2014/papers/thpp022.pdf`

[56] N. Baboi, et. al, *INVESTIGATION OF A HIGH-Q DIPOLE MODE AT THE TESLA CAVITIES*; Proceedings of EPAC 2000, Vienna, Austria

[57] J. Byrd, *RF Cavities and Linacs*, Lawrence Berkeley National Laboratory, 17.05.2018 url:`http://http://uspas.fnal.gov/materials/14UNM/RF_Structures.pdf`

[58] A. Sulimov et al., *Description and first experience with the RF measurement procedure for the european XFEL sc cavity production.*, San Sebastián, Spain, 2011, Proceedings of IPAC2011, url:`https://accelconf.web.cern.ch/accelconf/IPAC2011/posters/mopc086_poster.pdf`

[59] W. Xu, S. Belomestnykh, I. Ben-Zvi, H. Hahn, *Improvement of the Q-factor measurement in RF cavities*, BNL-98926-2012-IR, C-A/AP/472, November 2012

[60] S. Kotthoff A. Goessel, C. Mueller, *Development of a remote-controlled coupler-interlock for the XFEL Accelerator Module Test Tacility(AMTF)*, Berlin, SRF2009, 2009, THPPO039,
url:`http://accelconf.web.cern.ch/accelconf/SRF2009/papers/thppo039.pdf`

[61] T. Schichler, *Vector cum control of Pulsed Accelerating Fields in Lorentz Force Detuned Superconducting Cavities.*, 1998

[62] S. N. Simrock, *Achieving Phase and Amplitude Stability in Pulsed Superconducting Cavities*, The 10th Workshop on RF Superconductivity, 2001, Tsukuba, Japan

[63] L. Lilje, *Superconducting Radiofrequency Accelerating Structures*, TAS2008; `https://indico.desy.de/indico/event/699/session/3/contribution/5/material/slides/1.pdf`

[64] R. E. Collin, *Foundations for Microwave Engineering*, 2001

[65] M. Parise, *Prediction of the Lorentz Force Detuning andpressure sensitivity for a Pill-box cavity*,Journal of Instrumentation, `https://doi.org/10.1088/1748-0221/13/05/T05010`

[66] **K.Kasprzak**, B. Dzieza, W. Gaj, D. Karolczyk, L. Kolwicz-Chodak, A. Kotarba, A. Krawczyk, K. Krzysik, W. Maciocha, A. Marendziak, K. Myalski, Sz. Myalski, T. Ostrowicz, B. Prochal, M. Sienkiewicz, M. Skiba, J. Swierblewski, M. Wiencek, J. Zbroja, P. Ziolkowski, A. Zwozniak *First Cryomodule Test at Amtf Hall for the European X-Ray Free Electron Laser (XFEL)*, Proceedings of IPAC2014, Dresden, Germany, WEPRI032,
url: `http://accelconf.web.cern.ch/AccelConf/IPAC2014/papers/wepri032.pdf`

[67] M. Wiencek, B. Dzieza, W. Gaj, D. Karolczyk, **K.Kasprzak**, L. Kolwicz-Chodak, A. Kotarba, A. Krawczyk, K. Krzysik, W. Maciocha, A. Marendziak, K. Myalski, Sz. Myalski, T. Ostrowicz, B. Prochal, M. Sienkiewicz, M. Skiba, J. Swierblewski, J. Zbroja, A. Zwozniak, *Tests of the Accelerating Cryomodules for the European X-Ray Free Electron Laser*, Proceedings of SRF2013, Paris, France, MOP054,
url:`http://accelconf.web.cern.ch/AccelConf/SRF2013/papers/mop054.pdf`

[68] D. Kostin et al., *Update on module measurements for the XFEL prototype modules*, Proceedings of SRF2011, Chicago, 2011, MOPO010,
url:`https://accelconf.web.cern.ch/accelconf/SRF2011/papers/mopo010.pdf`

[69] D. Kostin, *XFEL Cryomodule Assembley: RF Measurments and Tuning*, 2008, [online: May 2011],
url:http://pubdb.desy.de/fulltext/getfulltext.php?lid=8177&fid=20966

[70] D. Kostin, *Cavity accelerating gradient measurement error*, 2014

[71] V. Katalev, et. al, *A New Type of Waveguide Distribution for Theaccelerator Module Test Facility of European XFEL*,Proceedings of LINAC2014, Geneva, Switzerland,TUPP021

[72] **K. Kasprzak**, D. Konwisorz, K. Krzysik, S. Myalski, J. Swierblewski, K. Turaj, M. Wiencek, A. Zwoniak, D. Kostin, K. Przygoda, *Automated Quench Limit test procedure for serial production of XFEL RF bibitem*, Richmond, USA, IPAC2015, 2015, WEPMN031,
url:http://accelconf.web.cern.ch/AccelConf/IPAC2015/papers/wepmn031.pdf

[73] M. Wiencek, **K. Kasprzak**, A. Zwozniak, D. Kostin, D. Reschke, N. Walker, *Update and Status of Test Results of the XFEL Series Accelerator Modules*, Proceedings of SRF2015, Whistler, BC, Canada, MOPB080,
url:http://accelconf.web.cern.ch/AccelConf/SRF2015/papers/mopb080.pdf

[74] **K. Kasprzak**, M. Wiencek, A. Zwozniak, D. Kostin, D. Reschke, N. Walker *Test Results of The European XFEL Serial-Production Accelerator Modules*, Proceedings of SRF2017, Lanzhou, China, MOPB106

[75] N. Walker, et. al,*Performance Analysis of the European XFEL SRF Cavities, From Vertical Test to Operation in Modules*, Proceedings of LINAC2016, East Lansing, MI, USAWE1A04

[76] S. Choroba, V. Katalev, E. Apostolov *Series Production of the RF Power Distribution for the European XFEL*, Proceedings of LINAC2016, East Lansing, MI, USA THPLR067
url:http://accelconf.web.cern.ch/AccelConf/linac2016/papers/thplr067.pdf

[77] V. Katalev, S. Choroba, *Compact Waveguide distribution with asymmetric shunt tees for the European XFEL*, Albuquerque, New Mexico, USA, 2007, MOPAN015,
url:https://accelconf.web.cern.ch/accelconf/p07/PAPERS/MOPAN015.PDF

[78] S. Barbanotti J Eschke, K. Jensch, W. Maschmann, O. Sawlanski, X.L.Wang, W.Gaj, L. Kolwicz-Chodak, W. Maciocha, *Cryo-losses measurements of the XFEL prototype cryomodule and pre-series cryomodules.*, Paris : SRF2013, 2013, MOP029,
url:http://accelconf.web.cern.ch/AccelConf/SRF2013/papers/mop029.pdf

[79] J. Branlard, V.Ayvazyan, T. Jezynski, H. Schlarb, W. Cichalewski, W. Jalmuzna, A. Piotrowskli, *LLRF Testing of the Superconducting Cryomodule for the European XFEL.*, New Orleans, IPAC2012, 2012, THEPPB014,
url:http://accelconf.web.cern.ch/accelconf/ipac2012/papers/theppb014.pdf

[80] J. Branlard, V.Ayvazyan, M.Grecki, H. Schlarb, C.Schmidt, W. Cichalewski, K.Gnidzinska, A. Piotrowski, K.Przygoda, W.Jalmuzna, *LLRF tests of the cryomodule at AMTF: First Experimental Results.*, Paris, SRF2013, 2013, THP087, url:http://accelconf.web.cern.ch/AccelConf/SRF2013/papers/thp087.pdf

[81] J. Swierblewski et al., *Improvements of the Mechanical, Vacuum and Cryogenic Procedures for European XFEL Cryomodule Testing*, Proceedings of SRF2015, Whistler, BC, Canada, TUPB115, url:http://accelconf.web.cern.ch/AccelConf/SRF2015/papers/tupb115.pdf

[82] M. Wiencek, **K.Kasprzak**, D. Konwisorz, S. Myalski, K. Turaj, A. Zwozniak, *Improvements of the RF Test Procedures for European XFEL Cryomodule Testing*, Proceedings of SRF2015, Whistler, BC, Canada, TUPB118, url: http://accelconf.web.cern.ch/AccelConf/SRF2015/papers/tupb118.pdf

[83] G. Kreps, *Private Communication.* 2010-2012, guennadi.kreps@desy.de.

[84] D. Kostin, *Private communication*, 2010-2016, denis.kostin@desy.de.

[85] H. D. Leslie *A review of the equivalent circuit model of RF accelerating bibitem in the context of an analysis of the 1.3 and 3.9 GHz bibitem at FLASH.*, MPhys project, 2011

[86] E. Sengpiel, [website], [online: February 2016], url: www.sengpielaudio.com/calculator-bandwidth.htm

[87] A. Zwozniak, *Private Communication.* 2016-2017, agnieszka.zwozniak@ifj.edu.pl.

[88] J.A. Mitchell et al., *Simulation and Measurements of Crab Cavity HOMs and HOM Couplers for HL-LHC*, Proceedings of SRF2017, Lanzhou, China, THPB059

[89] J. R. Delayen, G. K. Davis ,*PIEZOELECTRIC TUNER COMPENSATION OF LORENTZ DETUNING IN SUPERCONDUCTING CAVITIES*, THP22, srf2003

[90] G. Devanz et al.,*COMPENSATION OF LORENTZ FORCE DETUNING OF A TTF 9-CELL CAVITY WITH A NEW INTEGRATED PIEZO TUNER*, MOPCH140, Proceedings of EPAC 2006, Edinburgh, Scotland

[91] K. Przygoda, *Development of Control System for Fast Frequency Tuners of Superconductiong Resonant Cavities for FLASH and XFEL Experiments*, [Online: May 2011], EuCARD-DIS-2011-001, url:http://cdsweb.cern.ch/record/1349300

[92] NI, *NI tutorial:What is I/Q Data?*, url:http://www.ni.com/tutorial/4805/en/

[93] K. Przygoda, et. al, *Piezo Control for Lorentz Force Detuned SC Cavities of Desy Flash*, TUPEA053, Proceedings of IPAC'10, Kyoto, Japan

[94] K. Przygoda et al., *Lorentz Force Detuning Compensation for XFEL Pre-series Cavities at CMTB Test Stand in DESY*, LLRF, Lake Tahoe, California, 1-4 October 2013

[95] DOOCS, url:`http://tesla.desy.de/doocs/doocs.html`

[96] A. Brandt, *Development of a Finite State Machine for the Automated Operation of the LLRF Control at FLASH*, 2007

[97] W. Cichalewski, *Private communication*, 2014-2016, wojciech.cichalewski@desy.de

[98] K. Przygoda, J. Branlard, O. Hensler, H. Schlarb, C. Schmidt, **K. Kasprzak**, W. Cichalewski, *Testing Procedures for Fast Frequency Tuners of XFEL Cavities*, Proceedings of IPAC2015, Richmond, VA, USA, WEPMN030, url:`http://accelconf.web.cern.ch/AccelConf/IPAC2015/papers/wepmn030.pdf`

[99] Y. Yamamoto, W.D. Möller, D. Reschke, " *Error Estimation in Cavity Performance Test for the European XFEL at Desy*, WEPMB007, Proceedings of IPAC2016, Busan, Korea, url:`http://accelconf.web.cern.ch/AccelConf/ipac2016/papers/wepmb007.pdf`

[100] **K.Kasprzak**, A. Krawczyk, A. Zwozniak, *Superconducting RF tests*, 2016, url:`spas2016.ifj.edu.pl`

[101] O. Napoly, *RF acceleration*, 103rd Plenary ECFA meeting - CERN, CERN, 15 November 2018

[102] M. Omet, *Recent Status of Beam Commissioning at the European XFEL*, ALCW, Fukuoka, 2018/05/30

[103] Linear colliders *http://www.linearcollider.org*, [web page], [online: January 2017], url: `http://www.linearcollider.org`

[104] European Spallation Source *https://europeanspallationsource.se/*, [web page], [online: August 2019], url: `https://europeanspallationsource.se/`

[105] **K.Kasprzak**, M.Wiencek, *Fundamental Mode Spectrum Measurement of RF Cavities With RLC Equivalent Circuit*, Proceedings of SRF2013, Paris, France, THP093, url:`http:/http://accelconf.web.cern.ch/AccelConf/SRF2013/papers/thp093.pdf`

[106] Y. Wen-Chyuan, *Eigenvalues of several tridiagonal matrices.*, 2005, Applied Mathematics E-notes 5(2005), 66-74

[107] Y. Wen-Chyuan, Sui Sun, *Explict eigenvalues ands inverses of tridiagonal toeplitz matrices with four perturbated corners.*, 2008, The ANZIAM Journal, 49, 361-387

List of Figures

Acknowlegements

I would like to thank:

- Supervisors Piotr Malecki and Dariusz Bocian for their guidance. Piotr Malecki was an insightful reader of my work, while Dariusz Bocian was an inspiring leader.

- Denis Kostin for a marvellous theoretical support and advices during all my activities for the XFEL project. I am very grateful for answering all my questions and explanations.

- Guennadi Kreps and Alexey Sulimov for a guidance and a support leading to develop *FunMod* and *HomMod* package.

- Konrad Przygoda for a collaboration leading to develop the software of the piezo control and for the effort with revision of this thesis. His algorithm of the piezo control was successfully implemented and extended into the measurement conditions in the AMTF in the form of *TuneCAV* package.

- My team from IFJ PAN that was participating in the serial-production measurements for fruitful work in this project. Special thanks are addressed to Marek Stodulski, Andrzej Kotarba and Jacek Świerblewski.

- For helpful opinions, views, suggestions and a great time I want to thank my long term "RF team": Daniel Konwisorz, Krzysztof Krzysik, Szymon Myalski, Mateusz Wiencek and Agnieszka Zwozniak. I would like to offer my special thanks to Mateusz, who supported me with the first version of the *HomMod* software and many other activities.

- All supporters included in the serial production accelerator components testing. It was a great pleasure to work with You.

- To my parents for giving me the opportunities.

- To my wife - Dzidziuś. For patience.